Continuity of global MODIS terrestrial primary productivity estimates in the VIIRS era using model-data fusion

Preprint · March 2023

DOI: 10.22541/essoar.167768101.16068273/v1

4 authors, including:

K. Arthur Endsley
University of Montana
33 PUBLICATIONS **549** CITATIONS
SEE PROFILE

J. S. Kimball
University of Montana
402 PUBLICATIONS **24,393** CITATIONS
SEE PROFILE

Continuity of global MODIS terrestrial primary productivity estimates in the VIIRS era using model-data fusion

K. Arthur Endsley[1], Maosheng Zhao[2], John Kimball[3], and Sadashiva Devadiga[4]

[1]Numerical Terradynamic Simulation Group (NTSG), WA Franke College of Forestry and Conservation, University of Montana
[2]University of Maryland, College Park
[3]University of Montana
[4]Sigma Space Corporation

March 1, 2023

Abstract

The NASA Terra and Aqua satellites have been successfully operating for over two decades, exceeding their original 5-year design life. However, the era of NASA's Earth Observing System (EOS) may be coming to a close as early as 2023. Similarities between the Moderate Resolution Imaging Spectroradiometer (MODIS), aboard Aqua and Terra, and the Visible Infrared Imaging Radiometer Suite (VIIRS) sensors aboard the Suomi NPP, NOAA-20 and NOAA-21 satellites enable potential continuity of long-term earth observational records in the VIIRS era. We conducted a comprehensive calibration and validation of the MODIS MOD17 product, which provided the first global, continuous, weekly estimates of ecosystem gross primary productivity (GPP) and annual estimates of net primary productivity (NPP). Using Bayesian model-data fusion, we combined an 18-year record of tower fluxes with prior data on plant traits and hundreds of field measurements of NPP to benchmark MOD17 and to develop the first terrestrial productivity estimates from VIIRS. The updated mean global GPP (NPP) flux from MOD17 and the new VNP17 for 2012-2018 is 127 ±2.8 Pg C year-1 (58 ±1.1 Pg C year-1), which compares well with independent top-down and bottom-up estimates. Both MOD17 and VNP17 depict upward productivity trends over recent decades, with 2000-2018 MOD17 GPP (NPP) rising by 0.47 (0.25) Pg C year-2 but slowing to 0.35-0.44 (0.11-0.13) Pg C year-2 over 2012-2021, with a greater reduction in the NPP growth rate. The new VIIRS VNP17 product has the potential to extend these continuous estimates of global, terrestrial primary productivity beyond 2030.

Continuity of global MODIS terrestrial primary productivity estimates in the VIIRS era using model-data fusion

K. Arthur Endsley[1], Maosheng Zhao[2], John S. Kimball[1], Sadashiva Devadiga[3]

[1]Numerical Terradynamic Simulation Group (NTSG), W.A. Franke College of Forestry and Conservation, University of Montana, Missoula, MT, U.S.A.
[2]Science Systems and Applications, Inc.
[3]NASA Goddard Space Flight Center, Greenbelt, MD, U.S.A.

Key Points:

- Over two decades of global productivity estimates from MODIS cannot be continued without use of VIIRS data.
- We performed a comprehensive calibration and validation, and sensitivity and uncertainty analyses of MODIS MOD17 and new VIIRS VNP17.
- Both MOD17 and new VNP17 depict upward productivity trends and mean and interannual variability consistent with independent data.

Corresponding author: Maosheng Zhao, `maosheng.zhao@nasa.gov`

Abstract

The NASA Terra and Aqua satellites have been successfully operating for over two decades, exceeding their original 5-year design life. However, the era of NASA's Earth Observing System (EOS) may be coming to a close as early as 2023. Similarities between the Moderate Resolution Imaging Spectroradiometer (MODIS), aboard Aqua and Terra, and the Visible Infrared Imaging Radiometer Suite (VIIRS) sensors aboard the Suomi NPP, NOAA-20 and NOAA-21 satellites enable potential continuity of long-term earth observational records in the VIIRS era. We conducted a comprehensive calibration and validation of the MODIS MOD17 product, which provided the first global, continuous, weekly estimates of ecosystem gross primary productivity (GPP) and annual estimates of net primary productivity (NPP). Using Bayesian model-data fusion, we combined an 18-year record of tower fluxes with prior data on plant traits and hundreds of field measurements of NPP to benchmark MOD17 and to develop the first terrestrial productivity estimates from VIIRS. The updated mean global GPP (NPP) flux from MOD17 and the new VNP17 for 2012-2018 is 127 $\pm$2.8 Pg C year^{-1} (58 $\pm$1.1 Pg C year^{-1}), which compares well with independent top-down and bottom-up estimates. Both MOD17 and VNP17 depict upward productivity trends over recent decades, with 2000-2018 MOD17 GPP (NPP) rising by 0.47 (0.25) Pg C year^{-2} but slowing to 0.35-0.44 (0.11-0.13) Pg C year^{-2} over 2012-2021, with a greater reduction in the NPP growth rate. The new VIIRS VNP17 product has the potential to extend these continuous estimates of global, terrestrial primary productivity beyond 2030.

Plain Language Summary

The NASA Terra and Aqua satellites have been successfully operating for over two decades, far longer than their original 5-year design life. However, one or both satellites may run out of fuel as early as 2023. These satellites carry the Moderate Resolution Imaging Spectroradiometer (MODIS) sensors, which are very similar to the Visible Infrared Imaging Radiometer Suite (VIIRS) sensors aboard newer satellites. The long record of MODIS data collected so far may therefore be extended by the VIIRS sensors, particularly the global estimates of the amount of carbon in the atmosphere taken up and stored by plants. We used multiple independent datasets to figure out if and how the MODIS MOD17 computer model should be changed to improve its accuracy and to use data from VIIRS. The new VIIRS VNP17 data could extend our record of plant-atmosphere carbon exchange beyond the year 2030.

1 Introduction

The Moderate Resolution Imaging Spectroradiometer (MODIS), carried by the Terra and Aqua satellites, is a key component of NASA's Earth Observing System (EOS) (Justice et al., 2002), which has contributed observations of Earth's land, atmosphere, and oceans for over two decades. Although Terra and Aqua have far exceeded their original 5-year design life, the end of the EOS era is near, as one or both of the satellites may run out of fuel as early as 2023. Because of the dozens of products derived from the 36 MODIS spectral bands, and because of the similarity of the Visible Infrared Imaging Radiometer Suite (VIIRS) sensor aboard the Suomi NPP and NOAA-20 satellites, there has long been interest in using VIIRS to provide continuity of land surface observations (Murphy et al., 2001; Xiong et al., 2020). MODIS-like observations will continue to be important for global studies of terrestrial productivity, including ecosystem monitoring (Y. Zhang, Song, et al., 2017; M. O. Jones et al., 2020) and agricultural studies (Skakun et al., 2018).

Of particular interest are the on-going applications of MODIS to studies of the terrestrial carbon cycle, beginning with the first global, continuous, weekly estimates of ecosystem gross primary productivity (GPP) and annual estimates of net primary productivity (NPP): the Terra MODIS MOD17 product (Running et al., 2004; Zhao et al., 2005).

The MOD17 product, now exceeding 22 years of record, has been instrumental in diagnosing increasing water limitations on carbon uptake (Zhao & Running, 2010), highlighting the role of humans in wildfire ignition (Balch et al., 2017), and constraining human appropriations of biomass (Erb et al., 2018), among other diverse applications. It is no coincidence that MOD17 was developed at the same time that direct, ecosystem-level measurements of canopy gas exchange from eddy covariance (EC) flux towers first became widely available (Baldocchi et al., 2001). The simple light-use efficiency (LUE) approach allows for up-scaling the ecosystem-level estimate of GPP from towers using satellite observations of canopy vigor and gridded surface meteorological data (Ryu et al., 2019).

Here, we confront the MOD17 GPP and NPP models with data in a comprehensive calibration and validation study. We also present the first calibration and assessment of the MOD17 algorithm for use with the VIIRS sensor, enabling continuity of multi-decadal GPP and NPP estimates. The independent observational data used in this study include eddy covariance (EC) tower CO_2 fluxes, field surveys of productivity and biomass change, and a global database of species-level plant traits (Kattge et al., 2020). Previous MOD17 calibration efforts prescribed a set of general biophysical response characteristics for major land cover types, defined in the model's Biome Properties Look-up Table (BPLUT), and derived using a limited set of EC tower site observations as well as literature review, expert elicitation, and a smaller set of NPP estimates (Zhao et al., 2005). Here, we conducted a more extensive model calibration and formal analysis of model sensitivity and uncertainty in parameterization, which has been performed for similar diagnostic models (e.g., L. A. Jones et al., 2017; K. Zhang et al., 2019), but not yet for MOD17.

2 Data and Methods

Although there is a file-naming convention where "MOD" indicates a product granule based on Terra MODIS data (only, as opposed to Aqua MODIS), we use "MOD17" throughout this paper to refer to the combined GPP/NPP algorithm, which is currently operational using MODIS observations from both EOS Terra and Aqua satellites.

2.1 The MOD17 Algorithm

As MOD17 has been discussed thoroughly in the literature, we give only a brief overview of the model here. A complete description is available in the MOD17 Collection 6.1 User's Guide (Running & Zhao, 2021). MOD17 consists of three potentially independent submodels: 8-day GPP, 8-day net photosynthesis (PSN_{net}), and annual NPP. 8-day composite products are given the designation MOD17A2H, for Terra MODIS, or MYD17A2H, for Aqua MODIS. Annual products, including annual GPP (the sum of one year's 8-day GPP composites), are carried by MOD17A3H (or MYD17A3H). GPP is calculated using a classic light-use efficiency (LUE) approach (Running et al., 2004; Yuan et al., 2014; Madani et al., 2017), where the carbon (C) uptake by plants is assumed to be proportional to canopy absorbed photosynthetically active radiation (APAR) under prevailing daytime environmental conditions for diel or longer time scales. Low temperatures or high vapor pressure deficit (VPD) reduce the efficiency of photosynthetic C uptake, thus, MOD17 GPP is described as a product of APAR, the light-use efficiency under optimal conditions (ε_{max}), and environmental scalars:

$$\mathrm{GPP} = \mathrm{APAR} \times \varepsilon_{max} \times f(T_{min}) \times f(\mathrm{VPD}) \quad (1)$$

Where $f(T_{min})$ and $f(\mathrm{VPD})$ are numbers on $[0, 1]$ representing the decline in ε_{max} due to low daily minimum temperatures and high VPD, respectively. These environmental scalars are represented as linear ramp functions, where limiting conditions are interpolated between zero (completely limiting, i.e., photosynthesis cannot occur) and one (non-limiting). The key parameters in modeling GPP, in addition to ε_{max}, are the T_{min}

and VPD values that indicate the width of the ramp function and, consequently, the slope that determines how much $\varepsilon_{\max}$ is reduced for a unit decrease in $T_{\min}$ or unit increase in VPD.

Daily (or 8-day) net photosynthesis is calculated as GPP less maintenance respiration (R_M) from leaves and fine roots. Leaf R_M is based on a Q10 function (Tjoelker et al., 2001) and the current leaf C mass, which is estimated instantaneously as leaf area index (LAI) divided by specific leaf area (SLA). Fine root R_M is also based on a Q10 function and the fine root C mass is based on an allometric relationship with the leaf C mass. The same Q10 $\equiv 2$ is used for fine roots and livewood whereas leaves use a temperature-acclimated equation (ibid.). Notably, as MOD17 does not track biomass allocation, livewood respiration and growth respiration, R_G, are not included in $\mathrm{PSN_{net}}$. Annual NPP does account for R_G and livewood R_M, estimating livewood C mass through an allometric relationship with annual maximum leaf C mass. Based on empirical studies, R_G is estimated to consume 25% of annual NPP; thus, annual NPP is calculated as:

$$\mathrm{NPP} = \mathrm{GPP} - R_M - R_G = \frac{1}{1.25}(\mathrm{GPP} - R_M) \tag{2}$$

The complete list of parameters is included in Table 1. Each of the parameters is defined separately for 11 distinct plant functional types (PFTs), based on the MODIS MCD12Q1 Type 2 International Geosphere-Biospehre Programme (IGBP) land-cover classification (Friedl & Sulla-Menashe, 2019; Sulla-Menashe et al., 2019).

MOD17 Collection 6.1 (C61) depends on surface meteorological data including mean and minimum daily air temperature, photosynthetically active radiation (PAR), atmospheric pressure, and the water vapor mixing ratio. These inputs are derived from the NASA Global Modeling and Assimilation Office (GMAO) Goddard Earth Observing System 5 (GEOS-5), Forward Processing for Instrument Teams (GEOS FP-IT). It also depends on driver data from MOD15A2H (Myneni et al., 2015), a record of LAI and the fraction of the canopy absorbing PAR (fPAR). Taken together, these data determine the surface cover available to harvest light for C (CO_2) uptake and the environmental constraints on that process.

In this re-processing, there are some significant departures from earlier versions of MOD17. First, C61 and all previous versions of MOD17 used an estimate of short-wave radiation (GMAO "SWGNT") that is likely too low to be used in calculating PAR. Estimation of PAR is based on irradiance measurements indicating that approximately 45% of the daily (short-wave) solar irradiance is within the PAR waveband, 400-700 nm (Meek et al., 1984). However, MOD17 has historically used 45% of *net* short-wave radiation for calculating PAR, which might be an underestimate, as SWGNT accounts for surface albedo. Based on GMAO data over 2000-2017, the incoming daily short-wave irradiance (GMAO "SWGDN") is always greater than or equal to SWGNT. Previous MOD17 calibration (Zhao et al., 2005, 2006) has likely compensated for this underestimation of PAR.

Here, we re-calibrate MOD17 using GMAO SWGDN instead of SWGNT. In addition, whereas C61 and prior versions have fixed fine-root and livewood Q10 values at 2, we make these free parameters during model calibration, based on prior evidence that suggest this fixed value may be suboptimal (see "Model-Data Fusion"). Prior to calibration, we conducted a global sensitivity analysis of MOD17's free parameters, based on the Sobol' variance-based decomposition method (Sobol', 2001). This was performed in Python using SALib (Herman & Usher, 2017; Iwanaga et al., 2022), and obtains the proportion of the total variance in GPP or NPP that is contributed directly by a given parameter or by an interaction between that parameter and any combination of other parameters.

Table 1: Free parameters in MOD17, with units and a short description.

Parameter	Units	Description
$\varepsilon_{\max}$	kg C MJ^{-1}	LUE under optimal conditions
$T_{\min,\leftarrow}$	deg Celsius	Minimum temperature below which $\varepsilon = 0$
$T_{\min,\rightarrow}$	deg Celsius	Minimum temperature above which ε not limited by temperature
$\text{VPD}_{\leftarrow}$	Pa	VPD below which ε is not limited by VPD
$\text{VPD}_{\rightarrow}$	Pa	VPD above which $\varepsilon = 0$
SLA	LAI $(\text{kg C})^{-1}$	Projected leaf area per unit mass of leaf C
`froot_leaf_ratio`		Allometric ratio of fine root C to leaf C
`livewood_leaf_ratio`		Allometric ratio of livewood C to leaf C
`leaf_mr_base`	kg C $(\text{kg C})^{-1}$ day^{-1}	Maintenance respiration base rate, per unit leaf C, at 20 deg C
`froot_mr_base`	kg C $(\text{kg C})^{-1}$ day^{-1}	Maintenance respiration base rate, per unit fine root C, at 20 deg C
`livewood_mr_base`	kg C $(\text{kg C})^{-1}$ day^{-1}	Maintenance respiration base rate, per unit livewood C, at 20 deg C
`Q10_froot`		Exponent shape parameter relating fine root R_M to temperature
`Q10_livewood`		Exponent shape parameter relating livewood R_M to temperature

2.2 Model Calibration Data

For GPP model calibration, we used a globally representative network of 352 eddy covariance (EC) flux towers from the FLUXNET/La Thuile synthesis collection (Baldocchi, 2008). Based on a recent analysis of EC tower footprints (Chu et al., 2021), we chose a conservative tower footprint of 1.5 km, or a 3-by-3 grid of 500-m pixels centered on the tower. This area is used to integrate fPAR and LAI observations at 500-m scale and smooth the resulting GPP predictions through spatial averaging. Tower daily gap-filled GPP data were smoothed using a 2-day moving window filter with zero phase offset and observations were discarded when PAR was below 0.1 MJ m^{-2} per day. fPAR and LAI data were filtered to remove spurious spikes; low-quality fPAR and LAI data, based on the quality check (QC) band, were filled in from an fPAR or LAI climatology. Then, 8-day fPAR and LAI were interpolated to daily time steps using forward and backward filling. In addition to MODIS MOD15A2H fPAR and LAI, daily surface meteorological data were compiled for tower sites for the years 2000 through 2017 from the Modern-Era Retrospective Re-analysis (MERRA-2, Gelaro et al., 2017).

MOD17 is calibrated separately for each PFT. Each FLUXNET site is assigned a dominant PFT, the class that makes up the majority of 500-m pixels within the 1.5-km tower footprint. Tower sites used for model calibration were screened to ensure PFT consistency between the local tower footprints and overlying MOD17 windows. Calibration for a given PFT uses just those FLUXNET sites where that PFT is dominant (Table 2). Because no FLUXNET site is located within a majority-DNF canopy, we assigned to this PFT two majority-ENF sites that have DNF pixels within a 3-km radius. CSH is also poorly represented among FLUXNET sites, dominant at only 2 sites. We assigned 3 other sites that have CSH pixels within the 1.5-km footprint, but which are dominant elsewhere.

Table 2: The plant functional type (PFT) classification used in MOD17, which is based on the MODIS MCD12Q1 Type 2 classification. The number of FLUXNET sites with each PFT as the dominant ground cover (i.e., majority of 500-m pixels within a 1.5-km footprint) is also included.

Plant Functional Type (PFT)	Abbreviation	Number of FLUXNET sites
Evergreen needleleaf forest	ENF	30
Evergreen broadleaf forest	EBF	22
Deciduous needleleaf forest	DNF	2
Deciduous broadleaf forest	DBF	32
Mixed forest	MF	33
Closed shrublands	CSH	5
Open shrublands	OSH	15
Woody savannas	WSV	47
Savannas	SAV	35
Grasslands	GRS	77
Croplands	CRO	54

Annual NPP parameters have never before been directly calibrated against observations, with model misfit quantified by the difference between predictions and field estimates of NPP. Here, we use a multi-decadal inventory of global NPP estimates collected by the Oak Ridge National Laboratory (ORNL) Distributed Active Archive Center (DAAC). This "Multi-Biome" collection and other field datasets (Table 3) describe above-ground, below-ground, and/or total NPP at over 1,600 field sites, providing a basis for global calibration of terrestrial carbon models. There are some challenges, however.

Few of the datasets in this collection provide details on the land-use or management history and fewer still provide specific years or year ranges for the NPP estimates;

Table 3: Calibration and validation data used in this study, with citations. The majority of datasets come from the Oak Ridge National Laboratory (ORNL) Distributed Active Archive Center (DAAC). The last two entries refer to separate published papers.

Dataset	Citation
Summary Data from Intensive Studies at 125 Sites, 1936-2006	(Olson et al., 2017)
Global Osnabruck Data, 1937-1981, R1	(Esser, 2013)
Grassland, Boreal Forest, and Tropical Forest Sites, 1939-1996, R1	(Scurlock & Olson, 2012)
PIK Data for Northern Eurasia, 1940-1988 (Based on Bazilevich), R1	(Dennisenko et al., 2012)
TEM Calibration Data, 1992, R1	(Kicklighter, 2012)
Global IBP Woodlands Data, 1955-1975, R1	(DeAngelis et al., 2012)
Global Primary Production Data Initiative Products, R2	(Olson et al., 2013)
Boreal Forest Consistent Worldwide Site Estimates, 1965-1995, R1	(Gower et al., 2012)
NPP Estimates from Biomass Dynamics for 31 Sites, 1948-1994, R1	(Scurlock et al., 2003)
VAST Calibration Data, 1965-1998, R1	(Barrett, 2012)
"Biomass production…in temperate and boreal ecosystems"	(Campioli et al., 2015)
"Depth distribution of belowground net primary production…"	(Luo et al., 2021)

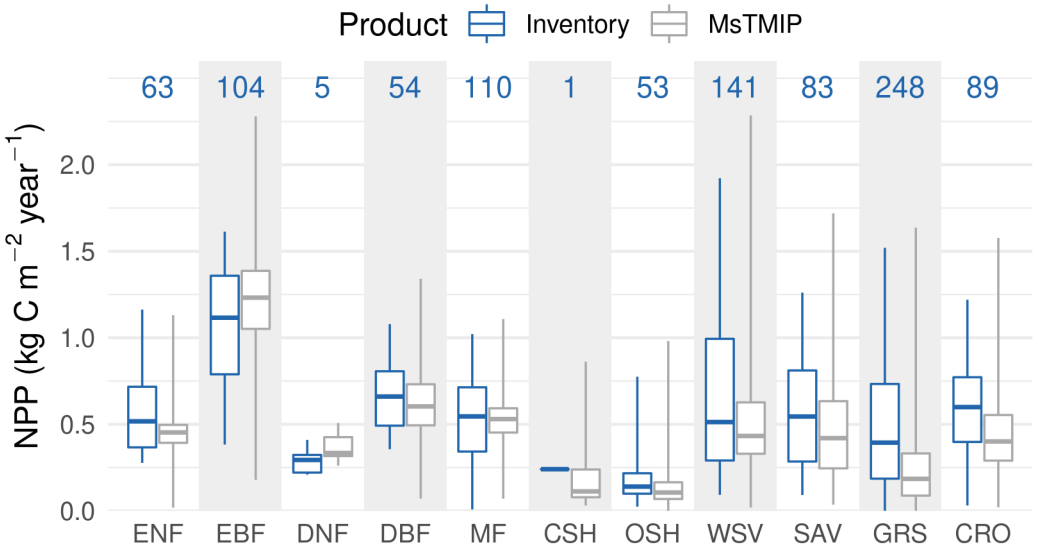

Figure 1: Boxplots of mean annual NPP, by Plant Functional Type (PFT), for the Cal-Val ("Inventory") data and the MsTMIP ensemble mean, based on a majority resampling of land-cover data to MsTMIP's half-degree grid. Numbers at top indicate the total number of site-years for the Inventory data. Whiskers show the minimum and maximum of each dataset. Sites with reported mean annual NPP greater than 2,385 g C m^{-2} year^{-1} were discarded.

the estimates span a range of years from 1936 to 2006. Sites in the inventory were classified into PFT groups based, first, on the reported biome or vegetation type; if no such information was provided, the site coordinates were used to map the PFT class from the MCD12Q1 Type 2 global mosaic for year 2015. A small number of sites were excluded because they did report intensive management histories (fertilizer, irrigation, mowing, or burning). NPP estimates from Gower et al. (2012) and Olson et al. (2013) were grouped by site (unique name or coordinates) and averaged. Because CSH describes such a small proportion of the global land domain (Madani et al., 2017), additional, randomly chosen CSH sites from the NPP validation datasets were added to the calibration dataset. In addition, data compiled by Campioli et al. (2015) and Luo et al. (2021) were added to the ORNL calibration dataset, after removing sites that were duplicated from the ORNL data, resulting in a total of 1,646 annual NPP measurements for calibration and validation ("Cal-Val").

As we cannot exclude the possibility that some sites are intensively managed to boost productivity (e.g., by fertilization or irrigation), we removed NPP samples that fell outside the PFT-group range of global mean (1980-2000) annual NPP, which was derived from a fusion of annual FLUXCOM NEE (Jung et al., 2020) and heterotrophic respiration (R_H) data from X. Tang et al. (2020). After also accounting for sites that fall outside of the MODIS global land domain (i.e., have no fPAR or LAI data), this resulted in a final total of 951 valid NPP measurements. The NPP Cal-Val data show expected differences by PFT and the median NPP agrees well with previously reported biome-level averages (e.g., Kicklighter et al., 1999; Zaks et al., 2007), and also with the Multi-Scale Synthesis and Terrestrial Model Intercomparison Project (MsTMIP, Huntzinger et al., 2013) "BG1" simulation (time-varying climate, land-cover, CO_2, and nitrogen deposition) ensemble mean (Figure 1). Reported values in DNF canopy (209-410 g C m^{-2}

year^{-1}) are low but consistent with reports from field measurements in forest stands (Kushida et al., 2007; Ji et al., 2020).

Corresponding NPP model meteorological drivers for 1980-2000 were obtained from the MERRA-2 re-analysis (Gelaro et al., 2017), which is derived from the GEOS-5 land model. As most sites do not specify the exact year of the NPP measurement, we used daily data from a randomly chosen year between 1980-2000 for each site, for the corresponding calendar day of a 365-day year, so as to capture the real, within-site, intra-annual variability in environmental drivers (as opposed to reducing the variance by using a climatology). As MOD17 does not have any state tracked between time steps, and as modeled NPP is calculated over the synthetic, 365-day year at each site, there are no issues with using different days for consecutive years. Because there are no MODIS data prior to 2000, MODIS fPAR and LAI climatologies were calculated for the 2000-2005 period for use in calibrating annual NPP.

2.3 Model-Data Fusion

The parameters in the MOD17 BPLUT, itemized in Table 1, were previously derived from literature review and some empirical studies. Today, there are numerous, direct ecological observations that can be used to inform model development and calibration, including extensive EC flux tower data and measured plant traits. We consulted the global TRY database (Kattge et al., 2020) for plant traits relevant to MOD17 parameters and developed prior parameter distributions for use in a Bayesian model-data fusion. Specifically, using Markov Chain Monte Carlo (MCMC), the observed distributions of plant traits were used as priors for estimating the likelihood of MOD17 parameters given the difference between modeled and observed GPP or NPP. Details of how plant traits informed priors are available in the Supplement.

Likelihood-ratio tests indicated that the SLA prior for each PFT was significantly different from the pooled distribution (i.e., based on values from all PFTs). We decided to fix SLA at its prior mean (from the TRY database), given the thousands of species observations for this parameter, because SLA was revealed to be the most sensitive model parameter and we believe the TRY data to be more reliable for fixing this parameter than the relatively small number of field NPP estimates.

Model calibration was performed using MCMC with the Differential Evolution Metropolis sampler described by Ter Braak and Vrugt (2008) and Vrugt et al. (2009), as implemented in the PyMC framework (Salvatier et al., 2016). Between 100,000 and 200,000 samples were drawn from the posterior for each of three chains, based on a root-mean squared error (RMSE) pseudo-likelihood function. Chains were qualitatively assessed for convergence and required burn-in; thinning to remove autocorrelation was one in every 20 (for GPP) or 200 (for NPP) samples. The optimal posterior point estimate, used in the updated BPLUT, was chosen as the mean *a posteriori* estimate.

2.4 Inter-calibration for the VIIRS Sensor

Within the 2000-2017 period for which FLUXNET data are available, the SNPP VIIRS mission provides data for 5 years (2012-2017). Because the VIIRS record is much shorter than the MODIS record, and also because of differences in fPAR and LAI between the corresponding VNP15A2H and MOD15A2H products, we opted to calibrate MOD17 for VIIRS differently. Instead of using data fusion for calibration against observed NPP (as with the updated MODIS MOD17 product), we derived bias-correction coefficients based on systematic differences in fPAR and LAI between the two sensors and apply these to the updated MOD17 BPLUT. The ratio between mean MOD15A2H fPAR and mean VNP15A2H fPAR is used as a multiplier to adjust the $\varepsilon_{\max}$ parameter in the resulting VNP17 BPLUT while the ratio between mean MOD15A2H LAI and

mean VNP15A2H LAI is used as a multiplier to adjust the SLA parameter. Besides $\varepsilon_{\max}$ and SLA, the updated MOD17 and new VNP17 BPLUT would be the same.

In deriving both coefficients, because GPP is only accumulated for part of the year (but R_M continues year-round), we calculated mean fPAR and LAI only during the growing season, defined as days when the daily temperature constraint on GPP (defined by $T_{\min,\leftarrow}$) is above zero. The input fPAR and LAI data to this process are the 5-km gap-filled datasets used for global simulation (see "Global Boundary Conditions" section). The fPAR-based $\varepsilon_{\max}$ coefficients range from 0.965 (ENF) to 1.01 (OSH) and the LAI-based SLA coefficients range from 1.007 (WSV) to 1.076 (EBF), confirming the consistency in fPAR, LAI values between MOD15A2H and VNP15A2H (Xu et al., 2018; Yan et al., 2021).

2.5 Global Boundary Conditions

To verify that global carbon use efficiency (CUE), or NPP:GPP ratios, are reasonable, we conducted global simulations of GPP and NPP using the re-calibrated BPLUT. To overcome resource limitations, global simulations were conducted at 5-km scale from 2000-2021 (for MODIS) or 2012-2021 (for VIIRS). This approach is similar to previous MOD17 global simulations conducted at 1-degree resolution (Zhao et al., 2005). The global 5-km dominant PFT is defined as the majority land-cover type within a 5-km window over the MODIS MCD12Q1 (500-m) grid. We then created gap-filled 5-km fPAR and LAI time series using the approach of Zhao et al. (2005); the gap filling addresses data gaps from either cloud contamination or missing data during non-retrieval periods due to lower solar altitude at high latitudes during winter. Based on these 5-km, multi-year runs, the average annual GPP, NPP, and CUE were calculated within each PFT group.

2.6 Model Validation

Some GPP data were withheld during model calibration. For most PFTs, between 20 and 25 site-years of (daily) EC flux tower data, for up to 5 different tower sites, were reserved for validation. Because there are few sites where the majority of land-cover pixels are MF, GRS, DNF, or CSH, only 15 site-years are used for MF and GRS canopies and only 4 site-years are used for DNF and CSH. Each site-year reserved had valid data on at least 97% of data-days, ensuring that nearly complete years were used. Any missing days (3% or less) were interpolated by forward-backward filling to ensure an annual total based on 365 days.

For NPP model validation, because of the dearth of reliable NPP measurements, we used a 3-fold cross-validation to simultaneously estimate best-fit parameters and goodness-of-fit. In combination with MCMC, this means that a random subset of the NPP measurements was reserved in each fold and that nine chains (three folds times three chains in each fold) were obtained. Chains within a fold were pooled and the posterior mean parameters were used to calculate the goodness-of-fit, including bias, root mean-squared error (RMSE), and Pearson's correlation. These metrics were then averaged across folds to obtain the final goodness-of-fit values.

Three official MOD17 products were validated: MOD17A2H daily GPP, MOD17A3H annual GPP, and MOD17A3H annual NPP. Validation metrics include RMSE, normalized RMSE (nRMSE), unbiased RMSE, and Pearson's correlation coefficient; these were computed for products based on the MOD17 C61 BPLUT, updated MOD17 BPLUT and new VNP17 BPLUT. For MOD17A2H, daily tower GPP fluxes were aggregated (summed) to 8-day intervals matching the MOD17A2H 8-day GPP. For MOD17A3H annual GPP, because there are so few towers with valid data for at least 97% of days per year, we did not use the reserved validation sites only; instead, all tower sites with valid data were

used. This may overestimate the accuracy of the updated annual GPP product, since the annual GPP validation dataset includes several data points used in calibration.

We also validated MOD17 and VNP17 interannual NPP predictions against one top-down and three bottom-up estimates of global, annual NPP. First, the 2020 Global Carbon Budget (Friedlingstein et al., 2020) provides mean monthly NEE (2000-2016) based on atmospheric inversion on a 1-degree global, equirectangular grid. We calculated total annual NEE from these data and then resampled them onto a 0.5-degree grid to combine with global, up-scaled estimates of R_H from X. Tang et al. (2020); NPP is then calculated as $R_H - NEE$ ("GCB2020"). Second, we estimated total annual NPP (2000-2017) from the TRENDYv7 ensemble mean monthly GPP and R_A fields (Le Quéré et al., 2018; Sitch et al., 2015), on a 1-degree grid. Third, the ensemble mean NPP (2000-2010) from MsTMIP (BG1 simulation), on a 0.5-degree grid, was used as another bottom-up estimate (Huntzinger et al., 2013). Fourth, the up-scaled flux-tower estimates from FLUXCOM, driven by remote sensing and surface meteorological data ("RS+METEO"), were also compared, based on driver data from ERA5 (Jung et al., 2020). These independent estimates were compared to MOD17 and VNP17 annual NPP and their correspondence quantified by RMSE and Pearson's correlation coefficient.

To compute global annual fluxes from the independent GCB2020, TRENDYv7, MsTMIP, and FLUXCOM datasets, given their coarse spatial resolution and lack of equal-area projection, we projected the annual data onto a 9-km Equal-Area Scalable Earth Grid (EASE-Grid 2.0) using nearest-neighbor resampling. Then, after masking the data to a similarly resampled MCD12Q1 land area map, totaled the flux densities after scaling each pixel by its land area. This may result in slightly different estimates than reported in the literature for these products, but was ultimately necessary as those publications do not always report annual flux estimates.

2.7 Uncertainty Analysis

To quantify uncertainty in MOD17 GPP estimates, we applied error propagation by computing the Jacobian, J, of the GPP model with respect to fPAR and $\varepsilon_{\max}$, separately, for each PFT. The variance in GPP due to model inputs or parameters θ is given:

$$\sigma^2_{\mathrm{GPP}}(\theta) = J_\theta C J_\theta^T \tag{3}$$

where C is the error covariance matrix. To quantify the separate contributions of fPAR and $\varepsilon_{\max}$, this equation reduces to a scalar product, where C is the error in fPAR or $\varepsilon_{\max}$. We focused on fPAR and $\varepsilon_{\max}$ because the error in these parameters is known. fPAR error is given as 10 fPAR units (Myneni, 2018) and the standard error in the $\varepsilon_{\max}$ posterior is assumed to be representative. To facilitate uncertainty quantification, we also assume that errors in fPAR and $\varepsilon_{\max}$ are uncorrelated. We used Gaussian error propagation to estimate the uncertainty in annual GPP due to the compensating errors in daily GPP estimates. Overall uncertainty was calculated by pooling data for all PFTs, using only the GPP validation data, which effectively stratifies the data so approximately equal site-days are included from each PFT.

To quantify uncertainty in MOD17 annual NPP estimates, we use a Monte Carlo approach because is it is much more difficult to compute partial derivatives of the NPP model. We repeatedly sampled from the posterior NPP parameters, with replacement, calculating the RMSE in mean annual NPP based on the Cal-Val dataset. The coefficient of variation in RMSE is then reported, separately, for each PFT.

3 Results

The Sobol' sensitivity analysis indicates that more than 80% of the variance in the GPP model is determined by the $\varepsilon_{\max}$ parameter alone (Figure 2). The upper bounds

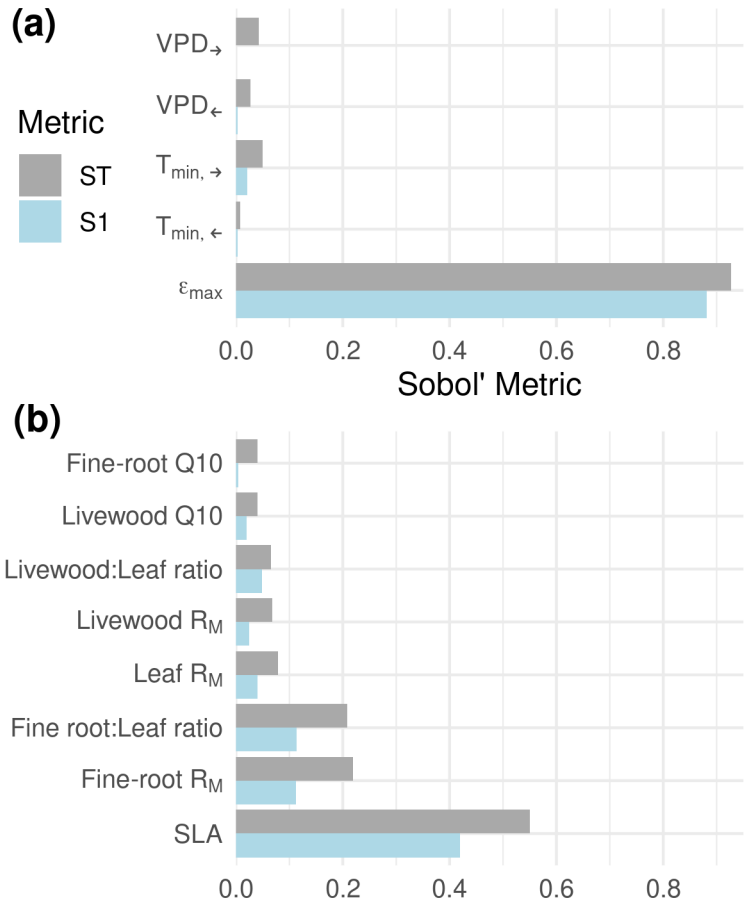

Figure 2: Sobol' sensitivity metrics for the MOD17 GPP (a) and NPP (b) models. The direct effect of the parameter on model estimates is indicated by S1; the total effect (including higher-order interactions) is indicated by ST. $T_{\text{min},\leftarrow}$ and $\text{VPD}_{\leftarrow}$ refer to the lower (left-hand) bounds of minimum temperature and VPD; the left-hand bound is the temperature (VPD) at which photosynthesis is completely limited (unlimited) by temperature (VPD). $T_{\text{min},\rightarrow}$ and $\text{VPD}_{\rightarrow}$ refer to the upper (right-hand) bounds of minimum temperature and VPD; the right-hand bound is the temperature (VPD) at which photosynthesis is completely unlimited (limited) by temperature (VPD).

of the environmental constraints, $T_{\text{min},\rightarrow}$ and $\text{VPD}_{\rightarrow}$, are more important than the lower bounds and have weak, second-order effects through ε_{max}. The annual NPP model has a strong direct effect of SLA (42%) but also moderately strong total effects from the fine root-leaf ratio (`froot_leaf_ratio`) and base R_M for fine roots. These sensitivities are partly reflected in the model-data fusion results. In the GPP calibration, the posterior distributions for the environmental scalars are fairly flat, resembling the uniform priors and indicating that the observed GPP data are consistent with a wide range of thresholds for T_{min} and VPD. Similarly, the `Q10_livewood` mean *a posteriori* estimate was close to the prior mean for most PFTs.

3.1 Optimal Parameters for BPLUT

The posterior distributions were compared to the C61 BPLUT and the wider literature, assessing both consistency with the previous product and realism. As an additional boundary condition, the mean global CUE values for each PFT were expected to be close to 0.46 (Collalti & Prentice, 2019) and much lower for EBF (Malhi, 2012). During NPP calibration, to ensure realism in the BPLUT values and the simulated, global CUE values, we rejected some of the mean *a posteriori* (MAP) estimates after calibration. When the MAP was rejected, it was replaced either by the prior mean for that PFT (Table S7) or by the MAP of a similar PFT. The updated MOD17 BPLUT and new VNP17 BPLUT can be found in the Supplement (Tables S9, S10).

Given the low sensitivity of the GPP model to the lower bounds of the environmental scalars (Figure 2), we opted to fix these at their C61 values; upper bounds remained free parameters during MOD17 calibration. The $\text{VPD}_{\rightarrow}$ posterior likelihood increased rapidly with VPD but, above ca. 3000 Pa the posterior flattens out. The $T_{\text{min},\rightarrow}$ posteriors are more complex, with most PFTs showing little sensitivity to this parameter. Consequently, the optimal values for both $\text{VPD}_{\rightarrow}$ and $T_{\text{min},\rightarrow}$ were chosen as the maximum *a posteriori* estimate, as the mean (or median), given a uniform prior, tends to fall near the middle of the prior bounds. The ε_{max} posteriors were symmetric and the prior mean was within the interquartile range (IQR) for all PFTs. The results are consistent with Madani et al. (2017), but the optimal ε_{max} appears to be significantly lower than its C61 value for shrublands and savannas, higher for croplands, and otherwise similar to C61 (Figure S9).

Consistent with the literature, the livewood Q10 posterior is narrow and resembles the prior. The fine-root Q10 posterior varies widely among PFTs, which is partly a reflection of the uncertainty in the literature. Deciduous canopies and Mixed Forest have the highest `Q10_froot` values. As `Q10_froot` is not likely to be less than 1.0 (Atkin et al., 2000), the posterior was rejected in favor of the prior in such cases. Posterior R_M for leaves and fine roots were generally lower than the prior means from TRY but within the range of the C61 BPLUT. The NPP data indicate that the optimal leaf R_M rate compares well with C61 for woody forest PFTs; however, posterior means for other PFTs were higher than the C61 value and close to the prior mean. The fine-root R_M posteriors vary widely and few are close to their C61 values. The posterior livewood R_M, however, compares well with the C61 BPLUT and the prior mean, except for EBF and shrublands, where it is significantly higher. The `livewood_mr_base` prior mean for EBF was used in place of the MAP.

3.2 Validation against Tower Fluxes and Field Data

The C61 annual GPP (MOD17A3H) estimates compare well with tower annual GPP among those sites with nearly complete years (Table 4). Under-estimation of GPP is apparent for ENF, but C61 also over-estimates GPP in medium-productivity EBF (Table S11). C61 GPP performs best in ENF, EBF, and GRS (nRMSE within 13-17%) but most severely under-estimates GPP in ENF and MF (nRMSE $\geq$ 49%). C61 8-day GPP (MOD17A2H), divided into daily units, indicates the algorithm performs best in shrublands, WSV, and GRS (nRSME $\leq$ 7%) and worst in CRO (nRMSE = 26%) because of under-estimation (mean bias = -1.2 g C m^{-2} day^{-1}) (Table S13).

GPP bias and RMSE were both reduced overall in the Updated product (Table 4), with the greatest improvements made at highly productive DBF and CRO sites (Table S13). Daily GPP improved for most PFTs, while annual GPP generally improved only for herbaceous and forested canopies. High negative bias in annual GPP was significantly reduced for ENF, GRS, and CRO (-196, -174 and -9 g C m^{-2} year^{-1} after recalibration, respectively). C61 MOD17 generally under-estimates GPP, particularly at high magnitudes (Heinsch et al., 2006; Y. Zhang et al., 2008), and slightly over-estimates annual

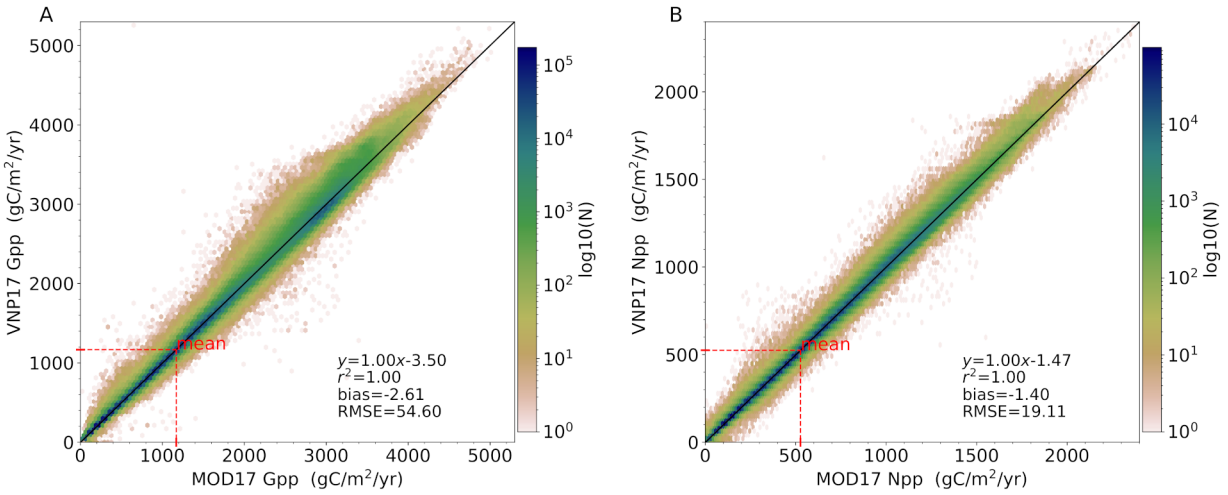

Figure 3: Comparison of mean annual GPP (left) and NPP (right) from the overlapping 10-year period for MODIS MOD17 and VIIRS VNP17 (2012-2021), based on global, 5-km simulations.

NPP, particularly in forested areas (Table S15). After re-calibration, GPP bias is reduced but is systematically similar to C61, while NPP bias is almost eliminated in individual PFTs, save for ENF, which has a strong, negative mean bias (Table S15). This also leads to an overall negative bias in the updated product (Table 4).

Annual NPP skill is improved in the MOD17 update, compared to C61 (Table 4, Figures S10-S11). C61 Annual NPP (MOD17A3H) performs best in shrublands, savannas, and herbaceous canopies (nRMSE $\leq$ 17 percent) and this pattern is similar for the updated product, though DNF, DBF, and MF are also considerably improved (Table S15). The magnitude of annual NPP RMSE in C terms is small ($\sim$ 0.7 g C m^{-2} day^{-1}) but performance varies widely by PFT, with the greatest nRMSE values in forest canopies. In the update, spatial correlation in annual NPP is improved for all PFTs ($\geq$ 0.5) except ENF. Annual NPP RMSE was also improved for all PFTs, except ENF.

Plant CUE (NPP:GPP ratio) is an emergent property of ecosystems simulated by MOD17. When the new annual GPP and NPP products are combined, we find that the BPLUT updates lead to substantial changes in CUE from C61. In terms of agreement with the MsTMIP ensemble, the updates improve plant CUE for all PFTs except DNF, SAV, and GRS (Figure S12). When compared to the measured CUE values compiled by Collalti and Prentice (2019) for woody plants, the updates improve plant CUE for all PFTs except EBF (Figure S13), for which median CUE is 0.49 (0.40 in MsTMIP ensemble, 0.44 in C61, and 0.37 in the update).

At global extent, the new VNP17 annual GPP and NPP products are very similar to the updated MOD17 products (Figure 3). The new VIIRS VNP17 BPLUT was used in the same validation scheme as for MOD17 GPP and NPP. However, because VIIRS fPAR and LAI data are only available starting in 2012 and many FLUXNET sites do not report data after 2012, there are far fewer site-weeks or site-years to use for validating VNP17 daily GPP than for MOD17. In particular, majority-DNF sites are not represented in the 2012-2017 period and no majority-DBF sites have years with at least 97% of valid data-days within this span. When using a common validation data mask, it is apparent that the VNP17 BPLUT produces daily GPP estimates quite similar to the updated MOD17 BPLUT (Table 4), except that VNP17 shows potential degrada-

Table 4: Validation statistics for the daily MOD17A2H/VNP17A2 GPP and annual MOD17A3H/VNP17A3 GPP and NPP products, as compared to EC flux tower and NPP cross-validation (Cal-Val) data, respectively. For daily GPP validation, daily tower GPP and updated simulations were aggregated to 8-day periods to match MOD17A2H. For annual GPP validation, all tower data were used instead of only reserved data. The normalized RMSE (%) is based on the overall observed range of daily GPP or annual NPP. The largest valid tower GPP observation was 20.4 g C m^{-2} day^{-1}. The largest NPP flux in the NPP Cal-Val dataset was 1,922 g C m^{-2} $year^{-1}$ (nRMSE for annual NPP is the cross-validation mean). 8-day GPP was evaluated for the entire FLUXNET record (2000-2017) but also on a common, reserved test dataset from 2012-2017, for compatibility with VIIRS; the latter case does not include any results from DNF due to missing FLUXNET data in this period. *VNP17 Annual GPP validation does not include DNF or DBF canopy, as none of the FLUXNET sites have any year with at least 97% of valid data-days during the period 2012-2017.

Model	Bias (g C m^{-2})	RMSE (g C m^{-2})	ubRMSE (g C m^{-2})	nRMSE (%)	r
MOD17 8-day GPP (C61), 2000-2017	-4.04 day^{-1}	2.69 day^{-1}	2.41 day^{-1}	13.7%	0.79
MOD17 8-day GPP (Update), 2000-2017	-2.77 day^{-1}	2.34 day^{-1}	2.07 day^{-1}	12.0%	0.84
MOD17 8-day GPP (C61), 2012-2017	-2.56 day^{-1}	2.25 day^{-1}	1.82 day^{-1}	11.0%	0.81
MOD17 8-day GPP (Update), 2012-2017	-2.06 day^{-1}	2.16 day^{-1}	1.72 day^{-1}	10.6%	0.82
VNP17 8-day GPP, 2012-2017	-1.75 day^{-1}	2.17 day^{-1}	1.72 day^{-1}	10.6%	0.82
MOD17 Annual GPP (C61)	-266 $year^{-1}$	546 $year^{-1}$	n.a.	14.4%	0.78
MOD17 Annual GPP (Update)	-210 $year^{-1}$	504 $year^{-1}$	n.a.	13.3%	0.80
VNP17 Annual GPP*	-179 $year^{-1}$	523 $year^{-1}$	n.a.	14.0%	0.82
MOD17 Annual NPP (C61)	9 $year^{-1}$	297 $year^{-1}$	n.a.	16.0%	0.49
MOD17 Annual NPP (Update)	-59 $year^{-1}$	261 $year^{-1}$	n.a.	14.1%	0.51
VNP17 Annual NPP	-46 $year^{-1}$	274 $year^{-1}$	n.a.	14.8%	0.49

tion in MF and improvement in OSH and a less-negative overall bias (Tables S13, S14). VNP17 annual NPP estimates, however, are generally less accurate than for MOD17, with particularly high RMSE in ENF, OSH, WSV, and SAV compared to the updated MOD17 (Tables S15, S16). Compared to the statistics in Table 4, when the longer validation record available to MODIS MOD17 is used instead, there is a more substantial improvement over C61 in daily GPP RMSE (2.69 g C m^{-2} day^{-1} for C61 versus 2.34 for the Updated BPLUT) and correlation (0.77 for C61 versus 0.84 for the Updated BPLUT).

Table 5: Root-mean squared difference (RMSD) in annual NPP (g C m^{-2} $year^{-1}$) at FLUXNET sites for each product, compared to independent NPP datasets.

NPP Dataset	C61	MOD17 Update	New VNP17
Global Carbon Budget (2000-2016)	341	272	276
TRENDYv7 Ensemble (2000-2017)	331	327	289
MsTMIP Ensemble (2000-2010)	341	313	n.a.

Compared to the independent NPP estimates at FLUXNET sites from bottom-up and top-down approaches, the updated MOD17 and VNP17 products also show substantial reductions in annual NPP RMSE over C61 (Table 5); again, VNP17 is very similar to MOD17 in this respect (Table S17). When broken out by PFT (Tables S18-S20), it's clear the updated MOD17 has improved skill in annual NPP for some of the most productive PFTs: EBF (C61 mean RMSE= 717 g C m^{-2} $year^{-1}$, updated MOD17 mean RMSE= 548 average across independent datasets), DBF (C61 mean RMSE= 247, updated MOD17 mean RMSE= 195), and CRO (C61 mean RMSE= 304, updated MOD17 mean RMSE= 272). Most importantly, the overall GPP and NPP magnitudes are very similar between VNP17 and the updated MOD17 (Figure 3).

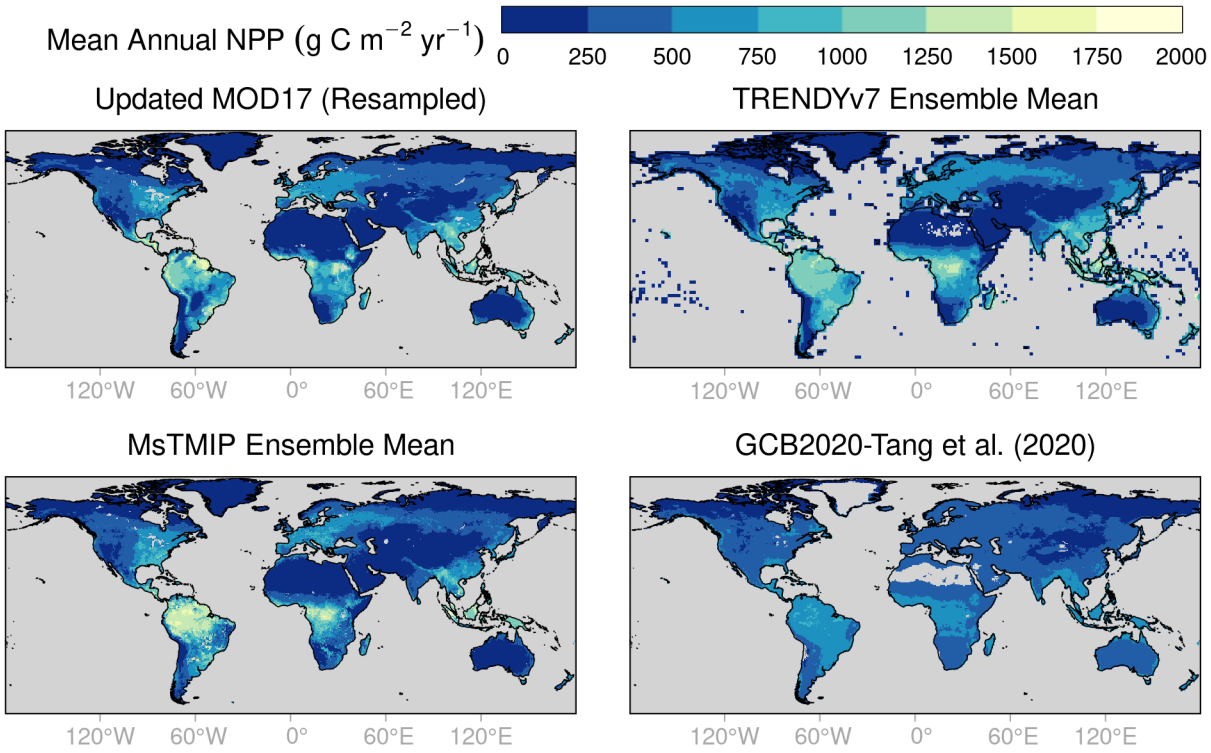

Figure 4: Comparison of mean annual NPP (2000-2010) across four products: the updated MOD17 product, based on the 5-km global simulation and resampled to 0.5-degrees; the TRENDYv7 ensemble mean, at 1-degree resolution; the MsTMIP ensemble mean at 0.5-degrees; and the synthetic NPP estimate from the 2020 Global Carbon Budget and Tang et al. (2020). In the MOD17 image, land areas not simulated in MOD17 (e.g., barren lands) are filled with zero annual NPP.

3.3 Mean, Trend, and Interannual Variability

The mean global GPP flux (2000-2018) in the updated MOD17 product is 127 ±2.8 Pg C year^{-1}, which compares well with that of the TRENDYv7 ensemble mean over the same period (126 ±2.4 Pg C year^{-1}), and is an increase over the estimate from C61 (119 ±2.9 Pg C year^{-1}). If we consider the period 2012-2018, mean global GPP flux from the new VNP17 is quite similar to the updated MOD17 estimate, 129.6 ±1.7 versus 129.7 ±1.7 Pg C year^{-1}, and both are higher than the C61 estimate over the same period (121.6 ±1.6 Pg C year^{-1}). Mean global NPP flux from the new products over 2012-2018 is 58.4-58.5 ±1.1 Pg C year^{-1}, compared to 60.7 ±1.1 in C61 (Table S21).

The updated MOD17 and new VNP17 annual NPP estimates exhibit strong spatial correlation (Figures 4, 5, and S14-S16) with bottom-up estimates from the TRENDYv7 (MOD17 $r = 0.85$, VNP17 $r = 0.86$) and MsTMIP ensembles (MOD17 $r = 0.79$) and also compares well with the top-down, global synthesis of NPP based on the Global Carbon Budget (MOD17 and VNP17 $r = 0.71$). Annual GPP estimates from both products show even stronger spatial correlations with TRENDYv7 (MOD17 and VNP17 $r = 0.91$). In terms of global, interannual NPP and R_A variability, MOD17 compares very well to the TRENDYv7 and MsTMIP ensembles, with the vast majority of the global land domain exhibiting strong, positive correlations (Figure S17); VNP17 IAV is very

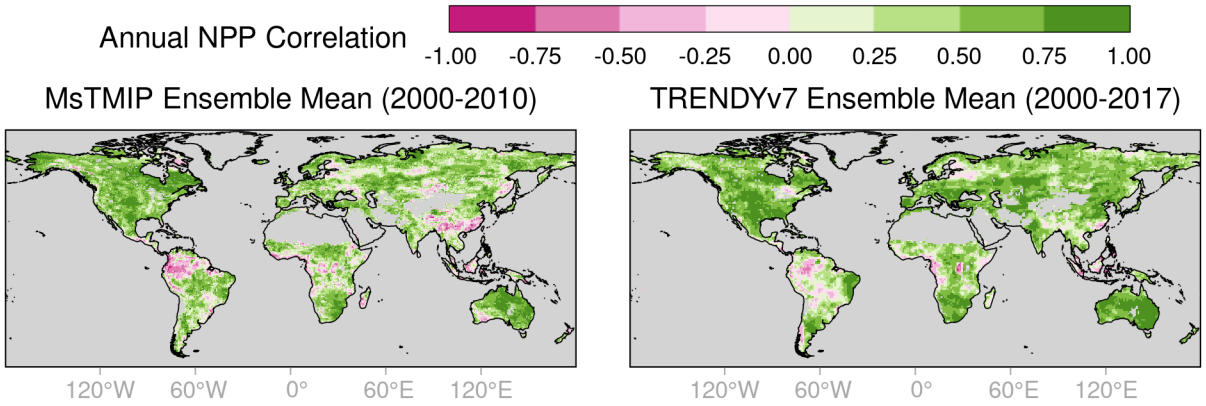

Figure 5: Comparison of interannual correlation in NPP between the updated MOD17 product (based on the 5-km global simulation) and the MsTMIP ensemble mean at 0.5-degrees or the TRENDYv7 ensemble mean at 1-degree resolution. The MOD17 product was resampled to match either product.

similar to that of MOD17 (Figures S18-S21). Negative correlations are found mainly in humid, tropical regions where IAV is low and persistent cloud cover leads to more reliance on fPAR climatology.

We also compared MOD17 C61 and the updated MOD17 to the MsTMIP and TRENDYv7 ensemble means in terms of interannual variation (IAV) in GPP and NPP (Figure 6). All products show a significant, upward trend, based on Theil-Sen median trend estimates. MOD17 C61 and the updated MOD17 display increasing GPP (NPP) trends of 0.45 and 0.47 (0.27 and 0.25) Pg C year^{-2}, respectively, over 2000-2018 compared with 0.41 (0.21) Pg C year^{-2} for the TRENDYv7 ensemble means. Trends are lower in the period 2012-2021; for MOD17 C61, the updated MOD17, and the new VNP17 we find GPP (NPP) trends of 0.38, 0.44, and 0.35 (0.17, 0.13, 0.11) Pg C year^{-2}. For the unified period of 2000-2010 (VNP17 drops out), both MOD17 products show greater IAV in GPP and NPP than MsTMIP and TRENDYv7. The IAV is slightly lower in the updated MOD17 compared to C61, which may reflect the bias-variance trade-off, i.e., a tendency in model calibration toward a narrower range of parameter variability.

3.4 Uncertainty Analysis

The error propagation indicates that a substantial portion of the error in daily and annual GPP estimates comes from error in fPAR (Tables S22, S23); at least 1.0 g C m^{-2} day^{-1} for all PFTs and greater than 1.5 g C m^{-2} day^{-1} for most. Uncertainty in $\varepsilon_{\max}$ is a negligible part of the error in GPP estimates, accounting for less than 0.12 g C m^{-2} day^{-1} in both MOD17 and VNP17, though with the greatest impact on EBF. The magnitude of the fPAR error contribution is generally proportional to the total error by PFT.

The error budget for annual NPP estimates generally corresponds to the sensitivity analysis: uncertainty in SLA is usually the largest source of error in NPP estimates, among free parameters (Tables S24, S25). However, some PFTs have large error contributions from other parameters. Uncertainty in `Q10_froot` is a major contributor to uncertainty in annual NPP for both ENF and EBF and the greatest contributor for CRO. Uncertainty in `froot_mr_base` is a major source of uncertainty in ENF and GRS, while uncertainty in `leaf_mr_base` is a major source for WSV. Uncertainty in SLA has surprisingly little impact on annual NPP estimates in shrublands; no model parameters an-

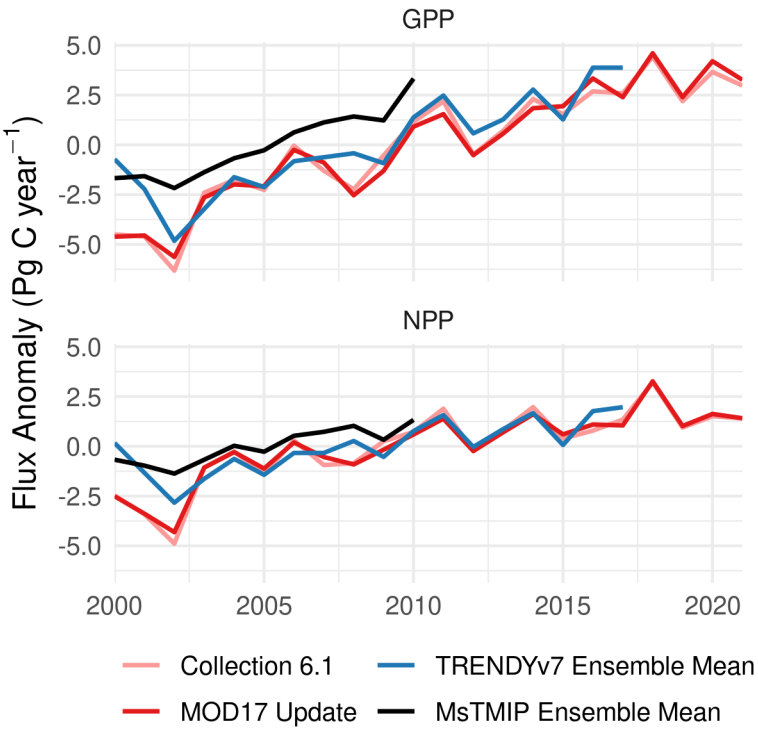

Figure 6: Interannual variation (IAV) in GPP, NPP (annual flux minus interannual mean) for the MOD17 products, shown alongside that of the Multi-Scale Synthesis and Terrestrial Model Intercomparison Project (MsTMIP) and TRENDYv7 ensemble means.

alyzed here contributed major uncertainty to estimates for this PFT, which is found predominantly at high latitudes.

4 Discussion

Prudent use of models requires that they are regularly evaluated, checking both the model predictions (validation) and assumptions (verification) against independent data. MOD17 is a good candidate for continued use in the VIIRS era, but requires validation and verification to contextualize its estimates of ecosystem productivity. Here, independent data on plant traits have been combined with GPP and NPP measurements from flux towers and field surveys to improve both the accuracy and the realism of MOD17.

4.1 Inferring the Optimal Biome Properties

Retrospectively, plant trait data from TRY and the literature allow for a qualitative validation of the MOD17 Collection 6.1 (C61) BPLUT. We found that maximum LUE ($\varepsilon_{\max}$) compared well to the global optimum LUE defined by Madani et al. (2017) for most PFTs, but C61 $\varepsilon_{\max}$ is likely too high for shrubland and savanna, and too low for croplands (Gan et al., 2021). Some studies have suggested higher $\varepsilon_{\max}$ in ENF (Coops et al., 2007) and in shrublands (J. Chen et al., 2014) while others find, as indicated here, it should be lower (Yuan et al., 2014; Madani et al., 2017). Previous generations of the MOD17 BPLUT used a comparatively small number of EC towers (and years of observation) in calibration, which may have led to biased $\varepsilon_{\max}$ estimates. Even among the expanded FLUXNET collection, there are only five CSH tower sites, three of which are within 2 km of one another, and all in regions of high aridity. Overall, lower $\varepsilon_{\max}$ in arid regions is expected (Garbulsky et al., 2010). This may explain the severe decrease in $\varepsilon_{\max}$ for CSH, relative to the C61 BPLUT, which is greater than the corresponding decrease in the better-represented OSH canopy.

While the TRY database indicates that R_M for all tissues should be higher than that of the C61 BPLUT (Figure S9, Table S7), posterior estimates are generally somewhere in the middle. Livewood R_M in C61 is close to that indicated by TRY. SLA in the C61 BPLUT also compares well to prior observations from TRY for evergreen and herbaceous (GRS and CRO) canopies but is too low otherwise. SLA values from TRY may seem high compared to field measurements of SLA (e.g., leaf area per unit leaf dry mass) but are consistent with the range of SLA in C terms (leaf area per unit leaf C), as the TRY database includes many values above 100 m^2 kg C^{-1} (Figure S8). Posterior SLA values also compare very well to a review by Wright and Westoby (2001).

The peculiarities of calibration results for CSH point to a larger issue with MOD17: too many poorly defined PFTs. Given that CSH is a tiny proportion (0.2%) of the global land surface (Madani et al., 2017), it is reasonable to ask whether this class should be combined with OSH in a global "Shrublands" class. This is especially salient in light of evidence that multiple PFTs may be over-differentiated (Yuan et al., 2014) and that environmental filtering (Funk et al., 2017) may lead to more robust plant response than static and somewhat arbitrary functional types (Y. Liu et al., 2021). One practical consequence is that the prior mean for SLA in both OSH and CSH may be too high, as indicated by the low posterior R_M rates in these PFTs.

Our uncertainty analysis of the NPP sub-model largely follows the sensitivity analysis but also emphasizes where parameters could be better constrained. SLA is the most important parameter for NPP estimation in MOD17 as, despite its relatively high certainty (Figure S9, based on prior information from TRY), it has the greatest impact on NPP error. Leaf properties in croplands are particularly uncertain (Figure S22), likely due to the wide variety of global crop types. Future LUE models like MOD17 might ben-

efit from modeling SLA instead of using a fixed value, given the sensitivity of SLA to phenology and environmental conditions (Gong & Gao, 2019; Z. Liu et al., 2022).

4.2 Performance of Global GPP and NPP Products

Relative to C61, model-data fusion lead to improvements in 8-day and annual GPP and annual NPP flux estimates, based on reserved EC tower data, NPP cross-validation with field data, and independent bottom-up and top-down NPP estimates. Since 2012, the persistent negative GPP bias of MOD17 was reduced by at least 0.5 g C m^{-2} day^{-1} and by over 50 g C m^{-2} $year^{-1}$; over a longer record, bias was reduced by more than twice as much (Table 4). These improvements put the updated MOD17 and new VNP17 8-day GPP product on par with other data-driven approaches combining satellite and flux-tower data (Joiner et al., 2018). Global annual GPP flux estimates in the new products (mean 2012-2021 annual GPP flux of 130 ±1.5 Pg C $year^{-1}$) are higher than the estimates of C61 (122 ±1.4 Pg C $year^{-1}$) and other satellite-based estimates but are more in line with oxygen isotope studies (Welp et al., 2011), recent syntheses (J. M. Chen et al., 2012; Piao et al., 2013; Anav et al., 2015) (Figure 7), and bottom-up studies (Madani et al., 2018, 2020), particularly for years since 2012 (Y. Zhang, Xiao, et al., 2017). The new GPP estimates also agree better with TRENDYv7 (128.6 ±1.4 for 2012-2021).

Annual NPP skill (nRMSE) was improved by almost 2 percentage points, a reduction in RMSE of about 30 g C m^{-2} $year^{-1}$. The updated and new products' reduction in global annual NPP flux (58.4-58.6 ±0.9 Pg C $year^{-1}$ for 2012-2021) is more consistent with estimates from the MsTMIP ensemble and combined results from the Global Carbon Budget (2020) and up-scaled soil respiration data (X. Tang et al., 2020); it's also closer than C61 to the estimate from the meta-analysis by Ito (2011) (56.2 ±14.3 Pg C $year^{-1}$). However, the mean annual NPP flux from the TRENDYv7 ensemble mean is higher and closer to the original estimate of MOD17 C61 (Table S21), as is the median of the spread in TRENDYv7 models (Figure 7). The inter-model spread of TRENDYv7 and earlier syntheses (Cramer et al., 1999; Ito, 2011) suggests persistent high uncertainty in any model's representation of terrestrial NPP. It also suggests at least the possibility that the field estimates of NPP used here (Table 3) may not be too large, despite concerns about their reliability and representativeness (Clark et al., 2001; Zhao et al., 2006).

The greatest strength of the MOD17 and VNP17 products is their long period of record, allowing an examination of interannual variability and trends. The strong increase in NPP observed over 2000-2010 (Figure 6) is inconsistent with the report of a reduction in NPP by Zhao and Running (2010). This could be attributed to a difference in the climate drivers used in different versions of MOD17 and the sensitivity of GPP to prevailing weather conditions (Zhao et al., 2006). The 1-km estimates of MOD17 Collection 5.1, from 2000 to 2015, used by Zhao and Running (2010) were driven by NCEP reanalysis data (Kanamitsu et al., 2002) whereas the operational MOD17 (and future VNP17) products use GMAO data; these differences have led to different anomalies in GPP and NPP (Zhao et al., 2005). The uncertainty in LUE models like MOD17 due to climate drivers merits further exploration.

However, even after recalibration, MOD17 and the new VNP17 GPP products still show large negative biases (Table 4). Previous studies have established that MOD17 generally under-estimates GPP (Heinsch et al., 2006; Coops et al., 2007; Propastin et al., 2012; Sjöström et al., 2013; J. Chen et al., 2014; Huang et al., 2018), especially in grasslands (Zhu et al., 2018) and in highly productive regions (Wang & Ogawa, 2017), and that this may be explained by a failure to account for diffuse PAR (Guan et al., 2022). Although it has been suggested that $\varepsilon_{\max}$ should be increased (Wang & Ogawa, 2017; Huang et al., 2018), this model-data fusion is consistent with the previous global analysis of Madani et al. (2017) indicating that $\varepsilon_{\max}$ should be *decreased* for low-productivity shrublands and savannas and *increased* in DBF, MF, and croplands, relative to C61. This

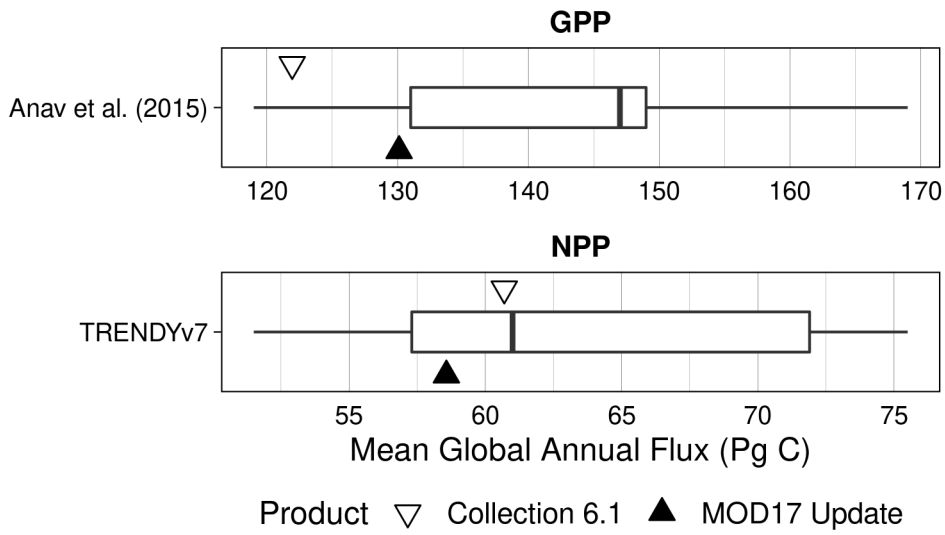

Figure 7: Comparison of MOD17 and VNP17 annual GPP and NPP fluxes with estimates from different models, as synthesized by Anav et al. (2015), for GPP, or represented by the inter-model spread of NPP estimates from the TRENDYv7 ensemble.

may reflect subsequent improvements in the gap-filled MOD15A2HGF fPAR and LAI data. Notably, the updated MOD17 and new VNP17 BPLUT both substantially reduced the negative bias in croplands, which was found to be severe in Collection 6 (Huang et al., 2018).

Annual NPP estimates were improved, over C61, to a greater degree than 8-day or annual GPP estimates (reduction in nRMSE of 0.4-1.0% for GPP but 1.2-1.9% for NPP), likely because there are more parameters to optimize in the NPP model. However, in the updated MOD17 and new VNP17 products, there is a large negative bias in ENF, likely introduced when fine-root R_M was increased to reduce the spuriously high CUE that emerged from global simulations. Leaf R_M and SLA (based on prior information from hundreds of species in TRY) are already both low for this PFT and the cross-validation RMSE is very low (compared to other PFTs); consequently, there are few options to mitigate this bias and avoid unrealistically high CUE values. The simultaneous improvement in annual NPP RMSE but decline in correlation likely reflects the sensitivity of NPP to local conditions that may not be adequately reflected by the 11 PFTs used in MOD17.

Another source of NPP variability is the variation in plant traits (and BPLUT parameters) themselves, over time and along environmental gradients, which is currently not reflected in the MOD17 model structure. SLA has been shown to vary with moisture and nutrient availability (Dwyer et al., 2014), and the spatial and temporal variation in SLA, if accounted for, might reduce estimated NPP magnitudes (Verheijen et al., 2015). It has also been established that fine-root respiration is at least partly coupled with canopy photosynthetic uptake (Högberg et al., 2001; Drake et al., 2008; Lynch et al., 2013).

How do the new products compare to previous generations? It is difficult to compare to previous performance assessments in carbon units (e.g., RMSE) because the quantity depends on the relative productivity of the EC tower sites included; more produc-

tive sites would generally lead to a higher RMSE. For example, the high RMSE of 8-day GPP in croplands (Table 13) exaggerates the overall RMSE estimated here (Table 4). As an alternative, normalized quantities have been used inconsistently, and while "relative error" (Heinsch et al., 2006) is a common choice, it is also highly sensitive to very low EC tower flux magnitudes. We suggest that only normalized RMSE, relative to the reported range of tower observations, be compared to other assessments. These would suggest that C61 is an improvement over earlier versions and the updated MOD17 BPLUT a further improvement. R. Tang et al. (2015), for example, find Collection 6 annual GPP biases generally twice as large as estimated here for C61, and nRMSE values significantly higher as well, based on less than half as many EC tower sites. Sjöström et al. (2013) found an overall Collection 5.1 GPP RMSE, compared to flux towers in Africa, of 2.58 g C m^{-1} d^{-1}, higher than our estimate of 2.25 g C m^{-1} d^{-1} for C61. The performance is sensitive to the driver data used and is generally much better when tower-observed surface meteorology is used (Coops et al., 2007; J. Chen et al., 2014), though some have found otherwise (Wang & Ogawa, 2017).

Error propagation indicates that error in MOD17 and VNP17 GPP estimates is primarily due to error in fPAR retrievals, as in multiple previous studies (Propastin et al., 2012; Fu et al., 2017; Wang & Ogawa, 2017). Given the low sensitivity of these models to environmental scalars, this suggests that dynamic changes in MOD17 modeled GPP are largely a function of changes in canopy extent and vigor, conveyed by changes in fPAR. This feature of LUE models has been an advantage during the EOS era and allowed models like MOD17 to capture trends in the land carbon sink (Figure 6) that are otherwise missed by purely data-driven approaches like FLUXCOM (Yang et al., 2022). And yet, given the modest improvement in the new MOD17 product compared to C61, it's also apparent that the accuracy of these global LUE models is strongly tied to the quality of input datasets, in addition to uncertainty in model parameters and model structure.

5 Conclusion

We combined prior information on plant productivity and respiration traits with eddy covariance estimates of GPP and field estimates of NPP for the recalibration of MOD17, the first model to provide global, continuous, weekly estimates of ecosystem productivity. This effort culminated in the final reprocessing of MODIS MOD17 and the development of new VNP17 GPP and NPP products based on VIIRS data. Relative to the current MODIS C61 MOD17 data, the updated MOD17 parameters substantially reduce the negative bias in 8-day GPP, by more than 1.2 g C m^{-2} day^{-1}; the RMSE in annual GPP was reduced by 42 g C m^{-2} $year^{-1}$ and RMSE in annual NPP was reduced by 36 g C m^{-2} $year^{-1}$ while maintaining or improving global correlations in the spatial pattern of GPP and NPP fluxes.

The combined records of the updated MOD17 and new VNP17 products enable weekly-to-annual terrestrial productivity estimates to be continued through 2030 and beyond. The updated estimates of mean global GPP and NPP for 2012-2021, 130.1 $\pm$1.6 and 58.6 $\pm$0.9 (respectively) agree very well with other bottom-up estimates. The long, extant record of MOD17 and VNP17 indicate that terrestrial productivity is increasing over recent decades (2000-2018), with GPP increasing annually by 0.47 Pg C $year^{-2}$ and NPP by 0.25 Pg C $year^{-2}$. These trends are supported by independent, bottom-up estimates and all the models examined here do indicate that the rate of increase in GPP and NPP may be slowing down in recent years.

Open Research Section

The 5-km global simulation outputs (for both MOD17 and the new VNP17) and the driver data required to run, calibrate, and validate MOD17 at FLUXNET sites (with the exception of tower fluxes, which we are not licensed to reproduce) are available at

697 <https://doi.org/10.5281/zenodo.7682806>. The repository of the MOD17 algo-
698 rithm's Python and C source code is available on GitHub at <https://github.com/arthur-e/MOD17>.

699 **Acknowledgments**
700 This study was supported by a grant from NASA (NNH20ZDA001N-SNPPSP).

References

Anav, A., Friedlingstein, P., Beer, C., Ciais, P., Harper, A., Jones, C., … Zhao, M. (2015, September). Spatiotemporal patterns of terrestrial gross primary production: A review. *Reviews of Geophysics*, *53*(3), 785–818. Retrieved from http://doi.wiley.com/10.1002/2015RG000483 doi: 10.1002/2015RG000483

Atkin, O. K., Edwards, E. J., & Loveys, B. R. (2000, July). Response of root respiration to changes in temperature and its relevance to global warming. *New Phytologist*, *147*(1), 141–154. Retrieved from http://doi.wiley.com/10.1046/j.1469-8137.2000.00683.x doi: 10.1046/j.1469-8137.2000.00683.x

Bahn, M., Knapp, M., Garajova, Z., Pfahringer, N., & Cernusca, A. (2006, June). Root respiration in temperate mountain grasslands differing in land use. *Global Change Biology*, *12*(6), 995–1006. Retrieved 2022-06-27, from https://onlinelibrary.wiley.com/doi/10.1111/j.1365-2486.2006.01144.x doi: 10.1111/j.1365-2486.2006.01144.x

Balch, J. K., Bradley, B. A., Abatzoglou, J. T., Nagy, R. C., Fusco, E. J., & Mahood, A. L. (2017, March). Human-started wildfires expand the fire niche across the United States. *Proceedings of the National Academy of Sciences*, *114*(11), 2946–2951. Retrieved 2022-07-29, from https://pnas.org/doi/full/10.1073/pnas.1617394114 doi: 10.1073/pnas.1617394114

Baldocchi, D. (2008). 'Breathing' of the terrestrial biosphere: lessons learned from a global network of carbon dioxide flux measurement systems. *Australian Journal of Botany*, *56*(1), 1. Retrieved from http://www.publish.csiro.au/?paper=BT07151 doi: 10.1071/BT07151

Baldocchi, D., Falge, E., Gu, L., Olson, R., Hollinger, D., Running, S., … Wofsy, S. (2001, November). FLUXNET: A new tool to study the temporal and spatial variability of ecosystem–scale carbon dioxide, water vapor, and energy flux densities. *Bulletin of the American Meteorological Society*, *82*(11), 2415–2434. Retrieved from http://journals.ametsoc.org/doi/10.1175/1520-0477(2001)082%3C2415:FANTTS%3E2.3.CO;2 (ISBN: 0003-0007) doi: 10.1175/1520-0477(2001)082<2415:FANTTS>2.3.CO;2

Barrett, D. J. (2012). NPP Multi-Biome: VAST Calibration Data, 1965-1998, R1. Retrieved from http://daac.ornl.gov/cgi-bin/dsviewer.pl?ds_id=576 (Publisher: ORNL Distributed Active Archive Center) doi: 10.3334/ORNLDAAC/576

Bolstad, P. V., Davis, K. J., Martin, J., Cook, B. D., & Wang, W. (2004, May). Component and whole-system respiration fluxes in northern deciduous forests. *Tree Physiology*, *24*(5), 493–504. Retrieved 2022-06-24, from https://academic.oup.com/treephys/article-lookup/doi/10.1093/treephys/24.5.493 doi: 10.1093/treephys/24.5.493

Bridgewater, S., Ibáñez, A., Ratter, J. A., & Furley, P. (2002, November). Vegetation classification and floristics of the savannas and associated wetlands of the Rio Bravo Conservation and Management Area, Belize. *Edinburgh Journal of Botany*, *59*(3), 421–442. Retrieved 2022-05-06, from https://journals.rbge.org.uk/ejb/article/view/1265 doi: 10.1017/S0960428602000252

Burton, A. J., Melillo, J. M., & Frey, S. D. (2008). Adjustment of forest ecosystem root respiration as temperature warms. *Journal of Integrative Plant Biology*, *50*(11), 1467–1483. doi: 10.1111/j.1744-7909.2008.00750.x

Campioli, M., Vicca, S., Luyssaert, S., Bilcke, J., Ceschia, E., Chapin III, F. S., … Janssens, I. A. (2015, November). Biomass production efficiency controlled by management in temperate and boreal ecosystems. *Nature Geoscience*, *8*(11), 843–846. Retrieved 2022-07-18, from http://www.nature.com/articles/ngeo2553 doi: 10.1038/ngeo2553

Chen, J., Zhang, H., Liu, Z., Che, M., & Chen, B. (2014, April). Evaluating pa-

rameter adjustment in the MODIS gross primary production algorithm based on eddy covariance tower measurements. *Remote Sensing*, *6*(4), 3321–3348. Retrieved 2022-07-20, from http://www.mdpi.com/2072-4292/6/4/3321 doi: 10.3390/rs6043321

Chen, J. M., Mo, G., Pisek, J., Liu, J., Deng, F., Ishizawa, M., & Chan, D. (2012, March). Effects of foliage clumping on the estimation of global terrestrial gross primary productivity. *Global Biogeochemical Cycles*, *26*(1), n/a–n/a. Retrieved 2023-01-29, from http://doi.wiley.com/10.1029/2010GB003996 doi: 10.1029/2010GB003996

Chu, H., Luo, X., Ouyang, Z., Chan, W. S., Dengel, S., Biraud, S. C., … Zona, D. (2021). Representativeness of eddy-covariance flux footprints for areas surrounding AmeriFlux sites. *Agricultural and Forest Meteorology*, *301-302*(February). doi: 10.1016/j.agrformet.2021.108350

Clark, D. A., Brown, S., Kicklighter, D. W., Chambers, J. Q., Thomlinson, J. R., & Ni, J. (2001, April). Measuring net primary production in forests: Concepts and field methods. *Ecological Applications*, *11*(2), 356–370. Retrieved 2023-02-02, from http://doi.wiley.com/10.1890/1051-0761(2001)011[0356:MNPPIF]2.0.CO;2 doi: 10.1890/1051-0761(2001)011[0356:MNPPIF]2.0.CO;2

Collalti, A., & Prentice, I. C. (2019). Is NPP proportional to GPP? Waring's hypothesis 20 years on. *Tree Physiology*, *39*(8), 1473–1483. doi: 10.1093/treephys/tpz034

Coops, N. C., Jassal, R. S., Leuning, R., Black, A. T., & Morgenstern, K. (2007, December). Incorporation of a soil water modifier into MODIS predictions of temperate Douglas-fir gross primary productivity: Initial model development. *Agricultural and Forest Meteorology*, *147*(3-4), 99–109. Retrieved 2022-07-20, from https://linkinghub.elsevier.com/retrieve/pii/S0168192307001700 doi: 10.1016/j.agrformet.2007.07.001

Cramer, W., Kicklighter, D. W., Bondeau, A., Iii, B. M., Churkina, G., Nemry, B., … Intercomparison, T. P. O. T. P. (1999, April). Comparing global models of terrestrial net primary productivity (NPP): overview and key results. *Global Change Biology*, *5*(S1), 1–15. Retrieved 2023-02-02, from https://onlinelibrary.wiley.com/doi/10.1046/j.1365-2486.1999.00009.x doi: 10.1046/j.1365-2486.1999.00009.x

Damesin, C., Ceschia, E., Le Goff, N., Ottorini, J. M., & Dufrêne, E. (2002, January). Stem and branch respiration of beech: from tree measurements to estimations at the stand level. *New Phytologist*, *153*(1), 159–172. Retrieved 2022-06-24, from http://doi.wiley.com/10.1046/j.0028-646X.2001.00296.x doi: 10.1046/j.0028-646X.2001.00296.x

DeAngelis, D. L., Gardner, R. H., & Shugart, H. H. (2012). NPP Multi-Biome: Global IBP Woodlands Data, 1955-1975, R1. Retrieved from http://daac.ornl.gov/cgi-bin/dsviewer.pl?ds_id=198 (Publisher: ORNL Distributed Active Archive Center) doi: 10.3334/ORNLDAAC/198

Dennisenko, E. A., Brovkin, V., & Cramer, W. P. (2012). NPP Multi-Biome: PIK Data for Northern Eurasia, 1940-1988 (Based on Bazilevich), R1. Retrieved from http://daac.ornl.gov/cgi-bin/dsviewer.pl?ds_id=575 (Publisher: ORNL Distributed Active Archive Center) doi: 10.3334/ORNLDAAC/575

Desrochers, A., Landhausser, S. M., & Lieffers, V. J. (2002, July). Coarse and fine root respiration in aspen (Populus tremuloides). *Tree Physiology*, *22*(10), 725–732. Retrieved 2022-06-27, from https://academic.oup.com/treephys/article-lookup/doi/10.1093/treephys/22.10.725 doi: 10.1093/treephys/22.10.725

Drake, J. E., Stoy, P. C., Jackson, R. B., & DeLucia, E. H. (2008, November). Fine-root respiration in a loblolly pine (Pinus taeda L.) forest exposed to elevated CO2 and N fertilization. *Plant, Cell & Environment*, *31*(11), 1663–1672. Retrieved 2022-07-13, from https://onlinelibrary.wiley.com/doi/10.1111/

j.1365-3040.2008.01869.x doi: 10.1111/j.1365-3040.2008.01869.x

Dwyer, J. M., Hobbs, R. J., & Mayfield, M. M. (2014, February). Specific leaf area responses to environmental gradients through space and time. *Ecology*, *95*(2), 399–410. Retrieved 2022-06-03, from http://doi.wiley.com/10.1890/13-0412.1 doi: 10.1890/13-0412.1

Díaz, S., Kattge, J., Cornelissen, J. H. C., Wright, I. J., Lavorel, S., Dray, S., … Gorné, L. D. (2016, January). The global spectrum of plant form and function. *Nature*, *529*(7585), 167–171. Retrieved from http://www.nature.com/articles/nature16489 doi: 10.1038/nature16489

Erb, K.-H., Kastner, T., Plutzar, C., Bais, A. L. S., Carvalhais, N., Fetzel, T., … Luyssaert, S. (2018, January). Unexpectedly large impact of forest management and grazing on global vegetation biomass. *Nature*, *553*(7686), 73–76. Retrieved 2022-07-29, from http://www.nature.com/articles/nature25138 doi: 10.1038/nature25138

Esser, G. (2013). NPP Multi-Biome: Global Osnabruck Data, 1937-1981, R1. Retrieved from http://daac.ornl.gov/cgi-bin/dsviewer.pl?ds_id=214 (Publisher: ORNL Distributed Active Archive Center) doi: 10.3334/ORNLDAAC/214

FAO. (2010). *Appendix 4: Alphabetical List of Crops with Botanical Name and Crop Code* (Tech. Rep.). Retrieved 2022-06-17, from https://www.fao.org/fileadmin/templates/ess/documents/world_census_of_agriculture/appendix4_r7.pdf

Friedl, M., & Sulla-Menashe, D. (2019). MCD12Q1 MODIS/Terra+Aqua Land Cover Type Yearly L3 Global 500m SIN Grid V006 [Data set]. doi: https://doi.org/10.5067/MODIS/MCD12Q1.006

Friedlingstein, P., O'Sullivan, M., Jones, M. W., Andrew, R. M., Hauck, J., Olsen, A., … Zaehle, S. (2020, December). Global Carbon Budget 2020. *Earth System Science Data*, *12*(4), 3269–3340. Retrieved from https://essd.copernicus.org/articles/12/3269/2020/ doi: 10.5194/essd-12-3269-2020

Fu, G., Zhang, J., Shen, Z.-X., Shi, P.-L., He, Y.-T., & Zhang, X.-Z. (2017, August). Validation of collection of 6 MODIS/Terra and MODIS/Aqua gross primary production in an alpine meadow of the Northern Tibetan Plateau. *International Journal of Remote Sensing*, *38*(16), 4517–4534. Retrieved 2022-07-14, from https://www.tandfonline.com/doi/full/10.1080/01431161.2017.1323283 doi: 10.1080/01431161.2017.1323283

Funk, J. L., Larson, J. E., Ames, G. M., Butterfield, B. J., Cavender-Bares, J., Firn, J., … Wright, J. (2017). Revisiting the Holy Grail: Using plant functional traits to understand ecological processes. *Biological Reviews*, *92*(2), 1156–1173. (ISBN: 1714744795) doi: 10.1111/brv.12275

Gan, R., Zhang, L., Yang, Y., Wang, E., Woodgate, W., Zhang, Y., … Yu, Q. (2021, October). Estimating ecosystem maximum light use efficiency based on the water use efficiency principle. *Environmental Research Letters*, *16*(10), 104032. Retrieved 2022-07-20, from https://iopscience.iop.org/article/10.1088/1748-9326/ac263b doi: 10.1088/1748-9326/ac263b

Garbulsky, M. F., Peñuelas, J., Papale, D., Ardö, J., Goulden, M. L., Kiely, G., … Filella, I. (2010, March). Patterns and controls of the variability of radiation use efficiency and primary productivity across terrestrial ecosystems. *Global Ecology and Biogeography*, *19*(2), 253–267. Retrieved from http://doi.wiley.com/10.1111/j.1466-8238.2009.00504.x doi: 10.1111/j.1466-8238.2009.00504.x

Gelaro, R., McCarty, W., Suárez, M. J., Todling, R., Molod, A., Takacs, L., … Zhao, B. (2017, July). The Modern-Era Retrospective Analysis for Research and Applications, Version 2 (MERRA-2). *Journal of Climate*, *30*(14), 5419–5454. Retrieved from http://journals.ametsoc.org/doi/10.1175/JCLI-D-16-0758.1 doi: 10.1175/JCLI-D-16-0758.1

Gong, H., & Gao, J. (2019, October). Soil and climatic drivers of plant SLA (specific leaf area). *Global Ecology and Conservation*, *20*, e00696. Retrieved 2022-07-20, from https://linkinghub.elsevier.com/retrieve/pii/S2351989419302665 doi: 10.1016/j.gecco.2019.e00696

Gower, S. T., Krankina, O. N., Olson, R. J., Apps, M. J., Linder, S., & Wang, C. (2012). NPP Boreal Forest: Consistent Worldwide Site Estimates, 1965-1995, R1. Retrieved from http://daac.ornl.gov/cgi-bin/dsviewer.pl?ds_id=611 (Publisher: ORNL Distributed Active Archive Center) doi: 10.3334/ORNLDAAC/611

Gower, S. T., & Richards, J. H. (1990, December). Larches: Deciduous Conifers in an Evergreen World. *BioScience*, *40*(11), 818–826. Retrieved 2022-12-19, from https://academic.oup.com/bioscience/article-lookup/doi/10.2307/1311484 doi: 10.2307/1311484

Guan, X., Chen, J. M., Shen, H., Xie, X., & Tan, J. (2022, February). Comparison of big-leaf and two-leaf light use efficiency models for GPP simulation after considering a radiation scalar. *Agricultural and Forest Meteorology*, *313*, 108761. Retrieved 2022-07-20, from https://linkinghub.elsevier.com/retrieve/pii/S0168192321004470 doi: 10.1016/j.agrformet.2021.108761

Heinsch, F. A., Zhao, M., Running, S. W., Kimball, J. S., Nemani, R. R., Davis, K. J., … Flanagan, L. B. (2006, July). Evaluation of remote sensing based terrestrial productivity from MODIS using regional tower eddy flux network observations. *IEEE Transactions on Geoscience and Remote Sensing*, *44*(7), 1908–1923. Retrieved from http://ieeexplore.ieee.org/document/1645290/ doi: 10.1109/TGRS.2005.853936

Herman, J., & Usher, W. (2017, January). SALib: An open-source Python library for Sensitivity Analysis. *The Journal of Open Source Software*, *2*(9), 97. Retrieved 2022-06-18, from http://joss.theoj.org/papers/10.21105/joss.00097 doi: 10.21105/joss.00097

Huang, X., Ma, M., Wang, X., Tang, X., & Yang, H. (2018, December). The uncertainty analysis of the MODIS GPP product in global maize croplands. *Frontiers of Earth Science*, *12*(4), 739–749. Retrieved 2023-01-25, from http://link.springer.com/10.1007/s11707-018-0716-x doi: 10.1007/s11707-018-0716-x

Huntzinger, D. N., Schwalm, C., Michalak, A. M., Schaefer, K., King, A. W., Wei, Y., … Zhu, Q. (2013, December). The North American Carbon Program Multi-Scale Synthesis and Terrestrial Model Intercomparison Project – Part 1: Overview and experimental design. *Geoscientific Model Development*, *6*(6), 2121–2133. Retrieved 2014-01-23, from http://www.geosci-model-dev.net/6/2121/2013/ doi: 10.5194/gmd-6-2121-2013

Högberg, P., Nordgren, A., Buchmann, N., Taylor, A. F. S., Ekblad, A., Högberg, M. N., … Read, D. J. (2001, June). Large-scale forest girdling shows that current photosynthesis drives soil respiration. *Nature*, *411*(6839), 789–792. Retrieved from http://www.nature.com/articles/35081058 doi: 10.1038/35081058

Ito, A. (2011, October). A historical meta-analysis of global terrestrial net primary productivity: are estimates converging?: A HISTORICAL META-ANALYSIS OF GLOBAL LAND NPP. *Global Change Biology*, *17*(10), 3161–3175. Retrieved 2023-02-02, from https://onlinelibrary.wiley.com/doi/10.1111/j.1365-2486.2011.02450.x doi: 10.1111/j.1365-2486.2011.02450.x

Iversen, C. M., McCormack, M. L., Powell, A. S., Blackwood, C. B., Freschet, G. T., Kattge, J., … Violle, C. (2017, July). A global Fine-Root Ecology Database to address below-ground challenges in plant ecology. *New Phytologist*, *215*(1), 15–26. Retrieved 2022-05-17, from https://onlinelibrary.wiley.com/doi/10.1111/nph.14486 doi: 10.1111/nph.14486

Iwanaga, T., Usher, W., & Herman, J. (2022). Toward SALib 2.0: Advancing the accessibility and interpretability of global sensitivity analyses. *Socio-Environmental Systems Modeling*, *4*. doi: https://doi.org/10.18174/sesmo.18155

Ji, Y., Zhou, G., Luo, T., Dan, Y., Zhou, L., & Lv, X. (2020, December). Variation of net primary productivity and its drivers in China's forests during 2000–2018. *Forest Ecosystems*, *7*(1), 15. Retrieved 2022-08-03, from https://forestecosyst.springeropen.com/articles/10.1186/s40663-020-00229-0 doi: 10.1186/s40663-020-00229-0

Joiner, J., Yoshida, Y., Zhang, Y., Duveiller, G., Jung, M., Lyapustin, A., … Tucker, C. (2018, August). Estimation of Terrestrial Global Gross Primary Production (GPP) with Satellite Data-Driven Models and Eddy Covariance Flux Data. *Remote Sensing*, *10*(9), 1346. Retrieved 2023-01-29, from http://www.mdpi.com/2072-4292/10/9/1346 doi: 10.3390/rs10091346

Jones, L. A., Kimball, J. S., Reichle, R. H., Madani, N., Glassy, J., Ardizzone, J. V., … Scott, R. L. (2017). The SMAP Level 4 Carbon Product for Monitoring Ecosystem Land-Atmosphere CO2 Exchange. *IEEE Transactions on Geoscience and Remote Sensing*, *55*(11), 6517–6532. (ISBN: 9781509033324) doi: 10.1109/TGRS.2017.2729343

Jones, M. O., Running, S. W., Kimball, J. S., Robinson, N. P., & Allred, B. W. (2020, December). Terrestrial primary productivity indicators for inclusion in the National Climate Indicators System. *Climatic Change*, *163*(4), 1855–1868. Retrieved from http://link.springer.com/10.1007/s10584-018-2155-9 doi: 10.1007/s10584-018-2155-9

Jung, M., Schwalm, C., Migliavacca, M., Walther, S., Camps-Valls, G., Koirala, S., … Reichstein, M. (2020). Scaling carbon fluxes from eddy covariance sites to globe: Synthesis and evaluation of the FLUXCOM approach. *Biogeosciences*, *17*(5), 1343–1365. doi: 10.5194/bg-17-1343-2020

Justice, C., Townshend, J. R. G., Vermote, E. F., Masuoka, E., Wolfe, R., Saleous, N., … Morisette, J. T. (2002, November). An overview of MODIS Land data processing and product status. *Remote Sensing of Environment*, *83*(1-2), 3–15. Retrieved 2022-07-04, from https://linkinghub.elsevier.com/retrieve/pii/S0034425702000846 doi: 10.1016/S0034-4257(02)00084-6

Kanamitsu, M., Ebisuzaki, W., Woollen, J., Yang, S.-K., Hnilo, J. J., Fiorino, M., & Potter, G. L. (2002, November). NCEP–DOE AMIP-II Reanalysis (R-2). *Bulletin of the American Meteorological Society*, *83*(11), 1631–1644. Retrieved 2023-02-14, from https://journals.ametsoc.org/doi/10.1175/BAMS-83-11-1631 doi: 10.1175/BAMS-83-11-1631

Kattge, J., Bönisch, G., Díaz, S., Lavorel, S., Prentice, I. C., Leadley, P., … ... (2020). TRY plant trait database – enhanced coverage and open access. *Global Change Biology*, *26*(1), 119–188. doi: 10.1111/gcb.14904

Kicklighter, D. W. (2012). NPP Multi-Biome: TEM Calibration Data, 1992, R1. Retrieved from http://daac.ornl.gov/cgi-bin/dsviewer.pl?ds_id=471 (Publisher: ORNL Distributed Active Archive Center) doi: 10.3334/ORNLDAAC/471

Kicklighter, D. W., Bruno, M., DZönges, S., Esser, G., Heimann, M., Helfrich, J., … Würth, G. (1999, January). A first-order analysis of the potential role of CO2 fertilization to affect the global carbon budget: A comparison of four terrestrial biosphere models. *Tellus B: Chemical and Physical Meteorology*, *51*(2), 343–366. Retrieved from https://www.tandfonline.com/doi/full/10.3402/tellusb.v51i2.16303 doi: 10.3402/tellusb.v51i2.16303

Kloeppel, B. D., Treichel, I. W., Kharuk, S., & Gower, S. T. (1998, April). Foliar carbon isotope discrimination in Larix species and sympatric evergreen conifers: a global comparison. *Oecologia*, *114*(2), 153–159. Retrieved 2022-12-19, from http://link.springer.com/10.1007/s004420050431 doi:

10.1007/s004420050431

Kushida, K., Isaev, A. P., Maximov, T. C., Takao, G., & Fukuda, M. (2007, April). Remote sensing of upper canopy leaf area index and forest floor vegetation cover as indicators of net primary productivity in a Siberian larch forest. *Journal of Geophysical Research*, *112*(G2), G02003. Retrieved 2022-07-21, from http://doi.wiley.com/10.1029/2006JG000269 doi: 10.1029/2006JG000269

Lavigne, M. B., Franklin, S. E., & Hunt, E. R. (1996, August). Estimating stem maintenance respiration rates of dissimilar balsam fir stands. *Tree Physiology*, *16*(8), 687–695. Retrieved 2022-06-24, from https://academic.oup.com/treephys/article-lookup/doi/10.1093/treephys/16.8.687 doi: 10.1093/treephys/16.8.687

Le Quéré, C., Barbero, L., Hauck, J., Andrew, R. M., Canadell, J. G., Sitch, S., & Korsbakken, J. I. (2018). Global Carbon Budget 2018. *Earth System Science Data*, *10*, 2141–2194.

Liu, Y., Holtzman, N. M., & Konings, A. G. (2021, May). Global ecosystem-scale plant hydraulic traits retrieved using model–data fusion. *Hydrology and Earth System Sciences*, *25*(5), 2399–2417. Retrieved 2022-09-26, from https://hess.copernicus.org/articles/25/2399/2021/ doi: 10.5194/hess-25-2399-2021

Liu, Z., Zhao, M., Zhang, H., Ren, T., Liu, C., & He, N. (2022, November). Divergent response and adaptation of specific leaf area to environmental change at different spatio-temporal scales jointly improve plant survival. *Global Change Biology*, gcb.16518. Retrieved 2022-12-18, from https://onlinelibrary.wiley.com/doi/10.1111/gcb.16518 doi: 10.1111/gcb.16518

Luo, Z., Xiao, L., Wang, G., Chang, J., Chen, Y., Guo, X., … Jia, S. (2021, May). *Depth distribution of belowground net primary production across global biomes* (preprint). In Review. Retrieved 2022-07-28, from https://www.researchsquare.com/article/rs-65178/v3 doi: 10.21203/rs.3.rs-65178/v3

Lynch, D. J., Matamala, R., Iversen, C. M., Norby, R. J., & Gonzalez-Meler, M. A. (2013, July). Stored carbon partly fuels fine-root respiration but is not used for production of new fine roots. *New Phytologist*, *199*(2), 420–430. Retrieved 2022-07-15, from https://onlinelibrary.wiley.com/doi/10.1111/nph.12290 doi: 10.1111/nph.12290

Madani, N., Kimball, J. S., Ballantyne, A. P., Affleck, D. L. R., van Bodegom, P. M., Reich, P. B., … Running, S. W. (2018, February). Future global productivity will be affected by plant trait response to climate. *Scientific Reports*, *8*(1), 2870. Retrieved 2023-01-29, from https://www.nature.com/articles/s41598-018-21172-9 doi: 10.1038/s41598-018-21172-9

Madani, N., Kimball, J. S., & Running, S. W. (2017). Improving global gross primary productivity estimates by computing optimum light use efficiencies using flux tower data. *Journal of Geophysical Research: Biogeosciences*, *122*(11), 2939–2951. doi: 10.1002/2017JG004142

Madani, N., Parazoo, N. C., Kimball, J. S., Ballantyne, A. P., Reichle, R. H., Maneta, M., … Tagesson, T. (2020, December). Recent Amplified Global Gross Primary Productivity Due to Temperature Increase Is Offset by Reduced Productivity Due to Water Constraints. *AGU Advances*, *1*(4). Retrieved 2023-01-29, from https://onlinelibrary.wiley.com/doi/10.1029/2020AV000180 doi: 10.1029/2020AV000180

Malhi, Y. (2012, January). The productivity, metabolism and carbon cycle of tropical forest vegetation: Carbon cycle of tropical forests. *Journal of Ecology*, *100*(1), 65–75. Retrieved 2023-02-14, from https://onlinelibrary.wiley.com/doi/10.1111/j.1365-2745.2011.01916.x doi:

10.1111/j.1365-2745.2011.01916.x

Meek, D. W., Hatfield, J. L., Howell, T. A., Idso, S. B., & Reginato, R. J. (1984, November). A Generalized Relationship between Photosynthetically Active Radiation and Solar Radiation. *Agronomy Journal*, *76*(6), 939–945. Retrieved 2022-09-19, from https://onlinelibrary.wiley.com/doi/10.2134/agronj1984.00021962007600060018x doi: 10.2134/agronj1984.00021962007600060018x

Murphy, R. E., Barnes, W. L., Lyapustin, A. I., Privette, J., Welsch, C., DeLuccia, F., … Kealy, P. S. M. (2001). Using VIIRS to provide data continuity with MODIS. In *IGARSS 2001. Scanning the Present and Resolving the Future. Proceedings. IEEE 2001 International Geoscience and Remote Sensing Symposium (Cat. No.01CH37217)* (Vol. 3, pp. 1212–1214). Sydney, NSW, Australia: IEEE. Retrieved 2022-07-07, from http://ieeexplore.ieee.org/document/976795/ doi: 10.1109/IGARSS.2001.976795

Myneni, R. B. (2018). *VIIRS Leaf Area Index (LAI) and Fraction of Photosynthetically Active Radiation Absorbed by Vegetation (FPAR) User Guide* (Tech. Rep.). Department of Earth and Environment, Boston University. Retrieved 2022-07-22, from https://lpdaac.usgs.gov/documents/126/VNP15_User_Guide.pdf

Myneni, R. B., Knyazikhin, Y., & Park, T. (2015). *MODIS/Terra+Aqua Leaf Area Index/FPAR 8-day L4 Global 500m SIN Grid V006 [Data set].* Retrieved 2021-07-02, from https://doi.org/10.5067/MODIS/MOD15A2H.061 doi: https://doi.org/10.5067/MODIS/MOD15A2H.061

Olson, R. J., Scurlock, J. M. O., Prince, S. D., Zheng, D. L., & Johnson, K. R. (2013). NPP Multi-Biome: Global Primary Production Data Initiative Products, R2. Retrieved from http://daac.ornl.gov/cgi-bin/dsviewer.pl?ds_id=617 (Publisher: ORNL Distributed Active Archive Center) doi: 10.3334/ORNLDAAC/617

Olson, R. J., Scurlock, J. M. O., Walker, T. R., Hook, L. A., Curtis, C. N., & Cook, R. B. (2017). NPP Multi-Biome: Summary Data from Intensive Studies at 125 Sites, 1936-2006. Retrieved from https://daac.ornl.gov/cgi-bin/dsviewer.pl?ds_id=1352 (Publisher: ORNL Distributed Active Archive Center) doi: 10.3334/ORNLDAAC/1352

Piao, S., Sitch, S., Ciais, P., Friedlingstein, P., Peylin, P., Wang, X., … Zeng, N. (2013, July). Evaluation of terrestrial carbon cycle models for their response to climate variability and to CO $_2$ trends. *Global Change Biology*, *19*(7), 2117–2132. Retrieved 2023-01-29, from https://onlinelibrary.wiley.com/doi/10.1111/gcb.12187 doi: 10.1111/gcb.12187

Poorter, H., Niinemets, ., Poorter, L., Wright, I. J., & Villar, R. (2009, May). Causes and consequences of variation in leaf mass per area (LMA): a meta-analysis. *New Phytologist*, *182*(3), 565–588. Retrieved 2022-06-21, from https://onlinelibrary.wiley.com/doi/10.1111/j.1469-8137.2009.02830.x doi: 10.1111/j.1469-8137.2009.02830.x

Propastin, P., Ibrom, A., Knohl, A., & Erasmi, S. (2012, June). Effects of canopy photosynthesis saturation on the estimation of gross primary productivity from MODIS data in a tropical forest. *Remote Sensing of Environment*, *121*, 252–260. Retrieved 2022-07-04, from https://linkinghub.elsevier.com/retrieve/pii/S0034425712000892 doi: 10.1016/j.rse.2012.02.005

Reich, P. B., Ellsworth, D. S., & Walters, M. B. (1998, December). Leaf structure (specific leaf area) modulates photosynthesis-nitrogen relations: evidence from within and across species and functional groups: SLA regulates photosynthetic nitrogen use. *Functional Ecology*, *12*(6), 948–958. Retrieved 2022-06-21, from http://doi.wiley.com/10.1046/j.1365-2435.1998.00274.x doi: 10.1046/j.1365-2435.1998.00274.x

Running, S. W., Nemani, R. R., Heinsch, F. A., Zhao, M., Reeves, M., & Hashimoto, H. (2004). A continuous satellite-derived measure of global terrestrial primary production. *BioScience*, *54*(6), 547. Retrieved from https://academic.oup.com/bioscience/article/54/6/547-560/294347 (arXiv: 1011.1669v3 ISBN: 0006-3568) doi: 10.1641/0006-3568(2004)054[0547:acsmog]2.0.co;2

Running, S. W., & Zhao, M. (2021). *User's Guide Daily GPP and Annual NPP (MOD17A2H/A3H) and Year-end Gap- Filled (MOD17A2HGF/A3HGF) Products NASA Earth Observing System MODIS Land Algorithm (For Collection 6.1)* (Tech. Rep. No. Version 1.1). Retrieved 2022-06-16, from https://lpdaac.usgs.gov/documents/926/MOD15_User_Guide_V61.pdf

Ryan, M. G., Gower, S. T., Hubbard, R. M., Waring, R. H., Gholz, H. L., Cropper, W. P., & Running, S. W. (1995, February). Woody tissue maintenance respiration of four conifers in contrasting climates. *Oecologia*, *101*(2), 133–140. Retrieved 2022-06-27, from http://link.springer.com/10.1007/BF00317276 doi: 10.1007/BF00317276

Ryu, Y., Berry, J. A., & Baldocchi, D. D. (2019). What is global photosynthesis? History, uncertainties and opportunities. *Remote Sensing of Environment*, *223*(January), 95–114. Retrieved from https://doi.org/10.1016/j.rse.2019.01.016 (Publisher: Elsevier) doi: 10.1016/j.rse.2019.01.016

Salvatier, J., Wiecki, T. V., & Fonnesbeck, C. (2016, April). Probabilistic programming in Python using PyMC3. *PeerJ Computer Science*, *2*, e55. Retrieved 2022-06-27, from https://peerj.com/articles/cs-55 doi: 10.7717/peerj-cs.55

Scurlock, J. M. O., Johnson, K. R., & Olson, R. J. (2003). NPP Grassland: NPP Estimates from Biomass Dynamics for 31 Sites, 1948-1994, R1. Retrieved from http://daac.ornl.gov/cgi-bin/dsviewer.pl?ds_id=654 (Publisher: ORNL Distributed Active Archive Center) doi: 10.3334/ORNLDAAC/654

Scurlock, J. M. O., & Olson, R. J. (2012). NPP Multi-Biome: Grassland, Boreal Forest, and Tropical Forest Sites, 1939-1996, R1. Retrieved from http://daac.ornl.gov/cgi-bin/dsviewer.pl?ds_id=653 (Publisher: ORNL Distributed Active Archive Center) doi: 10.3334/ORNLDAAC/653

Sitch, S., Friedlingstein, P., Gruber, N., Jones, S. D., Murray-Tortarolo, G., Ahlström, A., … Myneni, R. (2015). Recent trends and drivers of regional sources and sinks of carbon dioxide. *Biogeosciences*, *12*(3), 653–679. doi: 10.5194/bg-12-653-2015

Sjöström, M., Zhao, M., Archibald, S., Arneth, A., Cappelaere, B., Falk, U., … Ardö, J. (2013, April). Evaluation of MODIS gross primary productivity for Africa using eddy covariance data. *Remote Sensing of Environment*, *131*, 275–286. Retrieved 2022-07-04, from https://linkinghub.elsevier.com/retrieve/pii/S0034425712004890 doi: 10.1016/j.rse.2012.12.023

Skakun, S., Justice, C. O., Vermote, E., & Roger, J.-C. (2018, February). Transitioning from MODIS to VIIRS: an analysis of inter-consistency of NDVI data sets for agricultural monitoring. *International Journal of Remote Sensing*, *39*(4), 971–992. Retrieved 2022-07-07, from https://www.tandfonline.com/doi/full/10.1080/01431161.2017.1395970 doi: 10.1080/01431161.2017.1395970

Sobol', I. M. (2001, February). Global sensitivity indices for nonlinear mathematical models and their Monte Carlo estimates. *Mathematics and Computers in Simulation*, *55*(1-3), 271–280. Retrieved 2022-06-18, from https://linkinghub.elsevier.com/retrieve/pii/S0378475400002706 doi: 10.1016/S0378-4754(00)00270-6

Stockfors, J., & Linder, S. (1998, March). Effect of nitrogen on the seasonal course of growth and maintenance respiration in stems of Norway spruce trees. *Tree Physiology*, *18*(3), 155–166. Retrieved 2022-06-24, from https://academic.oup.com/treephys/article-lookup/doi/10.1093/

treephys/18.3.155 doi: 10.1093/treephys/18.3.155

Sulla-Menashe, D., Gray, J. M., Abercrombie, S. P., & Friedl, M. A. (2019, March). Hierarchical mapping of annual global land cover 2001 to present: The MODIS Collection 6 Land Cover product. *Remote Sensing of Environment*, *222*, 183–194. Retrieved from https://linkinghub.elsevier.com/retrieve/pii/S0034425718305686 doi: 10.1016/j.rse.2018.12.013

Tang, R., Shao, K., Li, Z. L., Wu, H., Tang, B.-H., Zhou, G., & Zhang, L. (2015). Multiscale Validation of the 8-day MOD16 Evapotranspiration Product Using Flux Data Collected in China. *IEEE Journal of Selected Topics in Applied Earth Observations and Remote Sensing*, *8*(4), 1478–1486. doi: 10.1109/JSTARS.2015.2420105

Tang, X., Fan, S., Du, M., Zhang, W., Gao, S., Liu, S., … Yang, W. (2020, May). Spatial and temporal patterns of global soil heterotrophic respiration in terrestrial ecosystems. *Earth System Science Data*, *12*(2), 1037–1051. Retrieved from https://essd.copernicus.org/articles/12/1037/2020/ doi: 10.5194/essd-12-1037-2020

Ter Braak, C. J. F., & Vrugt, J. A. (2008). Differential Evolution Markov Chain with snooker updater and fewer chains. *Statistics and Computing*, *18*(4), 435–446. doi: 10.1007/s11222-008-9104-9

Tjoelker, M. G., Oleksyn, J., & Reich, P. B. (2001, February). Modelling respiration of vegetation: Evidence for a general temperature-dependent Q10. *Global Change Biology*, *7*(2), 223–230. Retrieved from http://doi.wiley.com/10.1046/j.1365-2486.2001.00397.x doi: 10.1046/j.1365-2486.2001.00397.x

Verheijen, L. M., Aerts, R., Brovkin, V., Cavender-Bares, J., Cornelissen, J. H. C., Kattge, J., & van Bodegom, P. M. (2015, August). Inclusion of ecologically based trait variation in plant functional types reduces the projected land carbon sink in an earth system model. *Global Change Biology*, *21*(8), 3074–3086. Retrieved 2022-07-20, from https://onlinelibrary.wiley.com/doi/10.1111/gcb.12871 doi: 10.1111/gcb.12871

Vrugt, J. A., Ter Braak, C. J. F., Diks, C. G. H., Robinson, B. A., Hyman, J. M., & Higdon, D. (2009). Accelerating Markov chain Monte Carlo simulation by differential evolution with self-adaptive randomized subspace sampling. *International Journal of Nonlinear Sciences and Numerical Simulation*, *10*(3), 273–290. doi: 10.1515/IJNSNS.2009.10.3.273

Wang, J., & Ogawa, S. (2017, February). Analysis of dynamic changes in land use based on landscape metrics in Nagasaki, Japan. *Journal of Applied Remote Sensing*, *11*(1), 016022. Retrieved from http://remotesensing.spiedigitallibrary.org/article.aspx?doi=10.1117/1.JRS.11.016022 doi: 10.1117/1.JRS.11.016022

Welp, L. R., Keeling, R. F., Meijer, H. A. J., Bollenbacher, A. F., Piper, S. C., Yoshimura, K., … Wahlen, M. (2011, September). Interannual variability in the oxygen isotopes of atmospheric CO2 driven by El Niño. *Nature*, *477*(7366), 579–582. Retrieved 2023-01-29, from http://www.nature.com/articles/nature10421 doi: 10.1038/nature10421

White, M. A., Thornton, P. E., Running, S. W., & Nemani, R. R. (2000, January). Parameterization and sensitivity analysis of the BIOME–BGC terrestrial ecosystem model: Net primary production controls. *Earth Interactions*, *4*(3), 1–85. Retrieved 2022-06-01, from http://journals.ametsoc.org/doi/10.1175/1087-3562(2000)004<0003:PASAOT>2.0.CO;2 doi: 10.1175/1087-3562(2000)004<0003:PASAOT>2.0.CO;2

White, R., & Engelen, G. (2000, September). High-resolution integrated modelling of the spatial dynamics of urban and regional systems. *Computers, Environment and Urban Systems*, *24*(5), 383–400. Retrieved from http://linkinghub.elsevier.com/retrieve/pii/S0198971500000120 doi: 10.1016/S0198-9715(00)00012-0

Wright, I. J., Reich, P. B., Westoby, M., Ackerly, D. D., Baruch, Z., Bongers, F., … Villar, R. (2004, April). The worldwide leaf economics spectrum. *Nature*, *428*(6985), 821–827. Retrieved from http://www.nature.com/articles/nature02403 doi: 10.1038/nature02403

Wright, I. J., & Westoby, M. (2001, March). Understanding seedling growth relationships through specific leaf area and leaf nitrogen concentration: generalisations across growth forms and growth irradiance. *Oecologia*, *127*(1), 21–29. Retrieved 2022-07-20, from http://link.springer.com/10.1007/s004420000554 doi: 10.1007/s004420000554

Xiong, X., Angal, A., Chang, T., Chiang, K., Lei, N., Li, Y., … Wu, A. (2020, September). MODIS and VIIRS calibration and characterization in support of producing long-term high-quality data products. *Remote Sensing*, *12*(19), 3167. Retrieved 2022-07-07, from https://www.mdpi.com/2072-4292/12/19/3167 doi: 10.3390/rs12193167

Xu, B., Park, T., Yan, K., Chen, C., Zeng, Y., Song, W., … Myneni, R. B. (2018). Analysis of global LAI/FPAR products from VIIRS and MODIS sensors for spatio-temporal consistency and uncertainty from 2012-2016. *Forests*, *9*(2), 1–21. doi: 10.3390/f9020073

Yan, K., Pu, J., Park, T., Xu, B., Zeng, Y., Yan, G., … Myneni, R. B. (2021, July). Performance stability of the MODIS and VIIRS LAI algorithms inferred from analysis of long time series of products. *Remote Sensing of Environment*, *260*, 112438. Retrieved from https://linkinghub.elsevier.com/retrieve/pii/S0034425721001565 doi: 10.1016/j.rse.2021.112438

Yang, R., Wang, J., Zeng, N., Sitch, S., Tang, W., McGrath, M. J., … Han, P. (2022). Divergent historical GPP trends among state-of-the-art multi-model simulations and satellite-based products. *Earth System Dynamics*(13), 833–849. doi: https://doi.org/10.5194/esd-13-833-2022

Yuan, W., Cai, W., Liu, S., Dong, W., Chen, J., Arain, M. A., … Xia, J. (2014, November). Vegetation-specific model parameters are not required for estimating gross primary production. *Ecological Modelling*, *292*, 1–10. Retrieved 2022-07-20, from https://linkinghub.elsevier.com/retrieve/pii/S0304380014003962 doi: 10.1016/j.ecolmodel.2014.08.017

Zaks, D. P. M., Ramankutty, N., Barford, C. C., & Foley, J. A. (2007, September). From Miami to Madison: Investigating the relationship between climate and terrestrial net primary production. *Global Biogeochemical Cycles*, *21*(3), n/a–n/a. Retrieved 2022-07-18, from http://doi.wiley.com/10.1029/2006GB002705 doi: 10.1029/2006GB002705

Zha, T., Kellomäki, S., Wang, K.-Y., Ryypö, A., & Niinistö, S. (2004, October). Seasonal and annual stem respiration of scots pine trees under boreal conditions. *Annals of Botany*, *94*(6), 889–896. Retrieved 2022-06-09, from https://academic.oup.com/aob/article-lookup/doi/10.1093/aob/mch218 doi: 10.1093/aob/mch218

Zhang, K., Zhu, G., Ma, J., Yang, Y., Shang, S., & Gu, C. (2019). Parameter analysis and estimates for the MODIS evapotranspiration algorithm and multiscale verification. *Water Resources Research*, *55*(3), 2211–2231. doi: 10.1029/2018WR023485

Zhang, Y., Song, C., Band, L. E., Sun, G., & Li, J. (2017, March). Reanalysis of global terrestrial vegetation trends from MODIS products: Browning or greening? *Remote Sensing of Environment*, *191*, 145–155. Retrieved 2023-02-10, from https://linkinghub.elsevier.com/retrieve/pii/S0034425716304977 doi: 10.1016/j.rse.2016.12.018

Zhang, Y., Xiao, X., Wu, X., Zhou, S., Zhang, G., Qin, Y., & Dong, J. (2017, October). A global moderate resolution dataset of gross primary production of vegetation for 2000–2016. *Scientific Data*, *4*(1), 170165. Retrieved 2023-01-29, from https://www.nature.com/articles/sdata2017165 doi: 10.1038/sdata

.2017.165

Zhang, Y., Yu, Q., Jiang, J., & Tang, Y. (2008, April). Calibration of Terra/MODIS gross primary production over an irrigated cropland on the North China Plain and an alpine meadow on the Tibetan Plateau. *Global Change Biology*, *14*(4), 757–767. Retrieved 2023-01-12, from `https://onlinelibrary.wiley.com/doi/10.1111/j.1365-2486.2008.01538.x` doi: 10.1111/j.1365-2486.2008.01538.x

Zhao, M., Heinsch, F. A., Nemani, R. R., & Running, S. W. (2005). Improvements of the MODIS terrestrial gross and net primary production global data set. *Remote Sensing of Environment*, *95*, 164–176. doi: 10.1016/j.rse.2004.12.011

Zhao, M., & Running, S. W. (2010). Drought-induced reduction in global terrestrial net Primary production from 2000 through 2009. *Science*, *329*, 940–943.

Zhao, M., Running, S. W., & Nemani, R. R. (2006). Sensitivity of Moderate Resolution Imaging Spectroradiometer (MODIS) terrestrial primary production to the accuracy of meteorological reanalyses. *Journal of Geophysical Research*, *111*(G1), G01002. Retrieved from `http://doi.wiley.com/10.1029/2004JG000004` doi: 10.1029/2004JG000004

Zhu, X., Pei, Y., Zheng, Z., Dong, J., Zhang, Y., Wang, J., … Xiao, X. (2018). Underestimates of grassland gross primary production in MODIS standard products. *Remote Sensing*, *10*(11). doi: 10.3390/rs10111771

Continuity of global MODIS terrestrial primary productivity estimates in the VIIRS era using model-data fusion

K. Arthur Endsley[1], Maosheng Zhao[2], John S. Kimball[1], Sadashiva Devadiga[3]

[1]Numerical Terradynamic Simulation Group (NTSG), W.A. Franke College of Forestry and Conservation, University of Montana, Missoula, MT, U.S.A.
[2]Science Systems and Applications, Inc.
[3]NASA Goddard Space Flight Center, Greenbelt, MD, U.S.A.

Key Points:

- Over two decades of global productivity estimates from MODIS cannot be continued without use of VIIRS data.
- We performed a comprehensive calibration and validation, and sensitivity and uncertainty analyses of MODIS MOD17 and new VIIRS VNP17.
- Both MOD17 and new VNP17 depict upward productivity trends and mean and interannual variability consistent with independent data.

Corresponding author: Maosheng Zhao, `maosheng.zhao@nasa.gov`

Abstract

The NASA Terra and Aqua satellites have been successfully operating for over two decades, exceeding their original 5-year design life. However, the era of NASA's Earth Observing System (EOS) may be coming to a close as early as 2023. Similarities between the Moderate Resolution Imaging Spectroradiometer (MODIS), aboard Aqua and Terra, and the Visible Infrared Imaging Radiometer Suite (VIIRS) sensors aboard the Suomi NPP, NOAA-20 and NOAA-21 satellites enable potential continuity of long-term earth observational records in the VIIRS era. We conducted a comprehensive calibration and validation of the MODIS MOD17 product, which provided the first global, continuous, weekly estimates of ecosystem gross primary productivity (GPP) and annual estimates of net primary productivity (NPP). Using Bayesian model-data fusion, we combined an 18-year record of tower fluxes with prior data on plant traits and hundreds of field measurements of NPP to benchmark MOD17 and to develop the first terrestrial productivity estimates from VIIRS. The updated mean global GPP (NPP) flux from MOD17 and the new VNP17 for 2012-2018 is 127 $\pm$2.8 Pg C year^{-1} (58 $\pm$1.1 Pg C year^{-1}), which compares well with independent top-down and bottom-up estimates. Both MOD17 and VNP17 depict upward productivity trends over recent decades, with 2000-2018 MOD17 GPP (NPP) rising by 0.47 (0.25) Pg C year^{-2} but slowing to 0.35-0.44 (0.11-0.13) Pg C year^{-2} over 2012-2021, with a greater reduction in the NPP growth rate. The new VIIRS VNP17 product has the potential to extend these continuous estimates of global, terrestrial primary productivity beyond 2030.

Plain Language Summary

The NASA Terra and Aqua satellites have been successfully operating for over two decades, far longer than their original 5-year design life. However, one or both satellites may run out of fuel as early as 2023. These satellites carry the Moderate Resolution Imaging Spectroradiometer (MODIS) sensors, which are very similar to the Visible Infrared Imaging Radiometer Suite (VIIRS) sensors aboard newer satellites. The long record of MODIS data collected so far may therefore be extended by the VIIRS sensors, particularly the global estimates of the amount of carbon in the atmosphere taken up and stored by plants. We used multiple independent datasets to figure out if and how the MODIS MOD17 computer model should be changed to improve its accuracy and to use data from VIIRS. The new VIIRS VNP17 data could extend our record of plant-atmosphere carbon exchange beyond the year 2030.

1 Introduction

The Moderate Resolution Imaging Spectroradiometer (MODIS), carried by the Terra and Aqua satellites, is a key component of NASA's Earth Observing System (EOS) (Justice et al., 2002), which has contributed observations of Earth's land, atmosphere, and oceans for over two decades. Although Terra and Aqua have far exceeded their original 5-year design life, the end of the EOS era is near, as one or both of the satellites may run out of fuel as early as 2023. Because of the dozens of products derived from the 36 MODIS spectral bands, and because of the similarity of the Visible Infrared Imaging Radiometer Suite (VIIRS) sensor aboard the Suomi NPP and NOAA-20 satellites, there has long been interest in using VIIRS to provide continuity of land surface observations (Murphy et al., 2001; Xiong et al., 2020). MODIS-like observations will continue to be important for global studies of terrestrial productivity, including ecosystem monitoring (Y. Zhang, Song, et al., 2017; M. O. Jones et al., 2020) and agricultural studies (Skakun et al., 2018).

Of particular interest are the on-going applications of MODIS to studies of the terrestrial carbon cycle, beginning with the first global, continuous, weekly estimates of ecosystem gross primary productivity (GPP) and annual estimates of net primary productivity (NPP): the Terra MODIS MOD17 product (Running et al., 2004; Zhao et al., 2005).

The MOD17 product, now exceeding 22 years of record, has been instrumental in diagnosing increasing water limitations on carbon uptake (Zhao & Running, 2010), highlighting the role of humans in wildfire ignition (Balch et al., 2017), and constraining human appropriations of biomass (Erb et al., 2018), among other diverse applications. It is no coincidence that MOD17 was developed at the same time that direct, ecosystem-level measurements of canopy gas exchange from eddy covariance (EC) flux towers first became widely available (Baldocchi et al., 2001). The simple light-use efficiency (LUE) approach allows for up-scaling the ecosystem-level estimate of GPP from towers using satellite observations of canopy vigor and gridded surface meteorological data (Ryu et al., 2019).

Here, we confront the MOD17 GPP and NPP models with data in a comprehensive calibration and validation study. We also present the first calibration and assessment of the MOD17 algorithm for use with the VIIRS sensor, enabling continuity of multi-decadal GPP and NPP estimates. The independent observational data used in this study include eddy covariance (EC) tower CO_2 fluxes, field surveys of productivity and biomass change, and a global database of species-level plant traits (Kattge et al., 2020). Previous MOD17 calibration efforts prescribed a set of general biophysical response characteristics for major land cover types, defined in the model's Biome Properties Look-up Table (BPLUT), and derived using a limited set of EC tower site observations as well as literature review, expert elicitation, and a smaller set of NPP estimates (Zhao et al., 2005). Here, we conducted a more extensive model calibration and formal analysis of model sensitivity and uncertainty in parameterization, which has been performed for similar diagnostic models (e.g., L. A. Jones et al., 2017; K. Zhang et al., 2019), but not yet for MOD17.

2 Data and Methods

Although there is a file-naming convention where "MOD" indicates a product granule based on Terra MODIS data (only, as opposed to Aqua MODIS), we use "MOD17" throughout this paper to refer to the combined GPP/NPP algorithm, which is currently operational using MODIS observations from both EOS Terra and Aqua satellites.

2.1 The MOD17 Algorithm

As MOD17 has been discussed thoroughly in the literature, we give only a brief overview of the model here. A complete description is available in the MOD17 Collection 6.1 User's Guide (Running & Zhao, 2021). MOD17 consists of three potentially independent submodels: 8-day GPP, 8-day net photosynthesis (PSN_{net}), and annual NPP. 8-day composite products are given the designation MOD17A2H, for Terra MODIS, or MYD17A2H, for Aqua MODIS. Annual products, including annual GPP (the sum of one year's 8-day GPP composites), are carried by MOD17A3H (or MYD17A3H). GPP is calculated using a classic light-use efficiency (LUE) approach (Running et al., 2004; Yuan et al., 2014; Madani et al., 2017), where the carbon (C) uptake by plants is assumed to be proportional to canopy absorbed photosynthetically active radiation (APAR) under prevailing daytime environmental conditions for diel or longer time scales. Low temperatures or high vapor pressure deficit (VPD) reduce the efficiency of photosynthetic C uptake, thus, MOD17 GPP is described as a product of APAR, the light-use efficiency under optimal conditions (ε_{max}), and environmental scalars:

$$\mathrm{GPP} = \mathrm{APAR} \times \varepsilon_{max} \times f(T_{min}) \times f(\mathrm{VPD}) \quad (1)$$

Where $f(T_{min})$ and $f(\mathrm{VPD})$ are numbers on $[0, 1]$ representing the decline in ε_{max} due to low daily minimum temperatures and high VPD, respectively. These environmental scalars are represented as linear ramp functions, where limiting conditions are interpolated between zero (completely limiting, i.e., photosynthesis cannot occur) and one (non-limiting). The key parameters in modeling GPP, in addition to ε_{max}, are the T_{min}

and VPD values that indicate the width of the ramp function and, consequently, the slope that determines how much $\varepsilon_{\max}$ is reduced for a unit decrease in $T_{\min}$ or unit increase in VPD.

Daily (or 8-day) net photosynthesis is calculated as GPP less maintenance respiration (R_M) from leaves and fine roots. Leaf R_M is based on a Q10 function (Tjoelker et al., 2001) and the current leaf C mass, which is estimated instantaneously as leaf area index (LAI) divided by specific leaf area (SLA). Fine root R_M is also based on a Q10 function and the fine root C mass is based on an allometric relationship with the leaf C mass. The same Q10 $\equiv 2$ is used for fine roots and livewood whereas leaves use a temperature-acclimated equation (ibid.). Notably, as MOD17 does not track biomass allocation, livewood respiration and growth respiration, R_G, are not included in $\mathrm{PSN_{net}}$. Annual NPP does account for R_G and livewood R_M, estimating livewood C mass through an allometric relationship with annual maximum leaf C mass. Based on empirical studies, R_G is estimated to consume 25% of annual NPP; thus, annual NPP is calculated as:

$$\mathrm{NPP} = \mathrm{GPP} - R_M - R_G = \frac{1}{1.25}(\mathrm{GPP} - R_M) \tag{2}$$

The complete list of parameters is included in Table 1. Each of the parameters is defined separately for 11 distinct plant functional types (PFTs), based on the MODIS MCD12Q1 Type 2 International Geosphere-Biospehre Programme (IGBP) land-cover classification (Friedl & Sulla-Menashe, 2019; Sulla-Menashe et al., 2019).

MOD17 Collection 6.1 (C61) depends on surface meteorological data including mean and minimum daily air temperature, photosynthetically active radiation (PAR), atmospheric pressure, and the water vapor mixing ratio. These inputs are derived from the NASA Global Modeling and Assimilation Office (GMAO) Goddard Earth Observing System 5 (GEOS-5), Forward Processing for Instrument Teams (GEOS FP-IT). It also depends on driver data from MOD15A2H (Myneni et al., 2015), a record of LAI and the fraction of the canopy absorbing PAR (fPAR). Taken together, these data determine the surface cover available to harvest light for C (CO_2) uptake and the environmental constraints on that process.

In this re-processing, there are some significant departures from earlier versions of MOD17. First, C61 and all previous versions of MOD17 used an estimate of short-wave radiation (GMAO "SWGNT") that is likely too low to be used in calculating PAR. Estimation of PAR is based on irradiance measurements indicating that approximately 45% of the daily (short-wave) solar irradiance is within the PAR waveband, 400-700 nm (Meek et al., 1984). However, MOD17 has historically used 45% of *net* short-wave radiation for calculating PAR, which might be an underestimate, as SWGNT accounts for surface albedo. Based on GMAO data over 2000-2017, the incoming daily short-wave irradiance (GMAO "SWGDN") is always greater than or equal to SWGNT. Previous MOD17 calibration (Zhao et al., 2005, 2006) has likely compensated for this underestimation of PAR.

Here, we re-calibrate MOD17 using GMAO SWGDN instead of SWGNT. In addition, whereas C61 and prior versions have fixed fine-root and livewood Q10 values at 2, we make these free parameters during model calibration, based on prior evidence that suggest this fixed value may be suboptimal (see "Model-Data Fusion"). Prior to calibration, we conducted a global sensitivity analysis of MOD17's free parameters, based on the Sobol' variance-based decomposition method (Sobol', 2001). This was performed in Python using SALib (Herman & Usher, 2017; Iwanaga et al., 2022), and obtains the proportion of the total variance in GPP or NPP that is contributed directly by a given parameter or by an interaction between that parameter and any combination of other parameters.

Table 1: Free parameters in MOD17, with units and a short description.

Parameter	Units	Description
$\varepsilon_{\max}$	kg C MJ^{-1}	LUE under optimal conditions
$T_{\min,\leftarrow}$	deg Celsius	Minimum temperature below which $\varepsilon = 0$
$T_{\min,\rightarrow}$	deg Celsius	Minimum temperature above which ε not limited by temperature
$\text{VPD}_{\leftarrow}$	Pa	VPD below which ε is not limited by VPD
$\text{VPD}_{\rightarrow}$	Pa	VPD above which $\varepsilon = 0$
SLA	LAI $(\text{kg C})^{-1}$	Projected leaf area per unit mass of leaf C
`froot_leaf_ratio`		Allometric ratio of fine root C to leaf C
`livewood_leaf_ratio`		Allometric ratio of livewood C to leaf C
`leaf_mr_base`	kg C $(\text{kg C})^{-1}$ day^{-1}	Maintenance respiration base rate, per unit leaf C, at 20 deg C
`froot_mr_base`	kg C $(\text{kg C})^{-1}$ day^{-1}	Maintenance respiration base rate, per unit fine root C, at 20 deg C
`livewood_mr_base`	kg C $(\text{kg C})^{-1}$ day^{-1}	Maintenance respiration base rate, per unit livewood C, at 20 deg C
`Q10_froot`		Exponent shape parameter relating fine root R_M to temperature
`Q10_livewood`		Exponent shape parameter relating livewood R_M to temperature

2.2 Model Calibration Data

For GPP model calibration, we used a globally representative network of 352 eddy covariance (EC) flux towers from the FLUXNET/La Thuile synthesis collection (Baldocchi, 2008). Based on a recent analysis of EC tower footprints (Chu et al., 2021), we chose a conservative tower footprint of 1.5 km, or a 3-by-3 grid of 500-m pixels centered on the tower. This area is used to integrate fPAR and LAI observations at 500-m scale and smooth the resulting GPP predictions through spatial averaging. Tower daily gap-filled GPP data were smoothed using a 2-day moving window filter with zero phase offset and observations were discarded when PAR was below 0.1 MJ m^{-2} per day. fPAR and LAI data were filtered to remove spurious spikes; low-quality fPAR and LAI data, based on the quality check (QC) band, were filled in from an fPAR or LAI climatology. Then, 8-day fPAR and LAI were interpolated to daily time steps using forward and backward filling. In addition to MODIS MOD15A2H fPAR and LAI, daily surface meteorological data were compiled for tower sites for the years 2000 through 2017 from the Modern-Era Retrospective Re-analysis (MERRA-2, Gelaro et al., 2017).

MOD17 is calibrated separately for each PFT. Each FLUXNET site is assigned a dominant PFT, the class that makes up the majority of 500-m pixels within the 1.5-km tower footprint. Tower sites used for model calibration were screened to ensure PFT consistency between the local tower footprints and overlying MOD17 windows. Calibration for a given PFT uses just those FLUXNET sites where that PFT is dominant (Table 2). Because no FLUXNET site is located within a majority-DNF canopy, we assigned to this PFT two majority-ENF sites that have DNF pixels within a 3-km radius. CSH is also poorly represented among FLUXNET sites, dominant at only 2 sites. We assigned 3 other sites that have CSH pixels within the 1.5-km footprint, but which are dominant elsewhere.

Table 2: The plant functional type (PFT) classification used in MOD17, which is based on the MODIS MCD12Q1 Type 2 classification. The number of FLUXNET sites with each PFT as the dominant ground cover (i.e., majority of 500-m pixels within a 1.5-km footprint) is also included.

Plant Functional Type (PFT)	Abbreviation	Number of FLUXNET sites
Evergreen needleleaf forest	ENF	30
Evergreen broadleaf forest	EBF	22
Deciduous needleleaf forest	DNF	2
Deciduous broadleaf forest	DBF	32
Mixed forest	MF	33
Closed shrublands	CSH	5
Open shrublands	OSH	15
Woody savannas	WSV	47
Savannas	SAV	35
Grasslands	GRS	77
Croplands	CRO	54

Annual NPP parameters have never before been directly calibrated against observations, with model misfit quantified by the difference between predictions and field estimates of NPP. Here, we use a multi-decadal inventory of global NPP estimates collected by the Oak Ridge National Laboratory (ORNL) Distributed Active Archive Center (DAAC). This "Multi-Biome" collection and other field datasets (Table 3) describe above-ground, below-ground, and/or total NPP at over 1,600 field sites, providing a basis for global calibration of terrestrial carbon models. There are some challenges, however.

Few of the datasets in this collection provide details on the land-use or management history and fewer still provide specific years or year ranges for the NPP estimates;

Table 3: Calibration and validation data used in this study, with citations. The majority of datasets come from the Oak Ridge National Laboratory (ORNL) Distributed Active Archive Center (DAAC). The last two entries refer to separate published papers.

Dataset	Citation
Summary Data from Intensive Studies at 125 Sites, 1936-2006	(Olson et al., 2017)
Global Osnabruck Data, 1937-1981, R1	(Esser, 2013)
Grassland, Boreal Forest, and Tropical Forest Sites, 1939-1996, R1	(Scurlock & Olson, 2012)
PIK Data for Northern Eurasia, 1940-1988 (Based on Bazilevich), R1	(Dennisenko et al., 2012)
TEM Calibration Data, 1992, R1	(Kicklighter, 2012)
Global IBP Woodlands Data, 1955-1975, R1	(DeAngelis et al., 2012)
Global Primary Production Data Initiative Products, R2	(Olson et al., 2013)
Boreal Forest Consistent Worldwide Site Estimates, 1965-1995, R1	(Gower et al., 2012)
NPP Estimates from Biomass Dynamics for 31 Sites, 1948-1994, R1	(Scurlock et al., 2003)
VAST Calibration Data, 1965-1998, R1	(Barrett, 2012)
"Biomass production…in temperate and boreal ecosystems"	(Campioli et al., 2015)
"Depth distribution of belowground net primary production…"	(Luo et al., 2021)

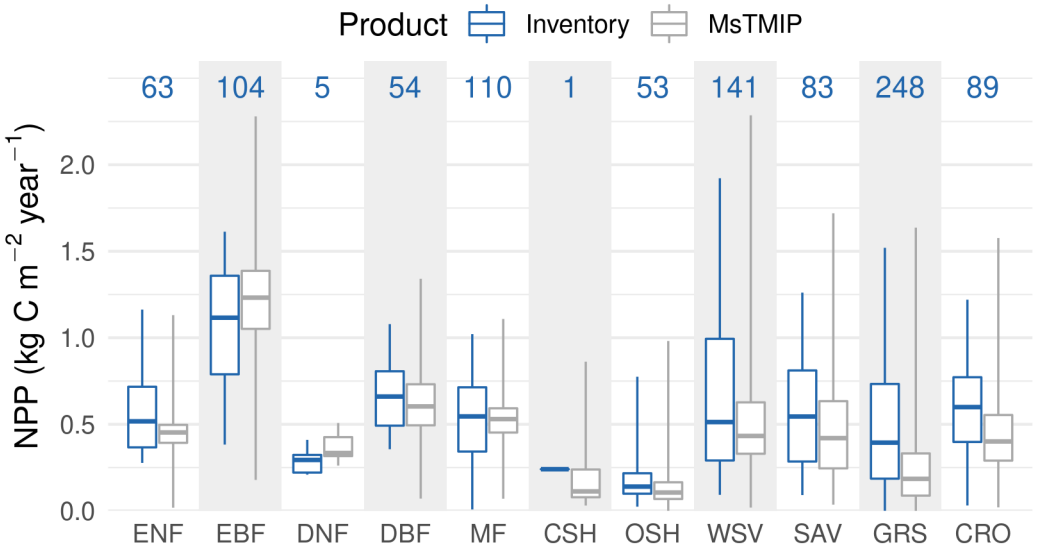

Figure 1: Boxplots of mean annual NPP, by Plant Functional Type (PFT), for the Cal-Val ("Inventory") data and the MsTMIP ensemble mean, based on a majority resampling of land-cover data to MsTMIP's half-degree grid. Numbers at top indicate the total number of site-years for the Inventory data. Whiskers show the minimum and maximum of each dataset. Sites with reported mean annual NPP greater than 2,385 g C m^{-2} year^{-1} were discarded.

the estimates span a range of years from 1936 to 2006. Sites in the inventory were classified into PFT groups based, first, on the reported biome or vegetation type; if no such information was provided, the site coordinates were used to map the PFT class from the MCD12Q1 Type 2 global mosaic for year 2015. A small number of sites were excluded because they did report intensive management histories (fertilizer, irrigation, mowing, or burning). NPP estimates from Gower et al. (2012) and Olson et al. (2013) were grouped by site (unique name or coordinates) and averaged. Because CSH describes such a small proportion of the global land domain (Madani et al., 2017), additional, randomly chosen CSH sites from the NPP validation datasets were added to the calibration dataset. In addition, data compiled by Campioli et al. (2015) and Luo et al. (2021) were added to the ORNL calibration dataset, after removing sites that were duplicated from the ORNL data, resulting in a total of 1,646 annual NPP measurements for calibration and validation ("Cal-Val").

As we cannot exclude the possibility that some sites are intensively managed to boost productivity (e.g., by fertilization or irrigation), we removed NPP samples that fell outside the PFT-group range of global mean (1980-2000) annual NPP, which was derived from a fusion of annual FLUXCOM NEE (Jung et al., 2020) and heterotrophic respiration (R_H) data from X. Tang et al. (2020). After also accounting for sites that fall outside of the MODIS global land domain (i.e., have no fPAR or LAI data), this resulted in a final total of 951 valid NPP measurements. The NPP Cal-Val data show expected differences by PFT and the median NPP agrees well with previously reported biome-level averages (e.g., Kicklighter et al., 1999; Zaks et al., 2007), and also with the Multi-Scale Synthesis and Terrestrial Model Intercomparison Project (MsTMIP, Huntzinger et al., 2013) "BG1" simulation (time-varying climate, land-cover, CO_2, and nitrogen deposition) ensemble mean (Figure 1). Reported values in DNF canopy (209-410 g C m^{-2}

year^{-1}) are low but consistent with reports from field measurements in forest stands (Kushida et al., 2007; Ji et al., 2020).

Corresponding NPP model meteorological drivers for 1980-2000 were obtained from the MERRA-2 re-analysis (Gelaro et al., 2017), which is derived from the GEOS-5 land model. As most sites do not specify the exact year of the NPP measurement, we used daily data from a randomly chosen year between 1980-2000 for each site, for the corresponding calendar day of a 365-day year, so as to capture the real, within-site, intra-annual variability in environmental drivers (as opposed to reducing the variance by using a climatology). As MOD17 does not have any state tracked between time steps, and as modeled NPP is calculated over the synthetic, 365-day year at each site, there are no issues with using different days for consecutive years. Because there are no MODIS data prior to 2000, MODIS fPAR and LAI climatologies were calculated for the 2000-2005 period for use in calibrating annual NPP.

2.3 Model-Data Fusion

The parameters in the MOD17 BPLUT, itemized in Table 1, were previously derived from literature review and some empirical studies. Today, there are numerous, direct ecological observations that can be used to inform model development and calibration, including extensive EC flux tower data and measured plant traits. We consulted the global TRY database (Kattge et al., 2020) for plant traits relevant to MOD17 parameters and developed prior parameter distributions for use in a Bayesian model-data fusion. Specifically, using Markov Chain Monte Carlo (MCMC), the observed distributions of plant traits were used as priors for estimating the likelihood of MOD17 parameters given the difference between modeled and observed GPP or NPP. Details of how plant traits informed priors are available in the Supplement.

Likelihood-ratio tests indicated that the SLA prior for each PFT was significantly different from the pooled distribution (i.e., based on values from all PFTs). We decided to fix SLA at its prior mean (from the TRY database), given the thousands of species observations for this parameter, because SLA was revealed to be the most sensitive model parameter and we believe the TRY data to be more reliable for fixing this parameter than the relatively small number of field NPP estimates.

Model calibration was performed using MCMC with the Differential Evolution Metropolis sampler described by Ter Braak and Vrugt (2008) and Vrugt et al. (2009), as implemented in the PyMC framework (Salvatier et al., 2016). Between 100,000 and 200,000 samples were drawn from the posterior for each of three chains, based on a root-mean squared error (RMSE) pseudo-likelihood function. Chains were qualitatively assessed for convergence and required burn-in; thinning to remove autocorrelation was one in every 20 (for GPP) or 200 (for NPP) samples. The optimal posterior point estimate, used in the updated BPLUT, was chosen as the mean *a posteriori* estimate.

2.4 Inter-calibration for the VIIRS Sensor

Within the 2000-2017 period for which FLUXNET data are available, the SNPP VIIRS mission provides data for 5 years (2012-2017). Because the VIIRS record is much shorter than the MODIS record, and also because of differences in fPAR and LAI between the corresponding VNP15A2H and MOD15A2H products, we opted to calibrate MOD17 for VIIRS differently. Instead of using data fusion for calibration against observed NPP (as with the updated MODIS MOD17 product), we derived bias-correction coefficients based on systematic differences in fPAR and LAI between the two sensors and apply these to the updated MOD17 BPLUT. The ratio between mean MOD15A2H fPAR and mean VNP15A2H fPAR is used as a multiplier to adjust the $\varepsilon_{\max}$ parameter in the resulting VNP17 BPLUT while the ratio between mean MOD15A2H LAI and

mean VNP15A2H LAI is used as a multiplier to adjust the SLA parameter. Besides $\varepsilon_{\max}$ and SLA, the updated MOD17 and new VNP17 BPLUT would be the same.

In deriving both coefficients, because GPP is only accumulated for part of the year (but R_M continues year-round), we calculated mean fPAR and LAI only during the growing season, defined as days when the daily temperature constraint on GPP (defined by $T_{\min,\leftarrow}$) is above zero. The input fPAR and LAI data to this process are the 5-km gap-filled datasets used for global simulation (see "Global Boundary Conditions" section). The fPAR-based $\varepsilon_{\max}$ coefficients range from 0.965 (ENF) to 1.01 (OSH) and the LAI-based SLA coefficients range from 1.007 (WSV) to 1.076 (EBF), confirming the consistency in fPAR, LAI values between MOD15A2H and VNP15A2H (Xu et al., 2018; Yan et al., 2021).

2.5 Global Boundary Conditions

To verify that global carbon use efficiency (CUE), or NPP:GPP ratios, are reasonable, we conducted global simulations of GPP and NPP using the re-calibrated BPLUT. To overcome resource limitations, global simulations were conducted at 5-km scale from 2000-2021 (for MODIS) or 2012-2021 (for VIIRS). This approach is similar to previous MOD17 global simulations conducted at 1-degree resolution (Zhao et al., 2005). The global 5-km dominant PFT is defined as the majority land-cover type within a 5-km window over the MODIS MCD12Q1 (500-m) grid. We then created gap-filled 5-km fPAR and LAI time series using the approach of Zhao et al. (2005); the gap filling addresses data gaps from either cloud contamination or missing data during non-retrieval periods due to lower solar altitude at high latitudes during winter. Based on these 5-km, multi-year runs, the average annual GPP, NPP, and CUE were calculated within each PFT group.

2.6 Model Validation

Some GPP data were withheld during model calibration. For most PFTs, between 20 and 25 site-years of (daily) EC flux tower data, for up to 5 different tower sites, were reserved for validation. Because there are few sites where the majority of land-cover pixels are MF, GRS, DNF, or CSH, only 15 site-years are used for MF and GRS canopies and only 4 site-years are used for DNF and CSH. Each site-year reserved had valid data on at least 97% of data-days, ensuring that nearly complete years were used. Any missing days (3% or less) were interpolated by forward-backward filling to ensure an annual total based on 365 days.

For NPP model validation, because of the dearth of reliable NPP measurements, we used a 3-fold cross-validation to simultaneously estimate best-fit parameters and goodness-of-fit. In combination with MCMC, this means that a random subset of the NPP measurements was reserved in each fold and that nine chains (three folds times three chains in each fold) were obtained. Chains within a fold were pooled and the posterior mean parameters were used to calculate the goodness-of-fit, including bias, root mean-squared error (RMSE), and Pearson's correlation. These metrics were then averaged across folds to obtain the final goodness-of-fit values.

Three official MOD17 products were validated: MOD17A2H daily GPP, MOD17A3H annual GPP, and MOD17A3H annual NPP. Validation metrics include RMSE, normalized RMSE (nRMSE), unbiased RMSE, and Pearson's correlation coefficient; these were computed for products based on the MOD17 C61 BPLUT, updated MOD17 BPLUT and new VNP17 BPLUT. For MOD17A2H, daily tower GPP fluxes were aggregated (summed) to 8-day intervals matching the MOD17A2H 8-day GPP. For MOD17A3H annual GPP, because there are so few towers with valid data for at least 97% of days per year, we did not use the reserved validation sites only; instead, all tower sites with valid data were

used. This may overestimate the accuracy of the updated annual GPP product, since the annual GPP validation dataset includes several data points used in calibration.

We also validated MOD17 and VNP17 interannual NPP predictions against one top-down and three bottom-up estimates of global, annual NPP. First, the 2020 Global Carbon Budget (Friedlingstein et al., 2020) provides mean monthly NEE (2000-2016) based on atmospheric inversion on a 1-degree global, equirectangular grid. We calculated total annual NEE from these data and then resampled them onto a 0.5-degree grid to combine with global, up-scaled estimates of R_H from X. Tang et al. (2020); NPP is then calculated as $R_H - NEE$ ("GCB2020"). Second, we estimated total annual NPP (2000-2017) from the TRENDYv7 ensemble mean monthly GPP and R_A fields (Le Quéré et al., 2018; Sitch et al., 2015), on a 1-degree grid. Third, the ensemble mean NPP (2000-2010) from MsTMIP (BG1 simulation), on a 0.5-degree grid, was used as another bottom-up estimate (Huntzinger et al., 2013). Fourth, the up-scaled flux-tower estimates from FLUXCOM, driven by remote sensing and surface meteorological data ("RS+METEO"), were also compared, based on driver data from ERA5 (Jung et al., 2020). These independent estimates were compared to MOD17 and VNP17 annual NPP and their correspondence quantified by RMSE and Pearson's correlation coefficient.

To compute global annual fluxes from the independent GCB2020, TRENDYv7, MsTMIP, and FLUXCOM datasets, given their coarse spatial resolution and lack of equal-area projection, we projected the annual data onto a 9-km Equal-Area Scalable Earth Grid (EASE-Grid 2.0) using nearest-neighbor resampling. Then, after masking the data to a similarly resampled MCD12Q1 land area map, totaled the flux densities after scaling each pixel by its land area. This may result in slightly different estimates than reported in the literature for these products, but was ultimately necessary as those publications do not always report annual flux estimates.

2.7 Uncertainty Analysis

To quantify uncertainty in MOD17 GPP estimates, we applied error propagation by computing the Jacobian, J, of the GPP model with respect to fPAR and $\varepsilon_{\max}$, separately, for each PFT. The variance in GPP due to model inputs or parameters θ is given:

$$\sigma^2_{\mathrm{GPP}}(\theta) = J_\theta C J_\theta^T \tag{3}$$

where C is the error covariance matrix. To quantify the separate contributions of fPAR and $\varepsilon_{\max}$, this equation reduces to a scalar product, where C is the error in fPAR or $\varepsilon_{\max}$. We focused on fPAR and $\varepsilon_{\max}$ because the error in these parameters is known. fPAR error is given as 10 fPAR units (Myneni, 2018) and the standard error in the $\varepsilon_{\max}$ posterior is assumed to be representative. To facilitate uncertainty quantification, we also assume that errors in fPAR and $\varepsilon_{\max}$ are uncorrelated. We used Gaussian error propagation to estimate the uncertainty in annual GPP due to the compensating errors in daily GPP estimates. Overall uncertainty was calculated by pooling data for all PFTs, using only the GPP validation data, which effectively stratifies the data so approximately equal site-days are included from each PFT.

To quantify uncertainty in MOD17 annual NPP estimates, we use a Monte Carlo approach because is it is much more difficult to compute partial derivatives of the NPP model. We repeatedly sampled from the posterior NPP parameters, with replacement, calculating the RMSE in mean annual NPP based on the Cal-Val dataset. The coefficient of variation in RMSE is then reported, separately, for each PFT.

3 Results

The Sobol' sensitivity analysis indicates that more than 80% of the variance in the GPP model is determined by the $\varepsilon_{\max}$ parameter alone (Figure 2). The upper bounds

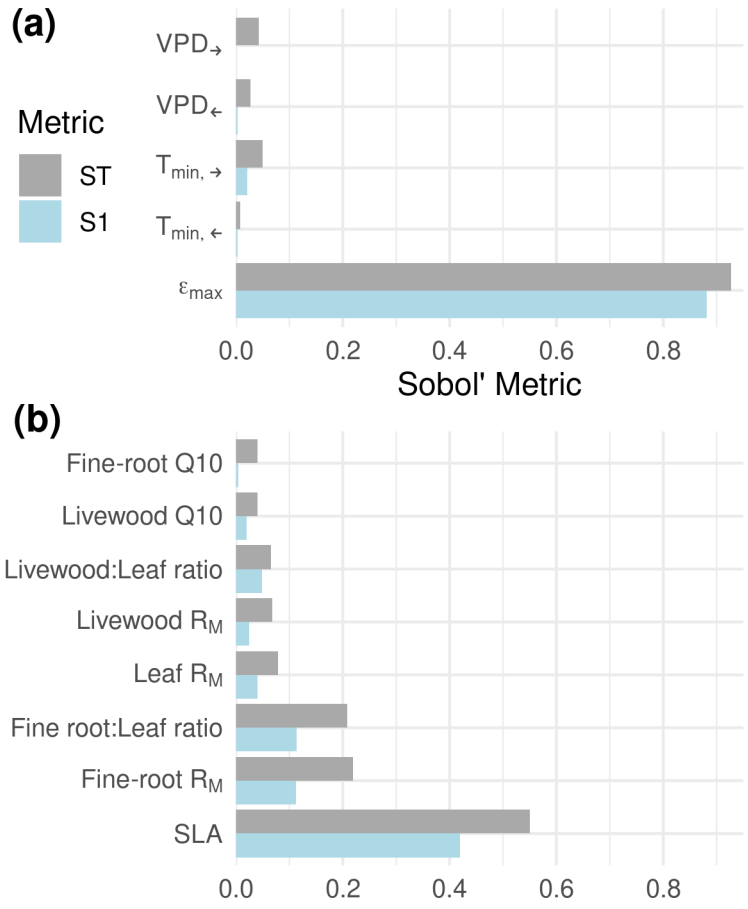

Figure 2: Sobol' sensitivity metrics for the MOD17 GPP (a) and NPP (b) models. The direct effect of the parameter on model estimates is indicated by S1; the total effect (including higher-order interactions) is indicated by ST. $T_{\text{min},\leftarrow}$ and $\text{VPD}_{\leftarrow}$ refer to the lower (left-hand) bounds of minimum temperature and VPD; the left-hand bound is the temperature (VPD) at which photosynthesis is completely limited (unlimited) by temperature (VPD). $T_{\text{min},\rightarrow}$ and $\text{VPD}_{\rightarrow}$ refer to the upper (right-hand) bounds of minimum temperature and VPD; the right-hand bound is the temperature (VPD) at which photosynthesis is completely unlimited (limited) by temperature (VPD).

of the environmental constraints, $T_{\text{min},\rightarrow}$ and $\text{VPD}_{\rightarrow}$, are more important than the lower bounds and have weak, second-order effects through ε_{max}. The annual NPP model has a strong direct effect of SLA (42%) but also moderately strong total effects from the fine root-leaf ratio (`froot_leaf_ratio`) and base R_M for fine roots. These sensitivities are partly reflected in the model-data fusion results. In the GPP calibration, the posterior distributions for the environmental scalars are fairly flat, resembling the uniform priors and indicating that the observed GPP data are consistent with a wide range of thresholds for T_{min} and VPD. Similarly, the `Q10_livewood` mean *a posteriori* estimate was close to the prior mean for most PFTs.

3.1 Optimal Parameters for BPLUT

The posterior distributions were compared to the C61 BPLUT and the wider literature, assessing both consistency with the previous product and realism. As an additional boundary condition, the mean global CUE values for each PFT were expected to be close to 0.46 (Collalti & Prentice, 2019) and much lower for EBF (Malhi, 2012). During NPP calibration, to ensure realism in the BPLUT values and the simulated, global CUE values, we rejected some of the mean *a posteriori* (MAP) estimates after calibration. When the MAP was rejected, it was replaced either by the prior mean for that PFT (Table S7) or by the MAP of a similar PFT. The updated MOD17 BPLUT and new VNP17 BPLUT can be found in the Supplement (Tables S9, S10).

Given the low sensitivity of the GPP model to the lower bounds of the environmental scalars (Figure 2), we opted to fix these at their C61 values; upper bounds remained free parameters during MOD17 calibration. The $\text{VPD}_{\rightarrow}$ posterior likelihood increased rapidly with VPD but, above ca. 3000 Pa the posterior flattens out. The $T_{\text{min},\rightarrow}$ posteriors are more complex, with most PFTs showing little sensitivity to this parameter. Consequently, the optimal values for both $\text{VPD}_{\rightarrow}$ and $T_{\text{min},\rightarrow}$ were chosen as the maximum *a posteriori* estimate, as the mean (or median), given a uniform prior, tends to fall near the middle of the prior bounds. The ε_{max} posteriors were symmetric and the prior mean was within the interquartile range (IQR) for all PFTs. The results are consistent with Madani et al. (2017), but the optimal ε_{max} appears to be significantly lower than its C61 value for shrublands and savannas, higher for croplands, and otherwise similar to C61 (Figure S9).

Consistent with the literature, the livewood Q10 posterior is narrow and resembles the prior. The fine-root Q10 posterior varies widely among PFTs, which is partly a reflection of the uncertainty in the literature. Deciduous canopies and Mixed Forest have the highest `Q10_froot` values. As `Q10_froot` is not likely to be less than 1.0 (Atkin et al., 2000), the posterior was rejected in favor of the prior in such cases. Posterior R_M for leaves and fine roots were generally lower than the prior means from TRY but within the range of the C61 BPLUT. The NPP data indicate that the optimal leaf R_M rate compares well with C61 for woody forest PFTs; however, posterior means for other PFTs were higher than the C61 value and close to the prior mean. The fine-root R_M posteriors vary widely and few are close to their C61 values. The posterior livewood R_M, however, compares well with the C61 BPLUT and the prior mean, except for EBF and shrublands, where it is significantly higher. The `livewood_mr_base` prior mean for EBF was used in place of the MAP.

3.2 Validation against Tower Fluxes and Field Data

The C61 annual GPP (MOD17A3H) estimates compare well with tower annual GPP among those sites with nearly complete years (Table 4). Under-estimation of GPP is apparent for ENF, but C61 also over-estimates GPP in medium-productivity EBF (Table S11). C61 GPP performs best in ENF, EBF, and GRS (nRMSE within 13-17%) but most severely under-estimates GPP in ENF and MF (nRMSE $\geq$ 49%). C61 8-day GPP (MOD17A2H), divided into daily units, indicates the algorithm performs best in shrublands, WSV, and GRS (nRSME $\leq$ 7%) and worst in CRO (nRMSE = 26%) because of under-estimation (mean bias = -1.2 g C m^{-2} day^{-1}) (Table S13).

GPP bias and RMSE were both reduced overall in the Updated product (Table 4), with the greatest improvements made at highly productive DBF and CRO sites (Table S13). Daily GPP improved for most PFTs, while annual GPP generally improved only for herbaceous and forested canopies. High negative bias in annual GPP was significantly reduced for ENF, GRS, and CRO (-196, -174 and -9 g C m^{-2} year^{-1} after recalibration, respectively). C61 MOD17 generally under-estimates GPP, particularly at high magnitudes (Heinsch et al., 2006; Y. Zhang et al., 2008), and slightly over-estimates annual

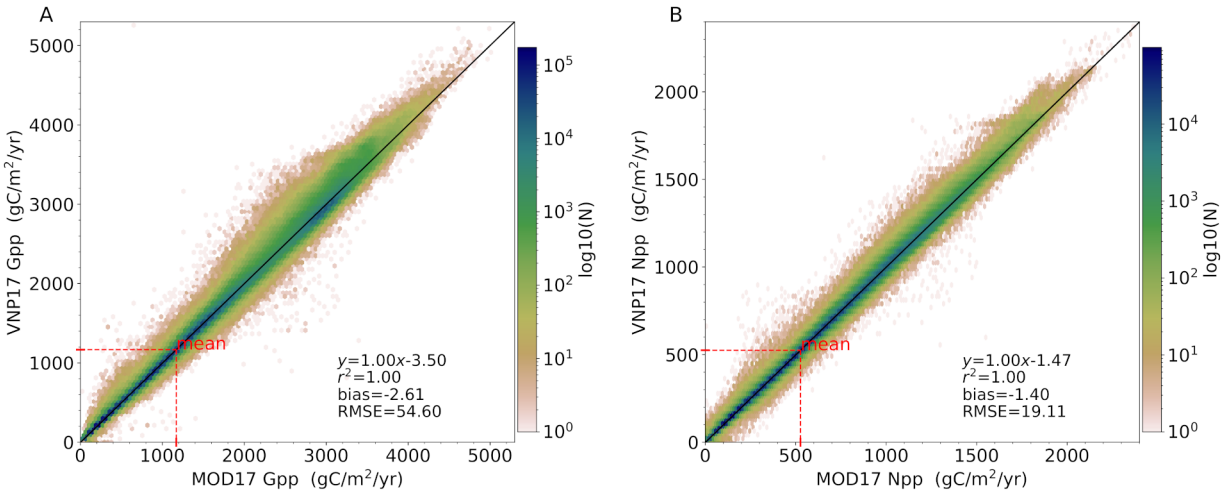

Figure 3: Comparison of mean annual GPP (left) and NPP (right) from the overlapping 10-year period for MODIS MOD17 and VIIRS VNP17 (2012-2021), based on global, 5-km simulations.

NPP, particularly in forested areas (Table S15). After re-calibration, GPP bias is reduced but is systematically similar to C61, while NPP bias is almost eliminated in individual PFTs, save for ENF, which has a strong, negative mean bias (Table S15). This also leads to an overall negative bias in the updated product (Table 4).

Annual NPP skill is improved in the MOD17 update, compared to C61 (Table 4, Figures S10-S11). C61 Annual NPP (MOD17A3H) performs best in shrublands, savannas, and herbaceous canopies (nRMSE $\leq$ 17 percent) and this pattern is similar for the updated product, though DNF, DBF, and MF are also considerably improved (Table S15). The magnitude of annual NPP RMSE in C terms is small ($\sim$ 0.7 g C m^{-2} day^{-1}) but performance varies widely by PFT, with the greatest nRMSE values in forest canopies. In the update, spatial correlation in annual NPP is improved for all PFTs ($\geq$ 0.5) except ENF. Annual NPP RMSE was also improved for all PFTs, except ENF.

Plant CUE (NPP:GPP ratio) is an emergent property of ecosystems simulated by MOD17. When the new annual GPP and NPP products are combined, we find that the BPLUT updates lead to substantial changes in CUE from C61. In terms of agreement with the MsTMIP ensemble, the updates improve plant CUE for all PFTs except DNF, SAV, and GRS (Figure S12). When compared to the measured CUE values compiled by Collalti and Prentice (2019) for woody plants, the updates improve plant CUE for all PFTs except EBF (Figure S13), for which median CUE is 0.49 (0.40 in MsTMIP ensemble, 0.44 in C61, and 0.37 in the update).

At global extent, the new VNP17 annual GPP and NPP products are very similar to the updated MOD17 products (Figure 3). The new VIIRS VNP17 BPLUT was used in the same validation scheme as for MOD17 GPP and NPP. However, because VIIRS fPAR and LAI data are only available starting in 2012 and many FLUXNET sites do not report data after 2012, there are far fewer site-weeks or site-years to use for validating VNP17 daily GPP than for MOD17. In particular, majority-DNF sites are not represented in the 2012-2017 period and no majority-DBF sites have years with at least 97% of valid data-days within this span. When using a common validation data mask, it is apparent that the VNP17 BPLUT produces daily GPP estimates quite similar to the updated MOD17 BPLUT (Table 4), except that VNP17 shows potential degrada-

Table 4: Validation statistics for the daily MOD17A2H/VNP17A2 GPP and annual MOD17A3H/VNP17A3 GPP and NPP products, as compared to EC flux tower and NPP cross-validation (Cal-Val) data, respectively. For daily GPP validation, daily tower GPP and updated simulations were aggregated to 8-day periods to match MOD17A2H. For annual GPP validation, all tower data were used instead of only reserved data. The normalized RMSE (%) is based on the overall observed range of daily GPP or annual NPP. The largest valid tower GPP observation was 20.4 g C m^{-2} day^{-1}. The largest NPP flux in the NPP Cal-Val dataset was 1,922 g C m^{-2} $year^{-1}$ (nRMSE for annual NPP is the cross-validation mean). 8-day GPP was evaluated for the entire FLUXNET record (2000-2017) but also on a common, reserved test dataset from 2012-2017, for compatibility with VIIRS; the latter case does not include any results from DNF due to missing FLUXNET data in this period. *VNP17 Annual GPP validation does not include DNF or DBF canopy, as none of the FLUXNET sites have any year with at least 97% of valid data-days during the period 2012-2017.

Model	Bias (g C m^{-2})	RMSE (g C m^{-2})	ubRMSE (g C m^{-2})	nRMSE (%)	r
MOD17 8-day GPP (C61), 2000-2017	-4.04 day^{-1}	2.69 day^{-1}	2.41 day^{-1}	13.7%	0.79
MOD17 8-day GPP (Update), 2000-2017	-2.77 day^{-1}	2.34 day^{-1}	2.07 day^{-1}	12.0%	0.84
MOD17 8-day GPP (C61), 2012-2017	-2.56 day^{-1}	2.25 day^{-1}	1.82 day^{-1}	11.0%	0.81
MOD17 8-day GPP (Update), 2012-2017	-2.06 day^{-1}	2.16 day^{-1}	1.72 day^{-1}	10.6%	0.82
VNP17 8-day GPP, 2012-2017	-1.75 day^{-1}	2.17 day^{-1}	1.72 day^{-1}	10.6%	0.82
MOD17 Annual GPP (C61)	-266 $year^{-1}$	546 $year^{-1}$	n.a.	14.4%	0.78
MOD17 Annual GPP (Update)	-210 $year^{-1}$	504 $year^{-1}$	n.a.	13.3%	0.80
VNP17 Annual GPP*	-179 $year^{-1}$	523 $year^{-1}$	n.a.	14.0%	0.82
MOD17 Annual NPP (C61)	9 $year^{-1}$	297 $year^{-1}$	n.a.	16.0%	0.49
MOD17 Annual NPP (Update)	-59 $year^{-1}$	261 $year^{-1}$	n.a.	14.1%	0.51
VNP17 Annual NPP	-46 $year^{-1}$	274 $year^{-1}$	n.a.	14.8%	0.49

tion in MF and improvement in OSH and a less-negative overall bias (Tables S13, S14). VNP17 annual NPP estimates, however, are generally less accurate than for MOD17, with particularly high RMSE in ENF, OSH, WSV, and SAV compared to the updated MOD17 (Tables S15, S16). Compared to the statistics in Table 4, when the longer validation record available to MODIS MOD17 is used instead, there is a more substantial improvement over C61 in daily GPP RMSE (2.69 g C m^{-2} day^{-1} for C61 versus 2.34 for the Updated BPLUT) and correlation (0.77 for C61 versus 0.84 for the Updated BPLUT).

Table 5: Root-mean squared difference (RMSD) in annual NPP (g C m^{-2} $year^{-1}$) at FLUXNET sites for each product, compared to independent NPP datasets.

NPP Dataset	C61	MOD17 Update	New VNP17
Global Carbon Budget (2000-2016)	341	272	276
TRENDYv7 Ensemble (2000-2017)	331	327	289
MsTMIP Ensemble (2000-2010)	341	313	n.a.

Compared to the independent NPP estimates at FLUXNET sites from bottom-up and top-down approaches, the updated MOD17 and VNP17 products also show substantial reductions in annual NPP RMSE over C61 (Table 5); again, VNP17 is very similar to MOD17 in this respect (Table S17). When broken out by PFT (Tables S18-S20), it's clear the updated MOD17 has improved skill in annual NPP for some of the most productive PFTs: EBF (C61 mean RMSE= 717 g C m^{-2} $year^{-1}$, updated MOD17 mean RMSE= 548 average across independent datasets), DBF (C61 mean RMSE= 247, updated MOD17 mean RMSE= 195), and CRO (C61 mean RMSE= 304, updated MOD17 mean RMSE= 272). Most importantly, the overall GPP and NPP magnitudes are very similar between VNP17 and the updated MOD17 (Figure 3).

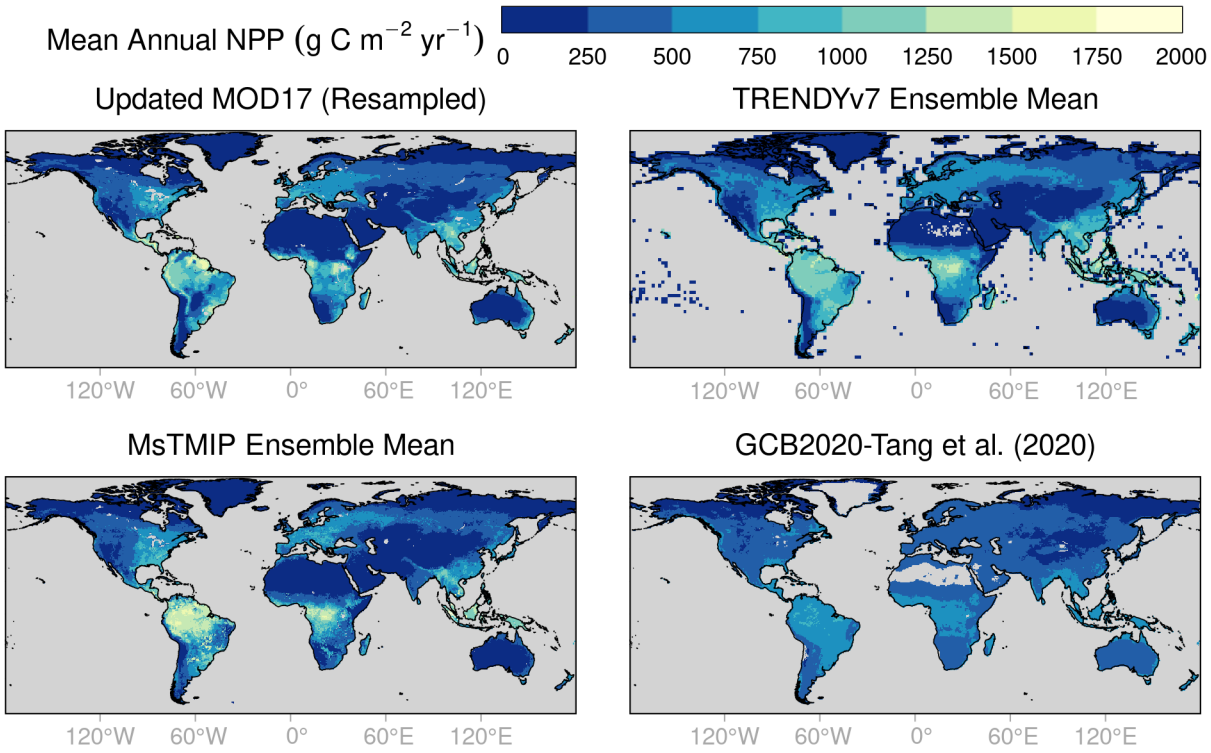

Figure 4: Comparison of mean annual NPP (2000-2010) across four products: the updated MOD17 product, based on the 5-km global simulation and resampled to 0.5-degrees; the TRENDYv7 ensemble mean, at 1-degree resolution; the MsTMIP ensemble mean at 0.5-degrees; and the synthetic NPP estimate from the 2020 Global Carbon Budget and Tang et al. (2020). In the MOD17 image, land areas not simulated in MOD17 (e.g., barren lands) are filled with zero annual NPP.

3.3 Mean, Trend, and Interannual Variability

The mean global GPP flux (2000-2018) in the updated MOD17 product is 127 ±2.8 Pg C year^{-1}, which compares well with that of the TRENDYv7 ensemble mean over the same period (126 ±2.4 Pg C year^{-1}), and is an increase over the estimate from C61 (119 ±2.9 Pg C year^{-1}). If we consider the period 2012-2018, mean global GPP flux from the new VNP17 is quite similar to the updated MOD17 estimate, 129.6 ±1.7 versus 129.7 ±1.7 Pg C year^{-1}, and both are higher than the C61 estimate over the same period (121.6 ±1.6 Pg C year^{-1}). Mean global NPP flux from the new products over 2012-2018 is 58.4-58.5 ±1.1 Pg C year^{-1}, compared to 60.7 ±1.1 in C61 (Table S21).

The updated MOD17 and new VNP17 annual NPP estimates exhibit strong spatial correlation (Figures 4, 5, and S14-S16) with bottom-up estimates from the TRENDYv7 (MOD17 $r = 0.85$, VNP17 $r = 0.86$) and MsTMIP ensembles (MOD17 $r = 0.79$) and also compares well with the top-down, global synthesis of NPP based on the Global Carbon Budget (MOD17 and VNP17 $r = 0.71$). Annual GPP estimates from both products show even stronger spatial correlations with TRENDYv7 (MOD17 and VNP17 $r = 0.91$). In terms of global, interannual NPP and R_A variability, MOD17 compares very well to the TRENDYv7 and MsTMIP ensembles, with the vast majority of the global land domain exhibiting strong, positive correlations (Figure S17); VNP17 IAV is very

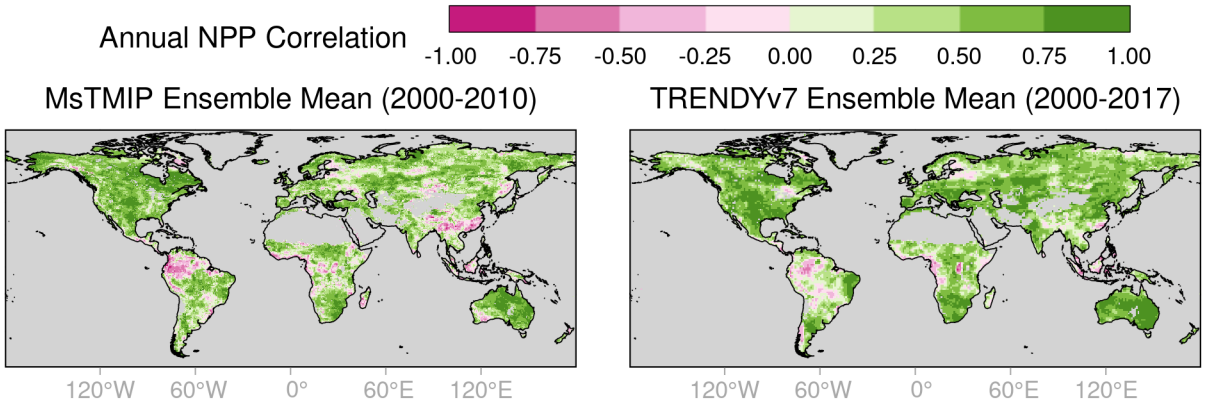

Figure 5: Comparison of interannual correlation in NPP between the updated MOD17 product (based on the 5-km global simulation) and the MsTMIP ensemble mean at 0.5-degrees or the TRENDYv7 ensemble mean at 1-degree resolution. The MOD17 product was resampled to match either product.

similar to that of MOD17 (Figures S18-S21). Negative correlations are found mainly in humid, tropical regions where IAV is low and persistent cloud cover leads to more reliance on fPAR climatology.

We also compared MOD17 C61 and the updated MOD17 to the MsTMIP and TRENDYv7 ensemble means in terms of interannual variation (IAV) in GPP and NPP (Figure 6). All products show a significant, upward trend, based on Theil-Sen median trend estimates. MOD17 C61 and the updated MOD17 display increasing GPP (NPP) trends of 0.45 and 0.47 (0.27 and 0.25) Pg C year^{-2}, respectively, over 2000-2018 compared with 0.41 (0.21) Pg C year^{-2} for the TRENDYv7 ensemble means. Trends are lower in the period 2012-2021; for MOD17 C61, the updated MOD17, and the new VNP17 we find GPP (NPP) trends of 0.38, 0.44, and 0.35 (0.17, 0.13, 0.11) Pg C year^{-2}. For the unified period of 2000-2010 (VNP17 drops out), both MOD17 products show greater IAV in GPP and NPP than MsTMIP and TRENDYv7. The IAV is slightly lower in the updated MOD17 compared to C61, which may reflect the bias-variance trade-off, i.e., a tendency in model calibration toward a narrower range of parameter variability.

3.4 Uncertainty Analysis

The error propagation indicates that a substantial portion of the error in daily and annual GPP estimates comes from error in fPAR (Tables S22, S23); at least 1.0 g C m^{-2} day^{-1} for all PFTs and greater than 1.5 g C m^{-2} day^{-1} for most. Uncertainty in $\varepsilon_{\max}$ is a negligible part of the error in GPP estimates, accounting for less than 0.12 g C m^{-2} day^{-1} in both MOD17 and VNP17, though with the greatest impact on EBF. The magnitude of the fPAR error contribution is generally proportional to the total error by PFT.

The error budget for annual NPP estimates generally corresponds to the sensitivity analysis: uncertainty in SLA is usually the largest source of error in NPP estimates, among free parameters (Tables S24, S25). However, some PFTs have large error contributions from other parameters. Uncertainty in `Q10_froot` is a major contributor to uncertainty in annual NPP for both ENF and EBF and the greatest contributor for CRO. Uncertainty in `froot_mr_base` is a major source of uncertainty in ENF and GRS, while uncertainty in `leaf_mr_base` is a major source for WSV. Uncertainty in SLA has surprisingly little impact on annual NPP estimates in shrublands; no model parameters an-

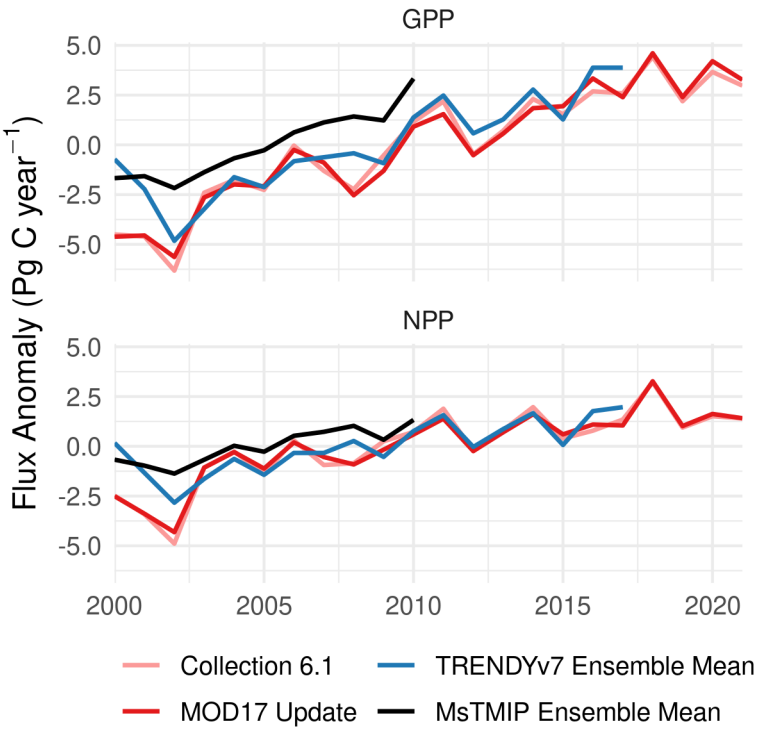

Figure 6: Interannual variation (IAV) in GPP, NPP (annual flux minus interannual mean) for the MOD17 products, shown alongside that of the Multi-Scale Synthesis and Terrestrial Model Intercomparison Project (MsTMIP) and TRENDYv7 ensemble means.

alyzed here contributed major uncertainty to estimates for this PFT, which is found predominantly at high latitudes.

4 Discussion

Prudent use of models requires that they are regularly evaluated, checking both the model predictions (validation) and assumptions (verification) against independent data. MOD17 is a good candidate for continued use in the VIIRS era, but requires validation and verification to contextualize its estimates of ecosystem productivity. Here, independent data on plant traits have been combined with GPP and NPP measurements from flux towers and field surveys to improve both the accuracy and the realism of MOD17.

4.1 Inferring the Optimal Biome Properties

Retrospectively, plant trait data from TRY and the literature allow for a qualitative validation of the MOD17 Collection 6.1 (C61) BPLUT. We found that maximum LUE ($\varepsilon_{\max}$) compared well to the global optimum LUE defined by Madani et al. (2017) for most PFTs, but C61 $\varepsilon_{\max}$ is likely too high for shrubland and savanna, and too low for croplands (Gan et al., 2021). Some studies have suggested higher $\varepsilon_{\max}$ in ENF (Coops et al., 2007) and in shrublands (J. Chen et al., 2014) while others find, as indicated here, it should be lower (Yuan et al., 2014; Madani et al., 2017). Previous generations of the MOD17 BPLUT used a comparatively small number of EC towers (and years of observation) in calibration, which may have led to biased $\varepsilon_{\max}$ estimates. Even among the expanded FLUXNET collection, there are only five CSH tower sites, three of which are within 2 km of one another, and all in regions of high aridity. Overall, lower $\varepsilon_{\max}$ in arid regions is expected (Garbulsky et al., 2010). This may explain the severe decrease in $\varepsilon_{\max}$ for CSH, relative to the C61 BPLUT, which is greater than the corresponding decrease in the better-represented OSH canopy.

While the TRY database indicates that R_M for all tissues should be higher than that of the C61 BPLUT (Figure S9, Table S7), posterior estimates are generally somewhere in the middle. Livewood R_M in C61 is close to that indicated by TRY. SLA in the C61 BPLUT also compares well to prior observations from TRY for evergreen and herbaceous (GRS and CRO) canopies but is too low otherwise. SLA values from TRY may seem high compared to field measurements of SLA (e.g., leaf area per unit leaf dry mass) but are consistent with the range of SLA in C terms (leaf area per unit leaf C), as the TRY database includes many values above 100 m^2 kg C^{-1} (Figure S8). Posterior SLA values also compare very well to a review by Wright and Westoby (2001).

The peculiarities of calibration results for CSH point to a larger issue with MOD17: too many poorly defined PFTs. Given that CSH is a tiny proportion (0.2%) of the global land surface (Madani et al., 2017), it is reasonable to ask whether this class should be combined with OSH in a global "Shrublands" class. This is especially salient in light of evidence that multiple PFTs may be over-differentiated (Yuan et al., 2014) and that environmental filtering (Funk et al., 2017) may lead to more robust plant response than static and somewhat arbitrary functional types (Y. Liu et al., 2021). One practical consequence is that the prior mean for SLA in both OSH and CSH may be too high, as indicated by the low posterior R_M rates in these PFTs.

Our uncertainty analysis of the NPP sub-model largely follows the sensitivity analysis but also emphasizes where parameters could be better constrained. SLA is the most important parameter for NPP estimation in MOD17 as, despite its relatively high certainty (Figure S9, based on prior information from TRY), it has the greatest impact on NPP error. Leaf properties in croplands are particularly uncertain (Figure S22), likely due to the wide variety of global crop types. Future LUE models like MOD17 might ben-

efit from modeling SLA instead of using a fixed value, given the sensitivity of SLA to phenology and environmental conditions (Gong & Gao, 2019; Z. Liu et al., 2022).

4.2 Performance of Global GPP and NPP Products

Relative to C61, model-data fusion lead to improvements in 8-day and annual GPP and annual NPP flux estimates, based on reserved EC tower data, NPP cross-validation with field data, and independent bottom-up and top-down NPP estimates. Since 2012, the persistent negative GPP bias of MOD17 was reduced by at least 0.5 g C m^{-2} day^{-1} and by over 50 g C m^{-2} $year^{-1}$; over a longer record, bias was reduced by more than twice as much (Table 4). These improvements put the updated MOD17 and new VNP17 8-day GPP product on par with other data-driven approaches combining satellite and flux-tower data (Joiner et al., 2018). Global annual GPP flux estimates in the new products (mean 2012-2021 annual GPP flux of 130 ±1.5 Pg C $year^{-1}$) are higher than the estimates of C61 (122 ±1.4 Pg C $year^{-1}$) and other satellite-based estimates but are more in line with oxygen isotope studies (Welp et al., 2011), recent syntheses (J. M. Chen et al., 2012; Piao et al., 2013; Anav et al., 2015) (Figure 7), and bottom-up studies (Madani et al., 2018, 2020), particularly for years since 2012 (Y. Zhang, Xiao, et al., 2017). The new GPP estimates also agree better with TRENDYv7 (128.6 ±1.4 for 2012-2021).

Annual NPP skill (nRMSE) was improved by almost 2 percentage points, a reduction in RMSE of about 30 g C m^{-2} $year^{-1}$. The updated and new products' reduction in global annual NPP flux (58.4-58.6 ±0.9 Pg C $year^{-1}$ for 2012-2021) is more consistent with estimates from the MsTMIP ensemble and combined results from the Global Carbon Budget (2020) and up-scaled soil respiration data (X. Tang et al., 2020); it's also closer than C61 to the estimate from the meta-analysis by Ito (2011) (56.2 ±14.3 Pg C $year^{-1}$). However, the mean annual NPP flux from the TRENDYv7 ensemble mean is higher and closer to the original estimate of MOD17 C61 (Table S21), as is the median of the spread in TRENDYv7 models (Figure 7). The inter-model spread of TRENDYv7 and earlier syntheses (Cramer et al., 1999; Ito, 2011) suggests persistent high uncertainty in any model's representation of terrestrial NPP. It also suggests at least the possibility that the field estimates of NPP used here (Table 3) may not be too large, despite concerns about their reliability and representativeness (Clark et al., 2001; Zhao et al., 2006).

The greatest strength of the MOD17 and VNP17 products is their long period of record, allowing an examination of interannual variability and trends. The strong increase in NPP observed over 2000-2010 (Figure 6) is inconsistent with the report of a reduction in NPP by Zhao and Running (2010). This could be attributed to a difference in the climate drivers used in different versions of MOD17 and the sensitivity of GPP to prevailing weather conditions (Zhao et al., 2006). The 1-km estimates of MOD17 Collection 5.1, from 2000 to 2015, used by Zhao and Running (2010) were driven by NCEP reanalysis data (Kanamitsu et al., 2002) whereas the operational MOD17 (and future VNP17) products use GMAO data; these differences have led to different anomalies in GPP and NPP (Zhao et al., 2005). The uncertainty in LUE models like MOD17 due to climate drivers merits further exploration.

However, even after recalibration, MOD17 and the new VNP17 GPP products still show large negative biases (Table 4). Previous studies have established that MOD17 generally under-estimates GPP (Heinsch et al., 2006; Coops et al., 2007; Propastin et al., 2012; Sjöström et al., 2013; J. Chen et al., 2014; Huang et al., 2018), especially in grasslands (Zhu et al., 2018) and in highly productive regions (Wang & Ogawa, 2017), and that this may be explained by a failure to account for diffuse PAR (Guan et al., 2022). Although it has been suggested that $\varepsilon_{\max}$ should be increased (Wang & Ogawa, 2017; Huang et al., 2018), this model-data fusion is consistent with the previous global analysis of Madani et al. (2017) indicating that $\varepsilon_{\max}$ should be *decreased* for low-productivity shrublands and savannas and *increased* in DBF, MF, and croplands, relative to C61. This

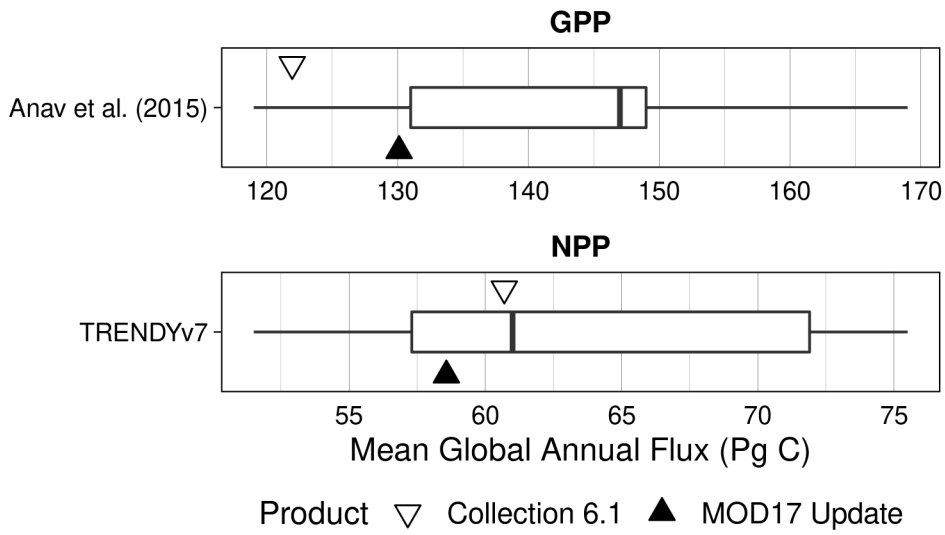

Figure 7: Comparison of MOD17 and VNP17 annual GPP and NPP fluxes with estimates from different models, as synthesized by Anav et al. (2015), for GPP, or represented by the inter-model spread of NPP estimates from the TRENDYv7 ensemble.

may reflect subsequent improvements in the gap-filled MOD15A2HGF fPAR and LAI data. Notably, the updated MOD17 and new VNP17 BPLUT both substantially reduced the negative bias in croplands, which was found to be severe in Collection 6 (Huang et al., 2018).

Annual NPP estimates were improved, over C61, to a greater degree than 8-day or annual GPP estimates (reduction in nRMSE of 0.4-1.0% for GPP but 1.2-1.9% for NPP), likely because there are more parameters to optimize in the NPP model. However, in the updated MOD17 and new VNP17 products, there is a large negative bias in ENF, likely introduced when fine-root R_M was increased to reduce the spuriously high CUE that emerged from global simulations. Leaf R_M and SLA (based on prior information from hundreds of species in TRY) are already both low for this PFT and the cross-validation RMSE is very low (compared to other PFTs); consequently, there are few options to mitigate this bias and avoid unrealistically high CUE values. The simultaneous improvement in annual NPP RMSE but decline in correlation likely reflects the sensitivity of NPP to local conditions that may not be adequately reflected by the 11 PFTs used in MOD17.

Another source of NPP variability is the variation in plant traits (and BPLUT parameters) themselves, over time and along environmental gradients, which is currently not reflected in the MOD17 model structure. SLA has been shown to vary with moisture and nutrient availability (Dwyer et al., 2014), and the spatial and temporal variation in SLA, if accounted for, might reduce estimated NPP magnitudes (Verheijen et al., 2015). It has also been established that fine-root respiration is at least partly coupled with canopy photosynthetic uptake (Högberg et al., 2001; Drake et al., 2008; Lynch et al., 2013).

How do the new products compare to previous generations? It is difficult to compare to previous performance assessments in carbon units (e.g., RMSE) because the quantity depends on the relative productivity of the EC tower sites included; more produc-

tive sites would generally lead to a higher RMSE. For example, the high RMSE of 8-day GPP in croplands (Table 13) exaggerates the overall RMSE estimated here (Table 4). As an alternative, normalized quantities have been used inconsistently, and while "relative error" (Heinsch et al., 2006) is a common choice, it is also highly sensitive to very low EC tower flux magnitudes. We suggest that only normalized RMSE, relative to the reported range of tower observations, be compared to other assessments. These would suggest that C61 is an improvement over earlier versions and the updated MOD17 BPLUT a further improvement. R. Tang et al. (2015), for example, find Collection 6 annual GPP biases generally twice as large as estimated here for C61, and nRMSE values significantly higher as well, based on less than half as many EC tower sites. Sjöström et al. (2013) found an overall Collection 5.1 GPP RMSE, compared to flux towers in Africa, of 2.58 g C m^{-1} d^{-1}, higher than our estimate of 2.25 g C m^{-1} d^{-1} for C61. The performance is sensitive to the driver data used and is generally much better when tower-observed surface meteorology is used (Coops et al., 2007; J. Chen et al., 2014), though some have found otherwise (Wang & Ogawa, 2017).

Error propagation indicates that error in MOD17 and VNP17 GPP estimates is primarily due to error in fPAR retrievals, as in multiple previous studies (Propastin et al., 2012; Fu et al., 2017; Wang & Ogawa, 2017). Given the low sensitivity of these models to environmental scalars, this suggests that dynamic changes in MOD17 modeled GPP are largely a function of changes in canopy extent and vigor, conveyed by changes in fPAR. This feature of LUE models has been an advantage during the EOS era and allowed models like MOD17 to capture trends in the land carbon sink (Figure 6) that are otherwise missed by purely data-driven approaches like FLUXCOM (Yang et al., 2022). And yet, given the modest improvement in the new MOD17 product compared to C61, it's also apparent that the accuracy of these global LUE models is strongly tied to the quality of input datasets, in addition to uncertainty in model parameters and model structure.

5 Conclusion

We combined prior information on plant productivity and respiration traits with eddy covariance estimates of GPP and field estimates of NPP for the recalibration of MOD17, the first model to provide global, continuous, weekly estimates of ecosystem productivity. This effort culminated in the final reprocessing of MODIS MOD17 and the development of new VNP17 GPP and NPP products based on VIIRS data. Relative to the current MODIS C61 MOD17 data, the updated MOD17 parameters substantially reduce the negative bias in 8-day GPP, by more than 1.2 g C m^{-2} day^{-1}; the RMSE in annual GPP was reduced by 42 g C m^{-2} $year^{-1}$ and RMSE in annual NPP was reduced by 36 g C m^{-2} $year^{-1}$ while maintaining or improving global correlations in the spatial pattern of GPP and NPP fluxes.

The combined records of the updated MOD17 and new VNP17 products enable weekly-to-annual terrestrial productivity estimates to be continued through 2030 and beyond. The updated estimates of mean global GPP and NPP for 2012-2021, 130.1 $\pm$1.6 and 58.6 $\pm$0.9 (respectively) agree very well with other bottom-up estimates. The long, extant record of MOD17 and VNP17 indicate that terrestrial productivity is increasing over recent decades (2000-2018), with GPP increasing annually by 0.47 Pg C $year^{-2}$ and NPP by 0.25 Pg C $year^{-2}$. These trends are supported by independent, bottom-up estimates and all the models examined here do indicate that the rate of increase in GPP and NPP may be slowing down in recent years.

Open Research Section

The 5-km global simulation outputs (for both MOD17 and the new VNP17) and the driver data required to run, calibrate, and validate MOD17 at FLUXNET sites (with the exception of tower fluxes, which we are not licensed to reproduce) are available at

697 <https://doi.org/10.5281/zenodo.7682806>. The repository of the MOD17 algo-
698 rithm's Python and C source code is available on GitHub at <https://github.com/arthur-e/MOD17>.

699 **Acknowledgments**
700 This study was supported by a grant from NASA (NNH20ZDA001N-SNPPSP).

References

Anav, A., Friedlingstein, P., Beer, C., Ciais, P., Harper, A., Jones, C., … Zhao, M. (2015, September). Spatiotemporal patterns of terrestrial gross primary production: A review. *Reviews of Geophysics*, *53*(3), 785–818. Retrieved from http://doi.wiley.com/10.1002/2015RG000483 doi: 10.1002/2015RG000483

Atkin, O. K., Edwards, E. J., & Loveys, B. R. (2000, July). Response of root respiration to changes in temperature and its relevance to global warming. *New Phytologist*, *147*(1), 141–154. Retrieved from http://doi.wiley.com/10.1046/j.1469-8137.2000.00683.x doi: 10.1046/j.1469-8137.2000.00683.x

Bahn, M., Knapp, M., Garajova, Z., Pfahringer, N., & Cernusca, A. (2006, June). Root respiration in temperate mountain grasslands differing in land use. *Global Change Biology*, *12*(6), 995–1006. Retrieved 2022-06-27, from https://onlinelibrary.wiley.com/doi/10.1111/j.1365-2486.2006.01144.x doi: 10.1111/j.1365-2486.2006.01144.x

Balch, J. K., Bradley, B. A., Abatzoglou, J. T., Nagy, R. C., Fusco, E. J., & Mahood, A. L. (2017, March). Human-started wildfires expand the fire niche across the United States. *Proceedings of the National Academy of Sciences*, *114*(11), 2946–2951. Retrieved 2022-07-29, from https://pnas.org/doi/full/10.1073/pnas.1617394114 doi: 10.1073/pnas.1617394114

Baldocchi, D. (2008). 'Breathing' of the terrestrial biosphere: lessons learned from a global network of carbon dioxide flux measurement systems. *Australian Journal of Botany*, *56*(1), 1. Retrieved from http://www.publish.csiro.au/?paper=BT07151 doi: 10.1071/BT07151

Baldocchi, D., Falge, E., Gu, L., Olson, R., Hollinger, D., Running, S., … Wofsy, S. (2001, November). FLUXNET: A new tool to study the temporal and spatial variability of ecosystem–scale carbon dioxide, water vapor, and energy flux densities. *Bulletin of the American Meteorological Society*, *82*(11), 2415–2434. Retrieved from http://journals.ametsoc.org/doi/10.1175/1520-0477(2001)082%3C2415:FANTTS%3E2.3.CO;2 (ISBN: 0003-0007) doi: 10.1175/1520-0477(2001)082<2415:FANTTS>2.3.CO;2

Barrett, D. J. (2012). NPP Multi-Biome: VAST Calibration Data, 1965-1998, R1. Retrieved from http://daac.ornl.gov/cgi-bin/dsviewer.pl?ds_id=576 (Publisher: ORNL Distributed Active Archive Center) doi: 10.3334/ORNLDAAC/576

Bolstad, P. V., Davis, K. J., Martin, J., Cook, B. D., & Wang, W. (2004, May). Component and whole-system respiration fluxes in northern deciduous forests. *Tree Physiology*, *24*(5), 493–504. Retrieved 2022-06-24, from https://academic.oup.com/treephys/article-lookup/doi/10.1093/treephys/24.5.493 doi: 10.1093/treephys/24.5.493

Bridgewater, S., Ibáñez, A., Ratter, J. A., & Furley, P. (2002, November). Vegetation classification and floristics of the savannas and associated wetlands of the Rio Bravo Conservation and Management Area, Belize. *Edinburgh Journal of Botany*, *59*(3), 421–442. Retrieved 2022-05-06, from https://journals.rbge.org.uk/ejb/article/view/1265 doi: 10.1017/S0960428602000252

Burton, A. J., Melillo, J. M., & Frey, S. D. (2008). Adjustment of forest ecosystem root respiration as temperature warms. *Journal of Integrative Plant Biology*, *50*(11), 1467–1483. doi: 10.1111/j.1744-7909.2008.00750.x

Campioli, M., Vicca, S., Luyssaert, S., Bilcke, J., Ceschia, E., Chapin III, F. S., … Janssens, I. A. (2015, November). Biomass production efficiency controlled by management in temperate and boreal ecosystems. *Nature Geoscience*, *8*(11), 843–846. Retrieved 2022-07-18, from http://www.nature.com/articles/ngeo2553 doi: 10.1038/ngeo2553

Chen, J., Zhang, H., Liu, Z., Che, M., & Chen, B. (2014, April). Evaluating pa-

rameter adjustment in the MODIS gross primary production algorithm based on eddy covariance tower measurements. *Remote Sensing*, *6*(4), 3321–3348. Retrieved 2022-07-20, from http://www.mdpi.com/2072-4292/6/4/3321 doi: 10.3390/rs6043321

Chen, J. M., Mo, G., Pisek, J., Liu, J., Deng, F., Ishizawa, M., & Chan, D. (2012, March). Effects of foliage clumping on the estimation of global terrestrial gross primary productivity. *Global Biogeochemical Cycles*, *26*(1), n/a–n/a. Retrieved 2023-01-29, from http://doi.wiley.com/10.1029/2010GB003996 doi: 10.1029/2010GB003996

Chu, H., Luo, X., Ouyang, Z., Chan, W. S., Dengel, S., Biraud, S. C., … Zona, D. (2021). Representativeness of eddy-covariance flux footprints for areas surrounding AmeriFlux sites. *Agricultural and Forest Meteorology*, *301-302*(February). doi: 10.1016/j.agrformet.2021.108350

Clark, D. A., Brown, S., Kicklighter, D. W., Chambers, J. Q., Thomlinson, J. R., & Ni, J. (2001, April). Measuring net primary production in forests: Concepts and field methods. *Ecological Applications*, *11*(2), 356–370. Retrieved 2023-02-02, from http://doi.wiley.com/10.1890/1051-0761(2001)011[0356:MNPPIF]2.0.CO;2 doi: 10.1890/1051-0761(2001)011[0356:MNPPIF]2.0.CO;2

Collalti, A., & Prentice, I. C. (2019). Is NPP proportional to GPP? Waring's hypothesis 20 years on. *Tree Physiology*, *39*(8), 1473–1483. doi: 10.1093/treephys/tpz034

Coops, N. C., Jassal, R. S., Leuning, R., Black, A. T., & Morgenstern, K. (2007, December). Incorporation of a soil water modifier into MODIS predictions of temperate Douglas-fir gross primary productivity: Initial model development. *Agricultural and Forest Meteorology*, *147*(3-4), 99–109. Retrieved 2022-07-20, from https://linkinghub.elsevier.com/retrieve/pii/S0168192307001700 doi: 10.1016/j.agrformet.2007.07.001

Cramer, W., Kicklighter, D. W., Bondeau, A., Iii, B. M., Churkina, G., Nemry, B., … Intercomparison, T. P. O. T. P. (1999, April). Comparing global models of terrestrial net primary productivity (NPP): overview and key results. *Global Change Biology*, *5*(S1), 1–15. Retrieved 2023-02-02, from https://onlinelibrary.wiley.com/doi/10.1046/j.1365-2486.1999.00009.x doi: 10.1046/j.1365-2486.1999.00009.x

Damesin, C., Ceschia, E., Le Goff, N., Ottorini, J. M., & Dufrêne, E. (2002, January). Stem and branch respiration of beech: from tree measurements to estimations at the stand level. *New Phytologist*, *153*(1), 159–172. Retrieved 2022-06-24, from http://doi.wiley.com/10.1046/j.0028-646X.2001.00296.x doi: 10.1046/j.0028-646X.2001.00296.x

DeAngelis, D. L., Gardner, R. H., & Shugart, H. H. (2012). NPP Multi-Biome: Global IBP Woodlands Data, 1955-1975, R1. Retrieved from http://daac.ornl.gov/cgi-bin/dsviewer.pl?ds_id=198 (Publisher: ORNL Distributed Active Archive Center) doi: 10.3334/ORNLDAAC/198

Dennisenko, E. A., Brovkin, V., & Cramer, W. P. (2012). NPP Multi-Biome: PIK Data for Northern Eurasia, 1940-1988 (Based on Bazilevich), R1. Retrieved from http://daac.ornl.gov/cgi-bin/dsviewer.pl?ds_id=575 (Publisher: ORNL Distributed Active Archive Center) doi: 10.3334/ORNLDAAC/575

Desrochers, A., Landhausser, S. M., & Lieffers, V. J. (2002, July). Coarse and fine root respiration in aspen (Populus tremuloides). *Tree Physiology*, *22*(10), 725–732. Retrieved 2022-06-27, from https://academic.oup.com/treephys/article-lookup/doi/10.1093/treephys/22.10.725 doi: 10.1093/treephys/22.10.725

Drake, J. E., Stoy, P. C., Jackson, R. B., & DeLucia, E. H. (2008, November). Fine-root respiration in a loblolly pine (Pinus taeda L.) forest exposed to elevated CO2 and N fertilization. *Plant, Cell & Environment*, *31*(11), 1663–1672. Retrieved 2022-07-13, from https://onlinelibrary.wiley.com/doi/10.1111/

j.1365-3040.2008.01869.x doi: 10.1111/j.1365-3040.2008.01869.x

Dwyer, J. M., Hobbs, R. J., & Mayfield, M. M. (2014, February). Specific leaf area responses to environmental gradients through space and time. *Ecology*, *95*(2), 399–410. Retrieved 2022-06-03, from http://doi.wiley.com/10.1890/13-0412.1 doi: 10.1890/13-0412.1

Díaz, S., Kattge, J., Cornelissen, J. H. C., Wright, I. J., Lavorel, S., Dray, S., … Gorné, L. D. (2016, January). The global spectrum of plant form and function. *Nature*, *529*(7585), 167–171. Retrieved from http://www.nature.com/articles/nature16489 doi: 10.1038/nature16489

Erb, K.-H., Kastner, T., Plutzar, C., Bais, A. L. S., Carvalhais, N., Fetzel, T., … Luyssaert, S. (2018, January). Unexpectedly large impact of forest management and grazing on global vegetation biomass. *Nature*, *553*(7686), 73–76. Retrieved 2022-07-29, from http://www.nature.com/articles/nature25138 doi: 10.1038/nature25138

Esser, G. (2013). NPP Multi-Biome: Global Osnabruck Data, 1937-1981, R1. Retrieved from http://daac.ornl.gov/cgi-bin/dsviewer.pl?ds_id=214 (Publisher: ORNL Distributed Active Archive Center) doi: 10.3334/ORNLDAAC/214

FAO. (2010). *Appendix 4: Alphabetical List of Crops with Botanical Name and Crop Code* (Tech. Rep.). Retrieved 2022-06-17, from https://www.fao.org/fileadmin/templates/ess/documents/world_census_of_agriculture/appendix4_r7.pdf

Friedl, M., & Sulla-Menashe, D. (2019). MCD12Q1 MODIS/Terra+Aqua Land Cover Type Yearly L3 Global 500m SIN Grid V006 [Data set]. doi: https://doi.org/10.5067/MODIS/MCD12Q1.006

Friedlingstein, P., O'Sullivan, M., Jones, M. W., Andrew, R. M., Hauck, J., Olsen, A., … Zaehle, S. (2020, December). Global Carbon Budget 2020. *Earth System Science Data*, *12*(4), 3269–3340. Retrieved from https://essd.copernicus.org/articles/12/3269/2020/ doi: 10.5194/essd-12-3269-2020

Fu, G., Zhang, J., Shen, Z.-X., Shi, P.-L., He, Y.-T., & Zhang, X.-Z. (2017, August). Validation of collection of 6 MODIS/Terra and MODIS/Aqua gross primary production in an alpine meadow of the Northern Tibetan Plateau. *International Journal of Remote Sensing*, *38*(16), 4517–4534. Retrieved 2022-07-14, from https://www.tandfonline.com/doi/full/10.1080/01431161.2017.1323283 doi: 10.1080/01431161.2017.1323283

Funk, J. L., Larson, J. E., Ames, G. M., Butterfield, B. J., Cavender-Bares, J., Firn, J., … Wright, J. (2017). Revisiting the Holy Grail: Using plant functional traits to understand ecological processes. *Biological Reviews*, *92*(2), 1156–1173. (ISBN: 1714744795) doi: 10.1111/brv.12275

Gan, R., Zhang, L., Yang, Y., Wang, E., Woodgate, W., Zhang, Y., … Yu, Q. (2021, October). Estimating ecosystem maximum light use efficiency based on the water use efficiency principle. *Environmental Research Letters*, *16*(10), 104032. Retrieved 2022-07-20, from https://iopscience.iop.org/article/10.1088/1748-9326/ac263b doi: 10.1088/1748-9326/ac263b

Garbulsky, M. F., Peñuelas, J., Papale, D., Ardö, J., Goulden, M. L., Kiely, G., … Filella, I. (2010, March). Patterns and controls of the variability of radiation use efficiency and primary productivity across terrestrial ecosystems. *Global Ecology and Biogeography*, *19*(2), 253–267. Retrieved from http://doi.wiley.com/10.1111/j.1466-8238.2009.00504.x doi: 10.1111/j.1466-8238.2009.00504.x

Gelaro, R., McCarty, W., Suárez, M. J., Todling, R., Molod, A., Takacs, L., … Zhao, B. (2017, July). The Modern-Era Retrospective Analysis for Research and Applications, Version 2 (MERRA-2). *Journal of Climate*, *30*(14), 5419–5454. Retrieved from http://journals.ametsoc.org/doi/10.1175/JCLI-D-16-0758.1 doi: 10.1175/JCLI-D-16-0758.1

Gong, H., & Gao, J. (2019, October). Soil and climatic drivers of plant SLA (specific leaf area). *Global Ecology and Conservation*, *20*, e00696. Retrieved 2022-07-20, from https://linkinghub.elsevier.com/retrieve/pii/S2351989419302665 doi: 10.1016/j.gecco.2019.e00696

Gower, S. T., Krankina, O. N., Olson, R. J., Apps, M. J., Linder, S., & Wang, C. (2012). NPP Boreal Forest: Consistent Worldwide Site Estimates, 1965-1995, R1. Retrieved from http://daac.ornl.gov/cgi-bin/dsviewer.pl?ds_id=611 (Publisher: ORNL Distributed Active Archive Center) doi: 10.3334/ORNLDAAC/611

Gower, S. T., & Richards, J. H. (1990, December). Larches: Deciduous Conifers in an Evergreen World. *BioScience*, *40*(11), 818–826. Retrieved 2022-12-19, from https://academic.oup.com/bioscience/article-lookup/doi/10.2307/1311484 doi: 10.2307/1311484

Guan, X., Chen, J. M., Shen, H., Xie, X., & Tan, J. (2022, February). Comparison of big-leaf and two-leaf light use efficiency models for GPP simulation after considering a radiation scalar. *Agricultural and Forest Meteorology*, *313*, 108761. Retrieved 2022-07-20, from https://linkinghub.elsevier.com/retrieve/pii/S0168192321004470 doi: 10.1016/j.agrformet.2021.108761

Heinsch, F. A., Zhao, M., Running, S. W., Kimball, J. S., Nemani, R. R., Davis, K. J., … Flanagan, L. B. (2006, July). Evaluation of remote sensing based terrestrial productivity from MODIS using regional tower eddy flux network observations. *IEEE Transactions on Geoscience and Remote Sensing*, *44*(7), 1908–1923. Retrieved from http://ieeexplore.ieee.org/document/1645290/ doi: 10.1109/TGRS.2005.853936

Herman, J., & Usher, W. (2017, January). SALib: An open-source Python library for Sensitivity Analysis. *The Journal of Open Source Software*, *2*(9), 97. Retrieved 2022-06-18, from http://joss.theoj.org/papers/10.21105/joss.00097 doi: 10.21105/joss.00097

Huang, X., Ma, M., Wang, X., Tang, X., & Yang, H. (2018, December). The uncertainty analysis of the MODIS GPP product in global maize croplands. *Frontiers of Earth Science*, *12*(4), 739–749. Retrieved 2023-01-25, from http://link.springer.com/10.1007/s11707-018-0716-x doi: 10.1007/s11707-018-0716-x

Huntzinger, D. N., Schwalm, C., Michalak, A. M., Schaefer, K., King, A. W., Wei, Y., … Zhu, Q. (2013, December). The North American Carbon Program Multi-Scale Synthesis and Terrestrial Model Intercomparison Project – Part 1: Overview and experimental design. *Geoscientific Model Development*, *6*(6), 2121–2133. Retrieved 2014-01-23, from http://www.geosci-model-dev.net/6/2121/2013/ doi: 10.5194/gmd-6-2121-2013

Högberg, P., Nordgren, A., Buchmann, N., Taylor, A. F. S., Ekblad, A., Högberg, M. N., … Read, D. J. (2001, June). Large-scale forest girdling shows that current photosynthesis drives soil respiration. *Nature*, *411*(6839), 789–792. Retrieved from http://www.nature.com/articles/35081058 doi: 10.1038/35081058

Ito, A. (2011, October). A historical meta-analysis of global terrestrial net primary productivity: are estimates converging?: A HISTORICAL META-ANALYSIS OF GLOBAL LAND NPP. *Global Change Biology*, *17*(10), 3161–3175. Retrieved 2023-02-02, from https://onlinelibrary.wiley.com/doi/10.1111/j.1365-2486.2011.02450.x doi: 10.1111/j.1365-2486.2011.02450.x

Iversen, C. M., McCormack, M. L., Powell, A. S., Blackwood, C. B., Freschet, G. T., Kattge, J., … Violle, C. (2017, July). A global Fine-Root Ecology Database to address below-ground challenges in plant ecology. *New Phytologist*, *215*(1), 15–26. Retrieved 2022-05-17, from https://onlinelibrary.wiley.com/doi/10.1111/nph.14486 doi: 10.1111/nph.14486

Iwanaga, T., Usher, W., & Herman, J. (2022). Toward SALib 2.0: Advancing the accessibility and interpretability of global sensitivity analyses. *Socio-Environmental Systems Modeling*, *4*. doi: https://doi.org/10.18174/sesmo.18155

Ji, Y., Zhou, G., Luo, T., Dan, Y., Zhou, L., & Lv, X. (2020, December). Variation of net primary productivity and its drivers in China's forests during 2000–2018. *Forest Ecosystems*, *7*(1), 15. Retrieved 2022-08-03, from https://forestecosyst.springeropen.com/articles/10.1186/s40663-020-00229-0 doi: 10.1186/s40663-020-00229-0

Joiner, J., Yoshida, Y., Zhang, Y., Duveiller, G., Jung, M., Lyapustin, A., … Tucker, C. (2018, August). Estimation of Terrestrial Global Gross Primary Production (GPP) with Satellite Data-Driven Models and Eddy Covariance Flux Data. *Remote Sensing*, *10*(9), 1346. Retrieved 2023-01-29, from http://www.mdpi.com/2072-4292/10/9/1346 doi: 10.3390/rs10091346

Jones, L. A., Kimball, J. S., Reichle, R. H., Madani, N., Glassy, J., Ardizzone, J. V., … Scott, R. L. (2017). The SMAP Level 4 Carbon Product for Monitoring Ecosystem Land-Atmosphere CO2 Exchange. *IEEE Transactions on Geoscience and Remote Sensing*, *55*(11), 6517–6532. (ISBN: 9781509033324) doi: 10.1109/TGRS.2017.2729343

Jones, M. O., Running, S. W., Kimball, J. S., Robinson, N. P., & Allred, B. W. (2020, December). Terrestrial primary productivity indicators for inclusion in the National Climate Indicators System. *Climatic Change*, *163*(4), 1855–1868. Retrieved from http://link.springer.com/10.1007/s10584-018-2155-9 doi: 10.1007/s10584-018-2155-9

Jung, M., Schwalm, C., Migliavacca, M., Walther, S., Camps-Valls, G., Koirala, S., … Reichstein, M. (2020). Scaling carbon fluxes from eddy covariance sites to globe: Synthesis and evaluation of the FLUXCOM approach. *Biogeosciences*, *17*(5), 1343–1365. doi: 10.5194/bg-17-1343-2020

Justice, C., Townshend, J. R. G., Vermote, E. F., Masuoka, E., Wolfe, R., Saleous, N., … Morisette, J. T. (2002, November). An overview of MODIS Land data processing and product status. *Remote Sensing of Environment*, *83*(1-2), 3–15. Retrieved 2022-07-04, from https://linkinghub.elsevier.com/retrieve/pii/S0034425702000846 doi: 10.1016/S0034-4257(02)00084-6

Kanamitsu, M., Ebisuzaki, W., Woollen, J., Yang, S.-K., Hnilo, J. J., Fiorino, M., & Potter, G. L. (2002, November). NCEP–DOE AMIP-II Reanalysis (R-2). *Bulletin of the American Meteorological Society*, *83*(11), 1631–1644. Retrieved 2023-02-14, from https://journals.ametsoc.org/doi/10.1175/BAMS-83-11-1631 doi: 10.1175/BAMS-83-11-1631

Kattge, J., Bönisch, G., Díaz, S., Lavorel, S., Prentice, I. C., Leadley, P., … ... (2020). TRY plant trait database – enhanced coverage and open access. *Global Change Biology*, *26*(1), 119–188. doi: 10.1111/gcb.14904

Kicklighter, D. W. (2012). NPP Multi-Biome: TEM Calibration Data, 1992, R1. Retrieved from http://daac.ornl.gov/cgi-bin/dsviewer.pl?ds_id=471 (Publisher: ORNL Distributed Active Archive Center) doi: 10.3334/ORNLDAAC/471

Kicklighter, D. W., Bruno, M., DZönges, S., Esser, G., Heimann, M., Helfrich, J., … Würth, G. (1999, January). A first-order analysis of the potential role of CO2 fertilization to affect the global carbon budget: A comparison of four terrestrial biosphere models. *Tellus B: Chemical and Physical Meteorology*, *51*(2), 343–366. Retrieved from https://www.tandfonline.com/doi/full/10.3402/tellusb.v51i2.16303 doi: 10.3402/tellusb.v51i2.16303

Kloeppel, B. D., Treichel, I. W., Kharuk, S., & Gower, S. T. (1998, April). Foliar carbon isotope discrimination in Larix species and sympatric evergreen conifers: a global comparison. *Oecologia*, *114*(2), 153–159. Retrieved 2022-12-19, from http://link.springer.com/10.1007/s004420050431 doi:

10.1007/s004420050431

Kushida, K., Isaev, A. P., Maximov, T. C., Takao, G., & Fukuda, M. (2007, April). Remote sensing of upper canopy leaf area index and forest floor vegetation cover as indicators of net primary productivity in a Siberian larch forest. *Journal of Geophysical Research*, *112*(G2), G02003. Retrieved 2022-07-21, from http://doi.wiley.com/10.1029/2006JG000269 doi: 10.1029/2006JG000269

Lavigne, M. B., Franklin, S. E., & Hunt, E. R. (1996, August). Estimating stem maintenance respiration rates of dissimilar balsam fir stands. *Tree Physiology*, *16*(8), 687–695. Retrieved 2022-06-24, from https://academic.oup.com/treephys/article-lookup/doi/10.1093/treephys/16.8.687 doi: 10.1093/treephys/16.8.687

Le Quéré, C., Barbero, L., Hauck, J., Andrew, R. M., Canadell, J. G., Sitch, S., & Korsbakken, J. I. (2018). Global Carbon Budget 2018. *Earth System Science Data*, *10*, 2141–2194.

Liu, Y., Holtzman, N. M., & Konings, A. G. (2021, May). Global ecosystem-scale plant hydraulic traits retrieved using model–data fusion. *Hydrology and Earth System Sciences*, *25*(5), 2399–2417. Retrieved 2022-09-26, from https://hess.copernicus.org/articles/25/2399/2021/ doi: 10.5194/hess-25-2399-2021

Liu, Z., Zhao, M., Zhang, H., Ren, T., Liu, C., & He, N. (2022, November). Divergent response and adaptation of specific leaf area to environmental change at different spatio-temporal scales jointly improve plant survival. *Global Change Biology*, gcb.16518. Retrieved 2022-12-18, from https://onlinelibrary.wiley.com/doi/10.1111/gcb.16518 doi: 10.1111/gcb.16518

Luo, Z., Xiao, L., Wang, G., Chang, J., Chen, Y., Guo, X., … Jia, S. (2021, May). *Depth distribution of belowground net primary production across global biomes* (preprint). In Review. Retrieved 2022-07-28, from https://www.researchsquare.com/article/rs-65178/v3 doi: 10.21203/rs.3.rs-65178/v3

Lynch, D. J., Matamala, R., Iversen, C. M., Norby, R. J., & Gonzalez-Meler, M. A. (2013, July). Stored carbon partly fuels fine-root respiration but is not used for production of new fine roots. *New Phytologist*, *199*(2), 420–430. Retrieved 2022-07-15, from https://onlinelibrary.wiley.com/doi/10.1111/nph.12290 doi: 10.1111/nph.12290

Madani, N., Kimball, J. S., Ballantyne, A. P., Affleck, D. L. R., van Bodegom, P. M., Reich, P. B., … Running, S. W. (2018, February). Future global productivity will be affected by plant trait response to climate. *Scientific Reports*, *8*(1), 2870. Retrieved 2023-01-29, from https://www.nature.com/articles/s41598-018-21172-9 doi: 10.1038/s41598-018-21172-9

Madani, N., Kimball, J. S., & Running, S. W. (2017). Improving global gross primary productivity estimates by computing optimum light use efficiencies using flux tower data. *Journal of Geophysical Research: Biogeosciences*, *122*(11), 2939–2951. doi: 10.1002/2017JG004142

Madani, N., Parazoo, N. C., Kimball, J. S., Ballantyne, A. P., Reichle, R. H., Maneta, M., … Tagesson, T. (2020, December). Recent Amplified Global Gross Primary Productivity Due to Temperature Increase Is Offset by Reduced Productivity Due to Water Constraints. *AGU Advances*, *1*(4). Retrieved 2023-01-29, from https://onlinelibrary.wiley.com/doi/10.1029/2020AV000180 doi: 10.1029/2020AV000180

Malhi, Y. (2012, January). The productivity, metabolism and carbon cycle of tropical forest vegetation: Carbon cycle of tropical forests. *Journal of Ecology*, *100*(1), 65–75. Retrieved 2023-02-14, from https://onlinelibrary.wiley.com/doi/10.1111/j.1365-2745.2011.01916.x doi:

10.1111/j.1365-2745.2011.01916.x

Meek, D. W., Hatfield, J. L., Howell, T. A., Idso, S. B., & Reginato, R. J. (1984, November). A Generalized Relationship between Photosynthetically Active Radiation and Solar Radiation. *Agronomy Journal*, *76*(6), 939–945. Retrieved 2022-09-19, from https://onlinelibrary.wiley.com/doi/10.2134/agronj1984.00021962007600060018x doi: 10.2134/agronj1984.00021962007600060018x

Murphy, R. E., Barnes, W. L., Lyapustin, A. I., Privette, J., Welsch, C., DeLuccia, F., … Kealy, P. S. M. (2001). Using VIIRS to provide data continuity with MODIS. In *IGARSS 2001. Scanning the Present and Resolving the Future. Proceedings. IEEE 2001 International Geoscience and Remote Sensing Symposium (Cat. No.01CH37217)* (Vol. 3, pp. 1212–1214). Sydney, NSW, Australia: IEEE. Retrieved 2022-07-07, from http://ieeexplore.ieee.org/document/976795/ doi: 10.1109/IGARSS.2001.976795

Myneni, R. B. (2018). *VIIRS Leaf Area Index (LAI) and Fraction of Photosynthetically Active Radiation Absorbed by Vegetation (FPAR) User Guide* (Tech. Rep.). Department of Earth and Environment, Boston University. Retrieved 2022-07-22, from https://lpdaac.usgs.gov/documents/126/VNP15_User_Guide.pdf

Myneni, R. B., Knyazikhin, Y., & Park, T. (2015). *MODIS/Terra+Aqua Leaf Area Index/FPAR 8-day L4 Global 500m SIN Grid V006 [Data set].* Retrieved 2021-07-02, from https://doi.org/10.5067/MODIS/MOD15A2H.061 doi: https://doi.org/10.5067/MODIS/MOD15A2H.061

Olson, R. J., Scurlock, J. M. O., Prince, S. D., Zheng, D. L., & Johnson, K. R. (2013). NPP Multi-Biome: Global Primary Production Data Initiative Products, R2. Retrieved from http://daac.ornl.gov/cgi-bin/dsviewer.pl?ds_id=617 (Publisher: ORNL Distributed Active Archive Center) doi: 10.3334/ORNLDAAC/617

Olson, R. J., Scurlock, J. M. O., Walker, T. R., Hook, L. A., Curtis, C. N., & Cook, R. B. (2017). NPP Multi-Biome: Summary Data from Intensive Studies at 125 Sites, 1936-2006. Retrieved from https://daac.ornl.gov/cgi-bin/dsviewer.pl?ds_id=1352 (Publisher: ORNL Distributed Active Archive Center) doi: 10.3334/ORNLDAAC/1352

Piao, S., Sitch, S., Ciais, P., Friedlingstein, P., Peylin, P., Wang, X., … Zeng, N. (2013, July). Evaluation of terrestrial carbon cycle models for their response to climate variability and to CO $_2$ trends. *Global Change Biology*, *19*(7), 2117–2132. Retrieved 2023-01-29, from https://onlinelibrary.wiley.com/doi/10.1111/gcb.12187 doi: 10.1111/gcb.12187

Poorter, H., Niinemets, ., Poorter, L., Wright, I. J., & Villar, R. (2009, May). Causes and consequences of variation in leaf mass per area (LMA): a meta-analysis. *New Phytologist*, *182*(3), 565–588. Retrieved 2022-06-21, from https://onlinelibrary.wiley.com/doi/10.1111/j.1469-8137.2009.02830.x doi: 10.1111/j.1469-8137.2009.02830.x

Propastin, P., Ibrom, A., Knohl, A., & Erasmi, S. (2012, June). Effects of canopy photosynthesis saturation on the estimation of gross primary productivity from MODIS data in a tropical forest. *Remote Sensing of Environment*, *121*, 252–260. Retrieved 2022-07-04, from https://linkinghub.elsevier.com/retrieve/pii/S0034425712000892 doi: 10.1016/j.rse.2012.02.005

Reich, P. B., Ellsworth, D. S., & Walters, M. B. (1998, December). Leaf structure (specific leaf area) modulates photosynthesis-nitrogen relations: evidence from within and across species and functional groups: SLA regulates photosynthetic nitrogen use. *Functional Ecology*, *12*(6), 948–958. Retrieved 2022-06-21, from http://doi.wiley.com/10.1046/j.1365-2435.1998.00274.x doi: 10.1046/j.1365-2435.1998.00274.x

Running, S. W., Nemani, R. R., Heinsch, F. A., Zhao, M., Reeves, M., & Hashimoto, H. (2004). A continuous satellite-derived measure of global terrestrial primary production. *BioScience*, *54*(6), 547. Retrieved from https://academic.oup.com/bioscience/article/54/6/547-560/294347 (arXiv: 1011.1669v3 ISBN: 0006-3568) doi: 10.1641/0006-3568(2004)054[0547:acsmog]2.0.co;2

Running, S. W., & Zhao, M. (2021). *User's Guide Daily GPP and Annual NPP (MOD17A2H/A3H) and Year-end Gap- Filled (MOD17A2HGF/A3HGF) Products NASA Earth Observing System MODIS Land Algorithm (For Collection 6.1)* (Tech. Rep. No. Version 1.1). Retrieved 2022-06-16, from https://lpdaac.usgs.gov/documents/926/MOD15_User_Guide_V61.pdf

Ryan, M. G., Gower, S. T., Hubbard, R. M., Waring, R. H., Gholz, H. L., Cropper, W. P., & Running, S. W. (1995, February). Woody tissue maintenance respiration of four conifers in contrasting climates. *Oecologia*, *101*(2), 133–140. Retrieved 2022-06-27, from http://link.springer.com/10.1007/BF00317276 doi: 10.1007/BF00317276

Ryu, Y., Berry, J. A., & Baldocchi, D. D. (2019). What is global photosynthesis? History, uncertainties and opportunities. *Remote Sensing of Environment*, *223*(January), 95–114. Retrieved from https://doi.org/10.1016/j.rse.2019.01.016 (Publisher: Elsevier) doi: 10.1016/j.rse.2019.01.016

Salvatier, J., Wiecki, T. V., & Fonnesbeck, C. (2016, April). Probabilistic programming in Python using PyMC3. *PeerJ Computer Science*, *2*, e55. Retrieved 2022-06-27, from https://peerj.com/articles/cs-55 doi: 10.7717/peerj-cs.55

Scurlock, J. M. O., Johnson, K. R., & Olson, R. J. (2003). NPP Grassland: NPP Estimates from Biomass Dynamics for 31 Sites, 1948-1994, R1. Retrieved from http://daac.ornl.gov/cgi-bin/dsviewer.pl?ds_id=654 (Publisher: ORNL Distributed Active Archive Center) doi: 10.3334/ORNLDAAC/654

Scurlock, J. M. O., & Olson, R. J. (2012). NPP Multi-Biome: Grassland, Boreal Forest, and Tropical Forest Sites, 1939-1996, R1. Retrieved from http://daac.ornl.gov/cgi-bin/dsviewer.pl?ds_id=653 (Publisher: ORNL Distributed Active Archive Center) doi: 10.3334/ORNLDAAC/653

Sitch, S., Friedlingstein, P., Gruber, N., Jones, S. D., Murray-Tortarolo, G., Ahlström, A., … Myneni, R. (2015). Recent trends and drivers of regional sources and sinks of carbon dioxide. *Biogeosciences*, *12*(3), 653–679. doi: 10.5194/bg-12-653-2015

Sjöström, M., Zhao, M., Archibald, S., Arneth, A., Cappelaere, B., Falk, U., … Ardö, J. (2013, April). Evaluation of MODIS gross primary productivity for Africa using eddy covariance data. *Remote Sensing of Environment*, *131*, 275–286. Retrieved 2022-07-04, from https://linkinghub.elsevier.com/retrieve/pii/S0034425712004890 doi: 10.1016/j.rse.2012.12.023

Skakun, S., Justice, C. O., Vermote, E., & Roger, J.-C. (2018, February). Transitioning from MODIS to VIIRS: an analysis of inter-consistency of NDVI data sets for agricultural monitoring. *International Journal of Remote Sensing*, *39*(4), 971–992. Retrieved 2022-07-07, from https://www.tandfonline.com/doi/full/10.1080/01431161.2017.1395970 doi: 10.1080/01431161.2017.1395970

Sobol', I. M. (2001, February). Global sensitivity indices for nonlinear mathematical models and their Monte Carlo estimates. *Mathematics and Computers in Simulation*, *55*(1-3), 271–280. Retrieved 2022-06-18, from https://linkinghub.elsevier.com/retrieve/pii/S0378475400002706 doi: 10.1016/S0378-4754(00)00270-6

Stockfors, J., & Linder, S. (1998, March). Effect of nitrogen on the seasonal course of growth and maintenance respiration in stems of Norway spruce trees. *Tree Physiology*, *18*(3), 155–166. Retrieved 2022-06-24, from https://academic.oup.com/treephys/article-lookup/doi/10.1093/

treephys/18.3.155 doi: 10.1093/treephys/18.3.155

Sulla-Menashe, D., Gray, J. M., Abercrombie, S. P., & Friedl, M. A. (2019, March). Hierarchical mapping of annual global land cover 2001 to present: The MODIS Collection 6 Land Cover product. *Remote Sensing of Environment*, *222*, 183–194. Retrieved from https://linkinghub.elsevier.com/retrieve/pii/S0034425718305686 doi: 10.1016/j.rse.2018.12.013

Tang, R., Shao, K., Li, Z. L., Wu, H., Tang, B.-H., Zhou, G., & Zhang, L. (2015). Multiscale Validation of the 8-day MOD16 Evapotranspiration Product Using Flux Data Collected in China. *IEEE Journal of Selected Topics in Applied Earth Observations and Remote Sensing*, *8*(4), 1478–1486. doi: 10.1109/JSTARS.2015.2420105

Tang, X., Fan, S., Du, M., Zhang, W., Gao, S., Liu, S., … Yang, W. (2020, May). Spatial and temporal patterns of global soil heterotrophic respiration in terrestrial ecosystems. *Earth System Science Data*, *12*(2), 1037–1051. Retrieved from https://essd.copernicus.org/articles/12/1037/2020/ doi: 10.5194/essd-12-1037-2020

Ter Braak, C. J. F., & Vrugt, J. A. (2008). Differential Evolution Markov Chain with snooker updater and fewer chains. *Statistics and Computing*, *18*(4), 435–446. doi: 10.1007/s11222-008-9104-9

Tjoelker, M. G., Oleksyn, J., & Reich, P. B. (2001, February). Modelling respiration of vegetation: Evidence for a general temperature-dependent Q10. *Global Change Biology*, *7*(2), 223–230. Retrieved from http://doi.wiley.com/10.1046/j.1365-2486.2001.00397.x doi: 10.1046/j.1365-2486.2001.00397.x

Verheijen, L. M., Aerts, R., Brovkin, V., Cavender-Bares, J., Cornelissen, J. H. C., Kattge, J., & van Bodegom, P. M. (2015, August). Inclusion of ecologically based trait variation in plant functional types reduces the projected land carbon sink in an earth system model. *Global Change Biology*, *21*(8), 3074–3086. Retrieved 2022-07-20, from https://onlinelibrary.wiley.com/doi/10.1111/gcb.12871 doi: 10.1111/gcb.12871

Vrugt, J. A., Ter Braak, C. J. F., Diks, C. G. H., Robinson, B. A., Hyman, J. M., & Higdon, D. (2009). Accelerating Markov chain Monte Carlo simulation by differential evolution with self-adaptive randomized subspace sampling. *International Journal of Nonlinear Sciences and Numerical Simulation*, *10*(3), 273–290. doi: 10.1515/IJNSNS.2009.10.3.273

Wang, J., & Ogawa, S. (2017, February). Analysis of dynamic changes in land use based on landscape metrics in Nagasaki, Japan. *Journal of Applied Remote Sensing*, *11*(1), 016022. Retrieved from http://remotesensing.spiedigitallibrary.org/article.aspx?doi=10.1117/1.JRS.11.016022 doi: 10.1117/1.JRS.11.016022

Welp, L. R., Keeling, R. F., Meijer, H. A. J., Bollenbacher, A. F., Piper, S. C., Yoshimura, K., … Wahlen, M. (2011, September). Interannual variability in the oxygen isotopes of atmospheric CO2 driven by El Niño. *Nature*, *477*(7366), 579–582. Retrieved 2023-01-29, from http://www.nature.com/articles/nature10421 doi: 10.1038/nature10421

White, M. A., Thornton, P. E., Running, S. W., & Nemani, R. R. (2000, January). Parameterization and sensitivity analysis of the BIOME–BGC terrestrial ecosystem model: Net primary production controls. *Earth Interactions*, *4*(3), 1–85. Retrieved 2022-06-01, from http://journals.ametsoc.org/doi/10.1175/1087-3562(2000)004<0003:PASAOT>2.0.CO;2 doi: 10.1175/1087-3562(2000)004<0003:PASAOT>2.0.CO;2

White, R., & Engelen, G. (2000, September). High-resolution integrated modelling of the spatial dynamics of urban and regional systems. *Computers, Environment and Urban Systems*, *24*(5), 383–400. Retrieved from http://linkinghub.elsevier.com/retrieve/pii/S0198971500000120 doi: 10.1016/S0198-9715(00)00012-0

Wright, I. J., Reich, P. B., Westoby, M., Ackerly, D. D., Baruch, Z., Bongers, F., … Villar, R. (2004, April). The worldwide leaf economics spectrum. *Nature*, *428*(6985), 821–827. Retrieved from http://www.nature.com/articles/nature02403 doi: 10.1038/nature02403

Wright, I. J., & Westoby, M. (2001, March). Understanding seedling growth relationships through specific leaf area and leaf nitrogen concentration: generalisations across growth forms and growth irradiance. *Oecologia*, *127*(1), 21–29. Retrieved 2022-07-20, from http://link.springer.com/10.1007/s004420000554 doi: 10.1007/s004420000554

Xiong, X., Angal, A., Chang, T., Chiang, K., Lei, N., Li, Y., … Wu, A. (2020, September). MODIS and VIIRS calibration and characterization in support of producing long-term high-quality data products. *Remote Sensing*, *12*(19), 3167. Retrieved 2022-07-07, from https://www.mdpi.com/2072-4292/12/19/3167 doi: 10.3390/rs12193167

Xu, B., Park, T., Yan, K., Chen, C., Zeng, Y., Song, W., … Myneni, R. B. (2018). Analysis of global LAI/FPAR products from VIIRS and MODIS sensors for spatio-temporal consistency and uncertainty from 2012-2016. *Forests*, *9*(2), 1–21. doi: 10.3390/f9020073

Yan, K., Pu, J., Park, T., Xu, B., Zeng, Y., Yan, G., … Myneni, R. B. (2021, July). Performance stability of the MODIS and VIIRS LAI algorithms inferred from analysis of long time series of products. *Remote Sensing of Environment*, *260*, 112438. Retrieved from https://linkinghub.elsevier.com/retrieve/pii/S0034425721001565 doi: 10.1016/j.rse.2021.112438

Yang, R., Wang, J., Zeng, N., Sitch, S., Tang, W., McGrath, M. J., … Han, P. (2022). Divergent historical GPP trends among state-of-the-art multi-model simulations and satellite-based products. *Earth System Dynamics*(13), 833–849. doi: https://doi.org/10.5194/esd-13-833-2022

Yuan, W., Cai, W., Liu, S., Dong, W., Chen, J., Arain, M. A., … Xia, J. (2014, November). Vegetation-specific model parameters are not required for estimating gross primary production. *Ecological Modelling*, *292*, 1–10. Retrieved 2022-07-20, from https://linkinghub.elsevier.com/retrieve/pii/S0304380014003962 doi: 10.1016/j.ecolmodel.2014.08.017

Zaks, D. P. M., Ramankutty, N., Barford, C. C., & Foley, J. A. (2007, September). From Miami to Madison: Investigating the relationship between climate and terrestrial net primary production. *Global Biogeochemical Cycles*, *21*(3), n/a–n/a. Retrieved 2022-07-18, from http://doi.wiley.com/10.1029/2006GB002705 doi: 10.1029/2006GB002705

Zha, T., Kellomäki, S., Wang, K.-Y., Ryypö, A., & Niinistö, S. (2004, October). Seasonal and annual stem respiration of scots pine trees under boreal conditions. *Annals of Botany*, *94*(6), 889–896. Retrieved 2022-06-09, from https://academic.oup.com/aob/article-lookup/doi/10.1093/aob/mch218 doi: 10.1093/aob/mch218

Zhang, K., Zhu, G., Ma, J., Yang, Y., Shang, S., & Gu, C. (2019). Parameter analysis and estimates for the MODIS evapotranspiration algorithm and multiscale verification. *Water Resources Research*, *55*(3), 2211–2231. doi: 10.1029/2018WR023485

Zhang, Y., Song, C., Band, L. E., Sun, G., & Li, J. (2017, March). Reanalysis of global terrestrial vegetation trends from MODIS products: Browning or greening? *Remote Sensing of Environment*, *191*, 145–155. Retrieved 2023-02-10, from https://linkinghub.elsevier.com/retrieve/pii/S0034425716304977 doi: 10.1016/j.rse.2016.12.018

Zhang, Y., Xiao, X., Wu, X., Zhou, S., Zhang, G., Qin, Y., & Dong, J. (2017, October). A global moderate resolution dataset of gross primary production of vegetation for 2000–2016. *Scientific Data*, *4*(1), 170165. Retrieved 2023-01-29, from https://www.nature.com/articles/sdata2017165 doi: 10.1038/sdata

.2017.165

Zhang, Y., Yu, Q., Jiang, J., & Tang, Y. (2008, April). Calibration of Terra/MODIS gross primary production over an irrigated cropland on the North China Plain and an alpine meadow on the Tibetan Plateau. *Global Change Biology*, *14*(4), 757–767. Retrieved 2023-01-12, from `https://onlinelibrary.wiley.com/doi/10.1111/j.1365-2486.2008.01538.x` doi: 10.1111/j.1365-2486.2008.01538.x

Zhao, M., Heinsch, F. A., Nemani, R. R., & Running, S. W. (2005). Improvements of the MODIS terrestrial gross and net primary production global data set. *Remote Sensing of Environment*, *95*, 164–176. doi: 10.1016/j.rse.2004.12.011

Zhao, M., & Running, S. W. (2010). Drought-induced reduction in global terrestrial net Primary production from 2000 through 2009. *Science*, *329*, 940–943.

Zhao, M., Running, S. W., & Nemani, R. R. (2006). Sensitivity of Moderate Resolution Imaging Spectroradiometer (MODIS) terrestrial primary production to the accuracy of meteorological reanalyses. *Journal of Geophysical Research*, *111*(G1), G01002. Retrieved from `http://doi.wiley.com/10.1029/2004JG000004` doi: 10.1029/2004JG000004

Zhu, X., Pei, Y., Zheng, Z., Dong, J., Zhang, Y., Wang, J., … Xiao, X. (2018). Underestimates of grassland gross primary production in MODIS standard products. *Remote Sensing*, *10*(11). doi: 10.3390/rs10111771

6 Supplement

6.1 Prior Information

First, plant species with valid, relevant trait data were manually classified into PFTs based on their genus, subject to a combination of expert knowledge, database searches (e.g., BudBurst.org, Kew's Plants of the World Online, WorldFloraOnline.org), photographs, and descriptions. For example, genera where most species were described as "shrubby" or "dwarf trees" where classified as "Shrub," to be utilized as prior information for both Open and Closed Shrublands (OSH and CSH). Similarly, a woody "Broadleaf" class, based on photographs and descriptions of the genus, was used to inform priors for both Evergreen Broadleaf and Deciduous Broadleaf classes, unless the genus was predominantly described as evergreen or deciduous. Graminoids and sedges were both classified into Grasslands (GRS). Genera that were too diverse ("cosmopolitan") were not classified and instead used only as a prior for PFTs that were not already represented by species with valid trait data. This includes Savannas (SAV) and Woody Savannas, which both refer to a potentially broad set of plant types (Bridgewater et al., 2002) that may also be found in other, more specific PFTs. The Mixed Forest (MF) prior for a given trait included trait data from species for any forest type. Species grouped into Cropland (CRO) were based on those that feature in the United Nation's Food and Agriculture Programme (FAO) 2010 agricultural census (FAO, 2010). After classification into PFTs, traits were aggregated by species, taking the median value.

A mapping of TRY database traits to MOD17 parameters is presented in Table 6. While some of the traits are directly represented in MOD17, others were used in combination to derive a given parameter. For example, the `froot_mr_base`, the R_M rate of fine roots per unit C, could be the ratio of two traits: "fine root respiration per fine root dry mass" to "fine root carbon (C) content per fine root dry mass." For `leaf_mr_base`, there is no measurement of R_M available but there are measurements of dark respiration. These were used along with the median value of "leaf respiration in light per leaf respiration rate in the dark" (45% with only 16 species available) in order to derive the leaf respiration rate in light (per unit C).

Table 6: List of traits from the TRY database and the MOD17 parameters they inform.

Trait from TRY Database	MOD17 Parameters Informed
Root respiration temperature dependence	`Q10_froot`
Stem respiration temperature dependence	`Q10_stem`
Fine root carbon (C) content per fine root dry mass	`froot_leaf_ratio`, `froot_mr_base`
Stem carbon (C) content per stem dry mass	`livewood_mr_base`
Leaf carbon (C) content per fine root dry mass	`froot_leaf_ratio`, `leaf_mr_base`
Leaf carbon (C) content per leaf area	SLA
Fine root respiration per fine root dry mass	`froot_mr_base`
Stem respiration rate per stem dry mass	`livewood_mr_base`
Leaf respiration rate in the dark per leaf dry mass	`leaf_mr_base`
Leaf respiration rate in light per [same] in the dark	`leaf_mr_base`

For some traits, there were too few species available to generate priors specific to each PFT. In such cases, all plant species were used to derive a single prior for all PFTs. Maximum likelihood estimation (MLE) was used to fit either Normal or Log-Normal distributions to traits, depending on whether the trait distribution was highly positively skewed, which was often. Table S7 lists the MOD17 free parameters and the priors that

were used for model calibration. For $\varepsilon_{\max}$, lacking relevant trait data from TRY, the mean and standard deviation of the "optimum" LUE from a global analysis by Madani et al. (2017) is used, instead.

By definition, livewood mass and respiration are zero in herbaceous plants (GRS and CRO), so these are set to a constant value of zero during calibration of those PFTs. Despite the effort to develop an informative prior for `froot_leaf_ratio`, there is little prior information on the partitioning of C allocation between fine roots and leaves for each PFT. TRY and the Fine-Root Ecology Database (FRED, Iversen et al., 2017) contain few species with this trait recorded and disagree about the relative magnitudes. For example, the mean fine root-leaf C ratio for ENF canopy is about 0.04 based on TRY but 1.33 according to FRED, perhaps due to obscured differences in units or sampling methodology. Using TRY, there are only 14 species in the TRY database for which all the necessary traits were recorded, and after removing the dry-mass normalization of fine-root and leaf C content, all ratios were very close to 1.0. There are also very few species in TRY with prior information on the livewood-leaf ratio. Given this uncertainty, and because we discovered that `livewood_leaf_ratio` is the least-sensitive parameter, we decided to fix both `livewood_leaf_ratio` and `froot_leaf_ratio` at their Collection 6.1 (C61) values, which were informed from a review by M. A. White et al. (2000).

Prior Q10 values for stem respiration in TRY are quite narrow, with a mean of 1.84, which also agrees very well with prior studies (Ryan et al., 1995; Damesin et al., 2002; Bolstad et al., 2004), and is slightly higher for ENF canopy. In TRY, the fine-root temperature dependence (Table S6) was recorded for only one species, so we referred to the literature instead. We adopted the cross-ecosystem Q10 value of 1.6 reported by Burton et al. (2008), which is consistent with the range reported by Atkin et al. (2000), though lower than measurements by Desrochers et al. (2002). With a Normal(1.6, 1.6) prior, the 80th percentile is approximately 3.0, which is consistent with the upper limit for the Q10 of fine root respiration reported by Bahn et al. (2006); it is also wide enough to reflect our uncertainty. Both the livewood (stem) and fine root respiration Q10 priors have means close to the C61 value, which is 2.0 for all PFTs.

The base R_M rates `leaf_mr_base`, `froot_mr_base`, and `livewood_mr_base` in C61 agree well with observations from the TRY database. However, TRY observations indicate that these rates should be higher for all PFTs. The middle 80% of the observed leaf R_M distribution is bounded by [0.005, 0.032] (kg C [kg C]$^{-1}$ day^{-1}), compared to the full range of [0.005, 0.010] in C61. For fine-root R_M, only 23 species are available in TRY, but the middle 80% of [0.006, 0.060] (kg C [kg C]$^{-1}$ day^{-1}) does include the two rates used in C61: 0.00819 for CRO and GRS and 0.00519 for all others. Similarly, though livewood R_M is represented by only 20 species in TRY, the middle 80% of [0.001, 0.042] (kg C [kg C]$^{-1}$ day^{-1}) does include C61's range of [0.0010, 0.0044]; the mean livewood R_M from TRY, 0.005 kg C [kg C]$^{-1}$ day^{-1}, is quite close. These estimates are in the middle of a wide range of reported stem respiration rates for forests (Ryan et al., 1995; Lavigne et al., 1996; Stockfors & Linder, 1998; Damesin et al., 2002; Zha et al., 2004; Bolstad et al., 2004).

SLA in MOD17 is defined as LAI per unit mass of leaf C, which is different from TRY and most field studies, where the numerator would be individual leaf area (m^2) and the denominator would be leaf dry mass. There are multiple TRY traits that could be used to derive SLA, which differ in whether the petiole, rhachis, or midrib are excluded from plant measurements (or whether this is known). When we compare all other "SLA" fields in dry-mass terms (inverse of leaf mass per area, or LMA) or in carbon terms ("Leaf carbon (C) content per leaf area" in TRY, which is the inverse of SLA as defined in MOD17), we find that carbon terms generally agree better with the C61 BPLUT (Table S8), which is based in part on a review by R. White and Engelen (2000). The relative magnitudes of SLA in carbon terms are also consistent with the leaf economics spectrum (Reich et al., 1998; Wright et al., 2004; Poorter et al., 2009); specifically, canopies with short-lived

leaves (DBF, CRO) tend to have higher SLA (lower LMA), and woody canopies tend to have lower SLA (higher LMA) than herbaceous canopies (Díaz et al., 2016). SLA for DNF likely should be higher, at least twice that of ENF (Gower & Richards, 1990; Kloeppel et al., 1998), and indeed some samples from TRY support a higher SLA (Figure S8), yet most are from R. White and Engelen (2000), which found a mean SLA of 22 m^{-2} $[kg\ C]^{-1}$.

6.2 Supplemental Figures & Tables

Table 8: Specific leaf area (SLA) can be defined in carbon terms ("Leaf carbon (C) content per leaf area" in TRY) or dry-mass terms (inverse of leaf mass per area, or LMA). Here, Collection 6.1 BPLUT values are compared to the median SLA in carbon terms (m^{-2} $[kg\ C]^{-1}$) and the median SLA across all dry-mass SLA fields (m^{-2} kg^{-1}), grouped by PFT, from the TRY database. Also shown is the overall median in each group as well as the mean value found in the literature review by White et al. (2000).

PFT	Collection 6.1	Carbon terms	Dry mass terms	White et al.
ENF	15.0	12.1	9.3	8.2
EBF	26.9	24.0	12.3	n.a.
DNF	16.9	23.5	10.7	22.0
DBF	24.7	34.5	16.6	32.0
MF	22.6	33.8	19.1	n.a.
CSH	9.4	24.8	13.3	n.a.
OSH	12.0	24.8	13.3	12.0
WSV	28.8	36.9	14.8	n.a.
SAV	28.9	34.9	15.7	n.a.
GRS	38.0	37.4	14.9	49.0
CRO	38.0	43.6	18.4	n.a.
Overall	24.7	29.5	14.8	n.a.

Table 11: Annual GPP (MOD17A3H) validation metrics, for Collection 6.1 ("C6.1") and the updated BPLUT ("Update"), for years in 2000-2017 with $\geq 97\%$ of valid data-days. FLUXNET sites used in calibration are combined with those reserved for validation due to the dearth of data-years available. Bias and RMSE are in units of g C m^{-2} $year^{-1}$. No FLUXNET sites with majority-DNF canopy have years with at least 97% of valid data-days within this span. The statistics are not shown for DBF (2 site-years) because only one site is represented; they are likely not reliable.

PFT	Site-Years	Bias (C6.1)	Bias (Update)	RMSE (C6.1)	RMSE (Update)	nRMSE (C6.1)	nRMSE (Update)
ENF	52	-307	-196	531	543	15.7%	16.1%
DNF	0	n.a.	n.a.	n.a.	n.a.	n.a.	n.a.
EBF	44	67	12	491	477	13.1%	12.8%
DBF	2	n.a.	n.a.	n.a.	n.a.	n.a.	n.a.
MF	31	-700	-640	763	694	48.5%	44.1%
CSH	7	77	46	103	108	32.3%	33.9%
OSH	6	-264	-336	718	751	33.0%	34.6%
WSV	29	-47	-155	376	416	28.7%	31.8%
SAV	44	-323	-341	532	506	30.4%	28.9%
GRS	56	-347	-174	589	452	17.2%	13.2%

PFT	Site-Years	Bias (C6.1)	Bias (Update)	RMSE (C6.1)	RMSE (Update)	nRMSE (C6.1)	nRMSE (Update)
CRO	20	-317	-9	433	324	37.0%	27.7%

Table 12: Annual GPP validation metrics at FLUXNET sites for years in 2012-2017 with $\geq$ 97% of valid data-days, based on the candidate VNP17 BPLUT. Bias and RMSE are in units of g C m^{-2} $year^{-1}$. As with MOD17, annual GPP validation includes both calibration and validation FLUXNET sites. No FLUXNET sites with majority-DNF or majority-DBF canopy have years with at least 97% of valid data-days within this span.

PFT	Site-Years	Bias	RMSE	nRMSE
ENF	6	-597	839	27.8%
DNF	0	n.a.	n.a.	n.a.
EBF	11	20	625	29.0%
DBF	0	n.a.	n.a.	n.a.
MF	6	-677	707	99.8%
CSH	7	42	93	29.2%
OSH	4	-1	30	9.0%
WSV	9	-98	491	40.8%
SAV	10	-282	602	39.7%
GRS	21	-181	454	17.9%
CRO	9	-27	327	29.9%

Table 14: 8-day GPP validation metrics based on the candidate VNP17 BPLUT, as compared to FLUXNET sites (2012-2017). Mean Bias, RMSE, and ubRMSE are in units of g C m^{-2} day^{-1}, while the parentheses under RMSE indicate the normalized RMSE. The normalized RMSE (%) is based on the overall observed range of daily GPP or annual NPP; for daily GPP, the observed range is restricted to years 2012-2017 to allow for meaningful comparisons between MODIS and VIIRS. DNF is not represented because no FLUXNET sites in this canopy report data during the period of available VIIRS fPAR and LAI retrievals, 2012-2017.

PFT	N	Bias	RMSE	ubRMSE	Corr
ENF	444	-1.6	2.8 (12%)	1.9	0.87
DNF	0	n.a.	n.a.	n.a.	n.a.
EBF	520	0.6	2.8 (13%)	1.5	0.59
DBF	637	0.2	1.5 (7%)	1.4	0.94
MF	684	-1.0	2.1 (9%)	1.6	0.89
CSH	188	0.1	0.5 (2%)	0.4	0.52
OSH	337	0.4	0.8 (4%)	0.6	0.63
WSV	588	0.0	1.5 (7%)	1.1	0.81
SAV	643	-0.7	2.6 (12%)	2.2	0.75
GRS	878	0.0	1.3 (6%)	0.9	0.77
CRO	614	0.3	3.4 (15%)	3.3	0.61

Table 7: Prior distributions for free parameters in MOD17, excluding temperature and VPD parameters in the GPP model. $\varepsilon_{\max}$, `Q10_froot`, and `Q10_livewood` follow a truncated (only positive) normal distribution with mean and standard deviation (in parentheses) shown. All other parameters follow a log-normal distribution with (log-)mean and (log-)standard deviation (in parentheses) shown.

PFT	$\varepsilon_{\max}$	log(SLA)	`Q10_livewood`	`Q10_froot`	log(`leaf_mr_base`)	log(`froot_mr_base`)	log(`livewood_mr_base`)
ENF	0.98 (0.32)	2.75 (0.78)	1.89 (0.27)	1.60 (1.60)	-4.65 (0.67)	-4.21 (0.84)	-5.27 (1.54)
EBF	1.40 (0.20)	3.21 (0.45)	1.84 (0.22)	1.60 (1.60)	-4.65 (0.67)	-4.21 (0.84)	-5.27 (1.54)
DNF	1.23 (0.20)	3.21 (0.27)	1.89 (0.27)	1.60 (1.60)	-4.35 (0.55)	-4.21 (0.84)	-5.27 (1.54)
DBF	1.68 (0.35)	3.61 (0.63)	1.84 (0.22)	1.60 (1.60)	-4.35 (0.55)	-4.21 (0.84)	-5.27 (1.54)
MF	1.43 (0.37)	3.56 (0.58)	1.84 (0.22)	1.60 (1.60)	-4.56 (0.61)	-4.21 (0.84)	-5.27 (1.54)
CSH	0.80 (0.38)	3.21 (0.31)	1.84 (0.22)	1.60 (1.60)	-4.36 (0.70)	-4.21 (0.84)	-5.27 (1.54)
OSH	0.74 (0.21)	3.21 (0.31)	1.84 (0.22)	1.60 (1.60)	-4.36 (0.70)	-4.21 (0.84)	-5.27 (1.54)
WSV	0.93 (0.37)	3.60 (0.70)	1.84 (0.22)	1.60 (1.60)	-4.36 (0.70)	-4.21 (0.84)	-5.27 (1.54)
SAV	0.93 (0.38)	3.58 (0.53)	1.84 (0.22)	1.60 (1.60)	-4.36 (0.70)	-4.21 (0.84)	-5.27 (1.54)
GRS	1.19 (0.45)	3.60 (0.54)	0.00 (0.00)	1.60 (1.60)	-4.03 (0.54)	-4.21 (0.84)	0.00 (0.00)
CRO	1.94 (0.55)	3.72 (0.60)	0.00 (0.00)	1.60 (1.60)	-3.78 (0.86)	-4.21 (0.84)	0.00 (0.00)

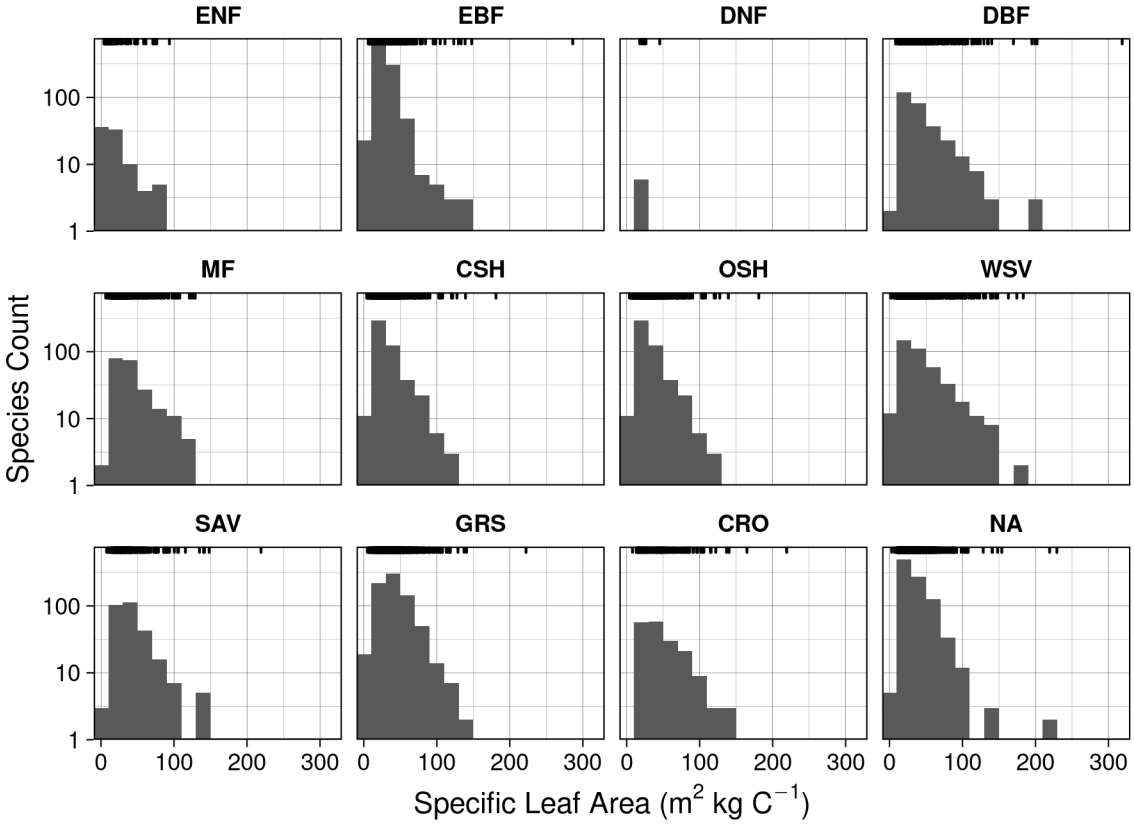

Figure 8: Histograms of specific leaf area (SLA) from the TRY database, in carbon (C) terms (i.e., leaf area per unit C) for each PFT. A rug plot at the top of each subplot shows the distribution of species-level observations.

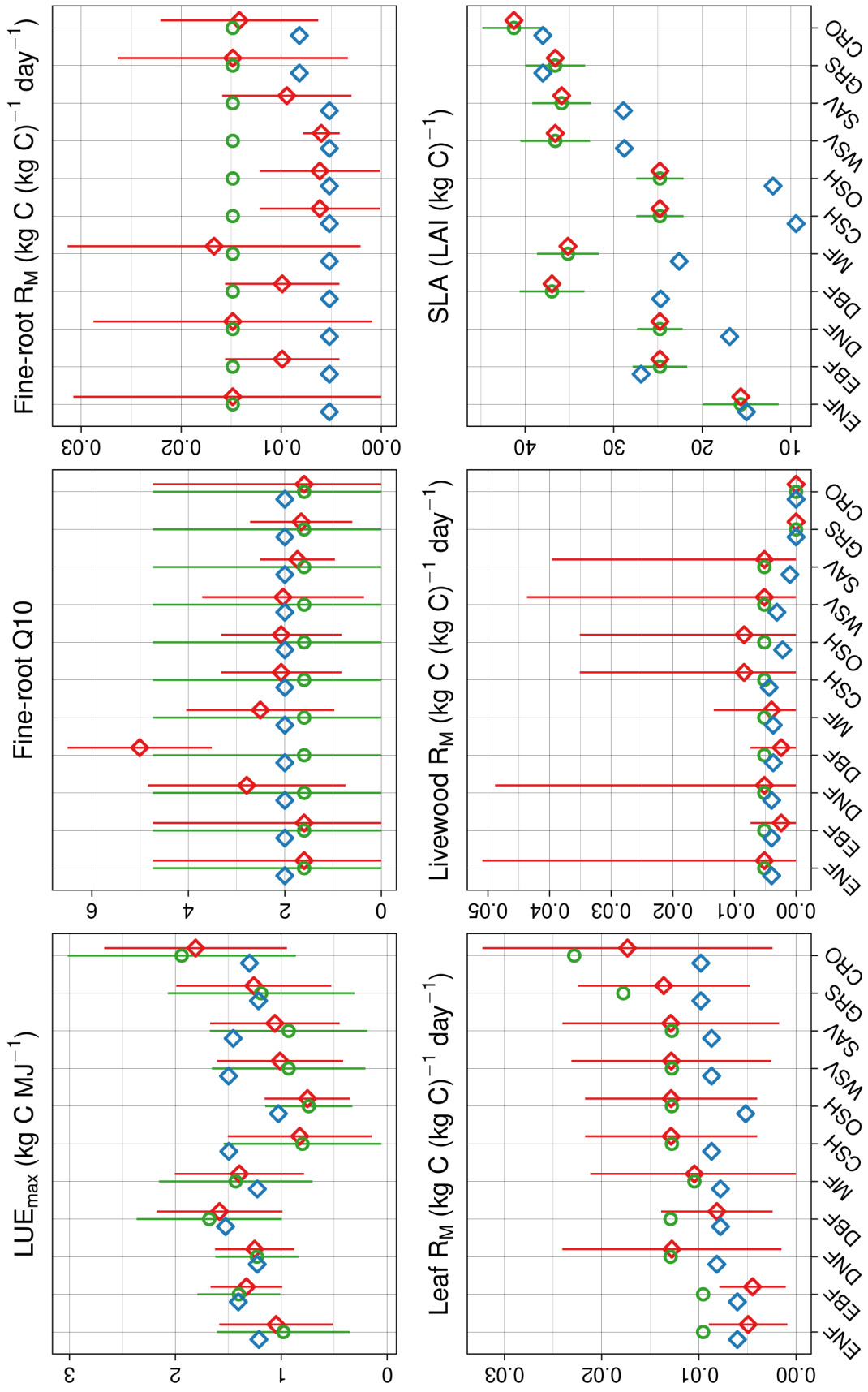

Figure 9: Distribution of BPLUT parameters for MOD17, comparing original Collection 6.1 (C61) values, the prior distribution and prior mean from TRY ("Prior"), and posterior distribution and mean ("Posterior"). For `froot_mr_base`, `leaf_mr_base`, and `livewood_mr_base`, the prior is derived from the literature or from a small number of species in TRY, so no distribution is shown. SLA was fixed at its prior mean, so only the prior distribution is shown and the "posterior" mean is the same as the prior mean.

Table 9: Updated BPLUT for the MOD17 and VNP17 GPP models, based on the optimal posterior estimates. Both MOD17 and VNP17 use the same parameters for the VPD and T_{min} environmental scalars. The lower bounds on T_{min} and VPD, respectively $T_{\text{min},\leftarrow}$ and $\text{VPD}_{\leftarrow}$, are fixed at their MOD17 Collection 6.1 values. To facilitate comparison, the upper bounds are rounded to the nearest 1 deg C or 50 Pascals, which is consistent with the model's low sensitivity to these parameters.

GPP Parameter	ENF	EBF	DNF	DBF	MF	CSH	OSH	WSV	SAV	GRS	CRO
MOD17 ε_{max} (g C MJ^{-1})	1.05	1.33	1.25	1.58	1.40	0.83	0.75	0.96	1.06	1.26	1.81
VNP17 ε_{max} (g C MJ^{-1})	1.01	1.29	1.24	1.56	1.36	0.81	0.76	1.00	1.05	1.24	1.80
$T_{\text{min},\leftarrow}$ (deg C)	-8	-8	-8	-6	-7	-8	-8	-8	-8	-8	-8
$T_{\text{min},\rightarrow}$ (deg C)	4	20	4	21	18	19	11	14	8	5	21
$\text{VPD}_{\leftarrow}$ (Pa)	650	1000	650	650	650	650	650	650	650	650	650
$\text{VPD}_{\rightarrow}$ (Pa)	4650	4300	2450	3450	3900	4650	5350	3650	5100	4150	4950

Table 10: Updated BPLUT for the MOD17 annual NPP model, based on the optimal posterior estimates. `froot_leaf_ratio` and `livewood_leaf_ratio` are fixed at their Collection 6.1 values.

Parameter	ENF	EBF	DNF	DBF	MF	CSH	OSH	WSV	SAV	GRS	CRO
MOD17 SLA (LAI [kg C]$^{-1}$)	15.6	24.8	24.8	37.0	35.2	24.8	24.8	36.6	35.9	36.6	41.3
VNP17 SLA (LAI [kg C]$^{-1}$)	16.2	26.7	25.3	38.2	36.2	25.4	25.0	37.2	36.8	37.8	41.9
`froot_leaf_ratio`	1.2	1.1	1.7	1.1	1.1	1.0	1.3	1.8	1.8	2.6	2.0
`livewood_leaf_ratio`	0.18	0.16	0.17	0.20	0.20	0.08	0.04	0.09	0.05	0.00	0.00
`froot_mr_base`	0.0148	0.0099	0.0148	0.0099	0.0167	0.0061	0.0061	0.0026	0.0094	0.0148	0.0142
`leaf_mr_base`	0.0049	0.0045	0.0128	0.0081	0.0105	0.0129	0.0129	0.0128	0.0129	0.0136	0.0173
`livewood_mr_base`	0.0051	0.0024	0.0051	0.0024	0.0040	0.0084	0.0084	0.0051	0.0051	0.0000	0.0000
`Q10_froot`	1.60	1.60	2.79	5.01	2.51	2.08	2.08	2.33	1.74	1.66	1.60
`Q10_livewood`	1.92	1.75	1.89	1.86	1.86	1.85	1.85	1.85	1.83	0.00	0.00

Table 13: 8-day GPP (MOD17A2H) validation metrics, for Collection 6.1 ("C6.1") and the updated BPLUT ("Update"), as compared to FLUXNET sites (2000-2017). Mean Bias, RMSE, and ubRMSE are in units of g C m^{-2} day^{-1}, while the parentheses under RMSE indicate the normalized RMSE. The normalized RMSE (%) is based on the overall observed range of daily GPP or annual NPP; for daily GPP, the observed range is restricted to years 2012-2017 to allow for meaningful comparisons between MODIS and VIIRS.

PFT	N	Bias (C61)	Bias (Update)	RMSE (C61)	RMSE (Update)	ubRMSE (C61)	ubRMSE (Update)	r (C61)	r (Update)
ENF	808	-1.0	-1.1	2.2 (11%)	2.2 (11%)	1.7	1.6	0.88	0.89
EBF	427	0.2	0.3	2.6 (13%)	2.4 (13%)	2.2	2.2	0.70	0.75
DNF	71	-0.7	-0.2	2.5 (13%)	2.5 (13%)	1.9	2.0	0.75	0.73
DBF	994	-0.2	-0.2	2.5 (13%)	2.0 (10%)	2.3	1.7	0.84	0.90
MF	667	-0.9	-0.7	2.0 (10%)	1.8 (9%)	1.6	1.5	0.90	0.90
CSH	94	0.2	0.1	0.6 (3%)	0.7 (3%)	0.4	0.5	0.25	0.04
OSH	406	0.4	0.3	0.9 (5%)	0.8 (4%)	0.7	0.6	0.69	0.72
WSV	562	-0.1	-0.4	1.3 (7%)	1.5 (8%)	1.1	1.0	0.86	0.84
SAV	788	-1.0	-0.8	2.5 (13%)	2.3 (12%)	2.1	2.0	0.74	0.77
GRS	604	0.2	0.5	1.4 (7%)	1.5 (7%)	1.2	1.1	0.77	0.76
CRO	853	-1.2	-0.3	5.1 (26%)	4.0 (21%)	4.8	4.0	0.74	0.83

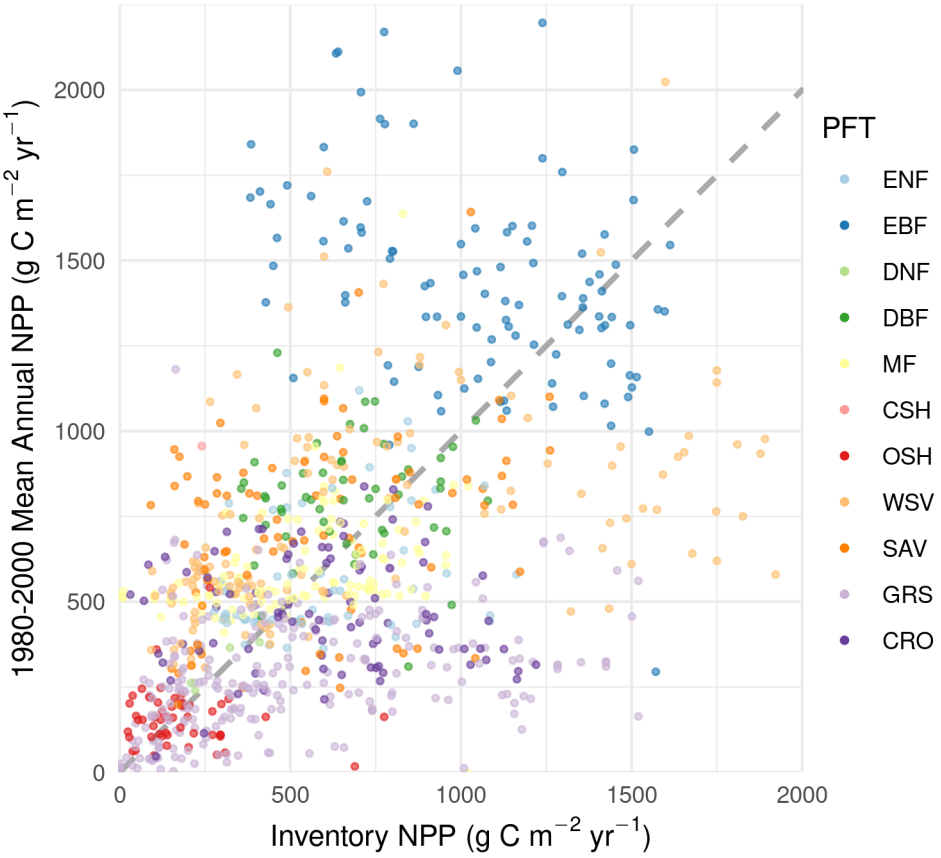

Figure 10: MOD17 predicted mean annual NPP, using the Collection 6.1 BPLUT, against observed mean annual NPP from the field. The dashed line indicates the 1:1 line.

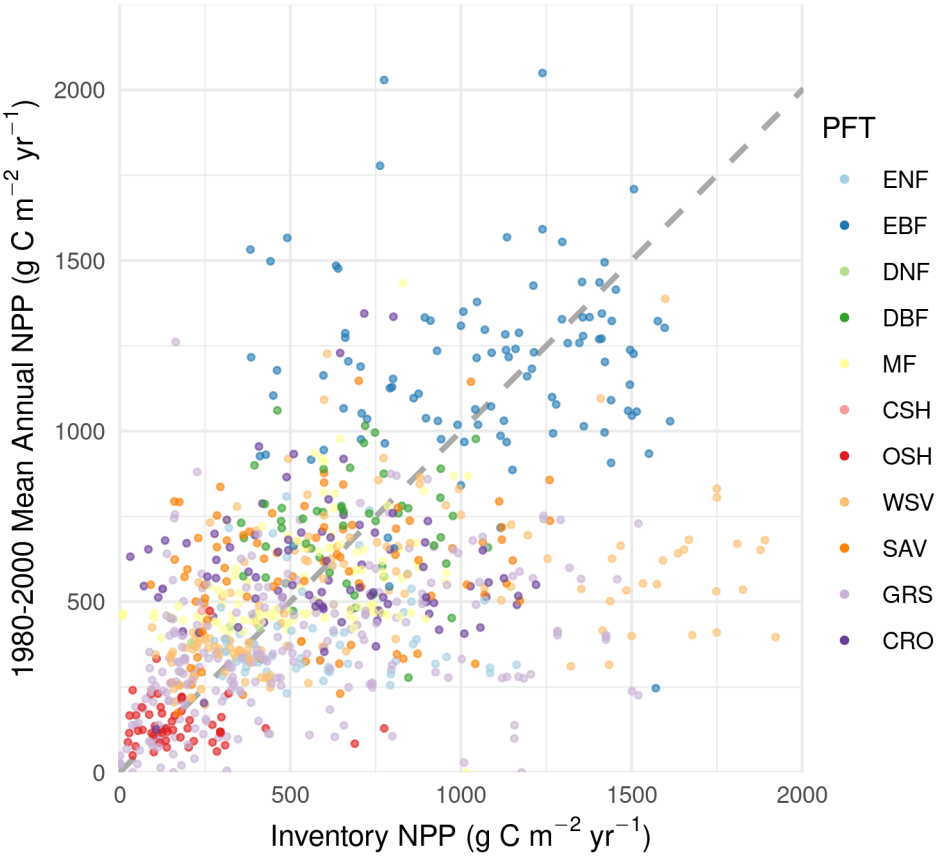

Figure 11: MOD17 predicted mean annual NPP, using the updated BPLUT, against observed mean annual NPP from the field. The dashed line indicates the 1:1 line.

Table 15: Annual MOD17 NPP validation metrics at Cal-Val inventory sites, based on k-folds cross-validation. RMSE is in units of g C m^{-2} $year^{-1}$. Statistics are not available for CSH because of too few sites.

PFT	Count	Bias (C6.1)	Bias (Update)	RMSE (C6.1)	RMSE (Update)	nRMSE (C6.1)	nRMSE (Update)	r (C6.1)	r (Update)
ENF	63	-11	-175	187	236	23.0%	29.0%	0.33	0.00
EBF	104	230	11	380	292	29.4%	22.7%	0.43	0.55
DNF	5	226	13	372	288	27.7%	21.4%	0.46	0.57
DBF	54	205	19	338	267	25.1%	19.9%	0.47	0.56
MF	110	158	18	292	243	18.9%	15.8%	0.54	0.58
CSH	1	n.a	n.a	n.a	n.a	n.a	n.a	n.a	n.a
OSH	53	134	11	268	225	17.2%	14.5%	0.64	0.68
WSV	141	113	-12	298	254	16.3%	13.9%	0.56	0.60
SAV	83	117	-22	301	257	16.5%	14.1%	0.54	0.57
GRS	248	22	-5	298	260	16.1%	14.1%	0.51	0.56
CRO	89	8	8	296	265	16.0%	14.3%	0.49	0.53

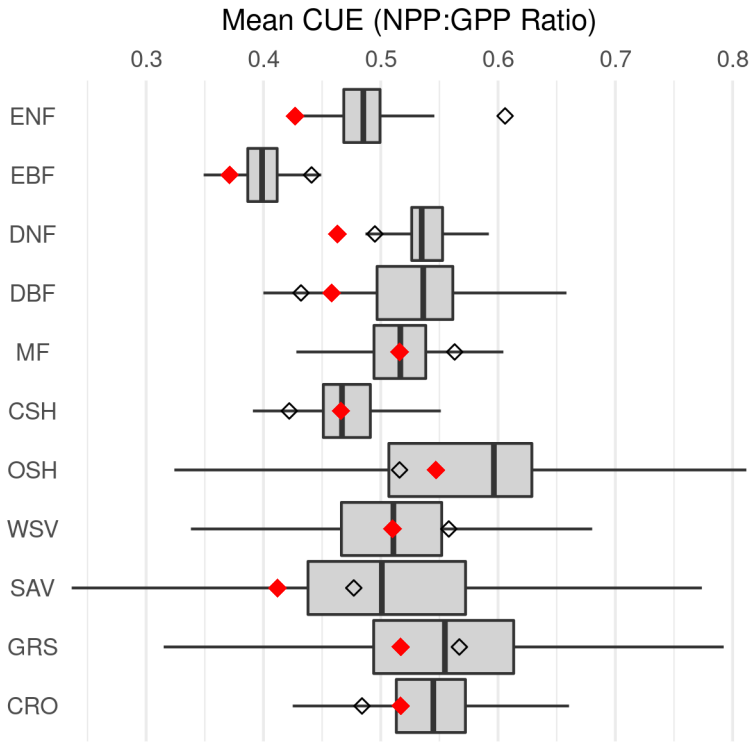

Figure 12: Plant carbon-use efficiency (CUE) values from the MsTMIP global, gridded ensemble mean (2000-2010), shown as boxplots, along with the overall mean CUE in the updated MOD17 product, shown as red diamonds. The new VNP17 BPLUT results in overall, global mean CUE values that are nearly identical to those shown here for MOD17.

Table 16: Annual VNP17 NPP validation metrics at Cal-Val inventory sites, based on k-folds cross-validation. RMSE is in units of g C m^{-2} $year^{-1}$. Statistics are not available for CSH because of too few sites.

PFT	Count	Bias	RMSE	nRMSE	r
ENF	63	-148	201	24.7%	0.37
EBF	104	90	335	26.0%	0.52
DNF	5	91	330	24.6%	0.54
DBF	54	78	300	22.3%	0.54
MF	110	61	265	17.2%	0.57
CSH	1	n.a.	n.a.	n.a.	n.a.
OSH	53	48	244	15.7%	0.67
WSV	141	-12	271	14.8%	0.54
SAV	83	-8	272	14.9%	0.53
GRS	247	-50	271	14.6%	0.51
CRO	89	-46	274	14.8%	0.49

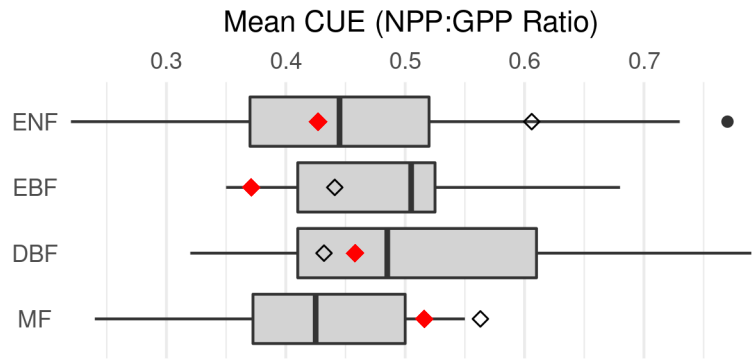

Figure 13: Plant carbon-use efficiency (CUE) values from the synthesis by Collalti & Prentice (2019), which included data only for forests, shown as boxplots, along with the overall mean CUE in the updated MOD17 product, shown as red diamonds. The new VNP17 BPLUT results in overall, global mean CUE values that are nearly identical to those shown here for MOD17.

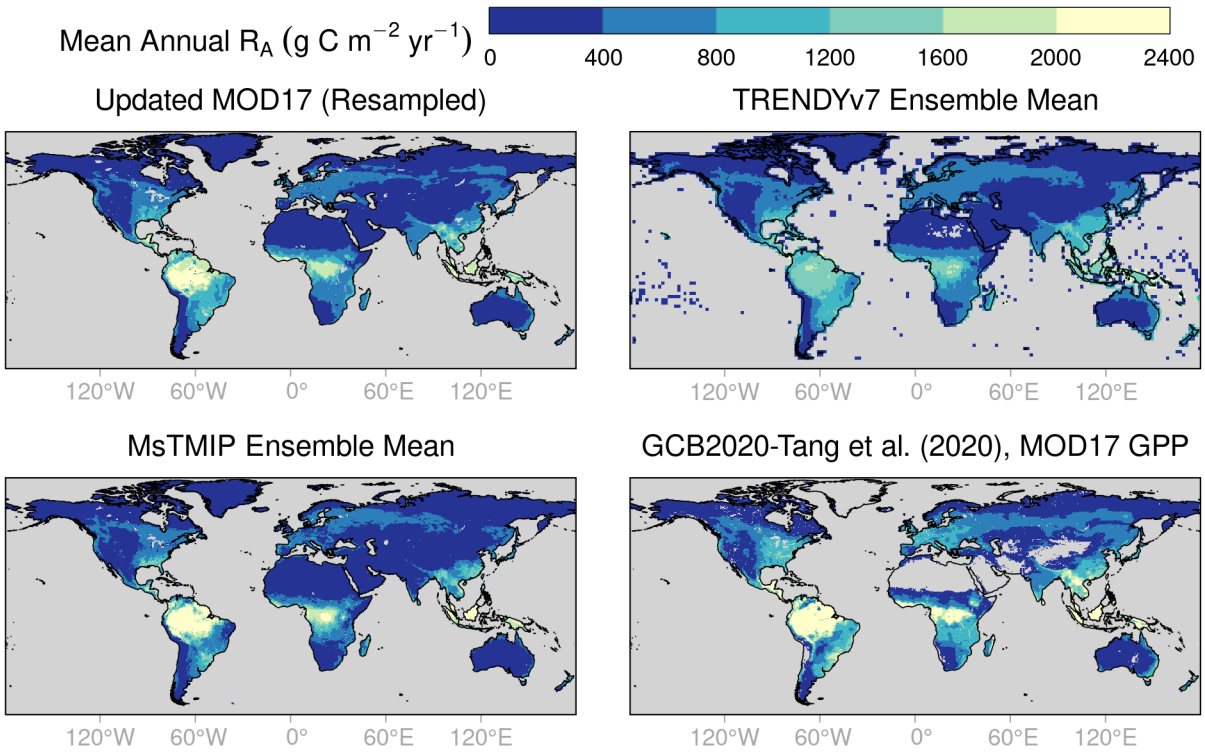

Figure 14: Plots of mean annual autotrophic respiration (R_A) for 2000-2010, which is a period of record common to all datasets. The TRENDYv7 Ensemble Mean is shown on a 1-degree equirectangular grid, all others are shown on a 0.5-degree grid. The Updated MOD17 map is based on a bilinear resampling from the original 5-km, MODIS Sinusoidal projection. The Global Carbon Budget-Tange et al. (2020) synthesis, "GCB2020-Tang et al. (2020)" is computed by subtracting that annual NPP product from the Updated MOD17 annual GPP product.)

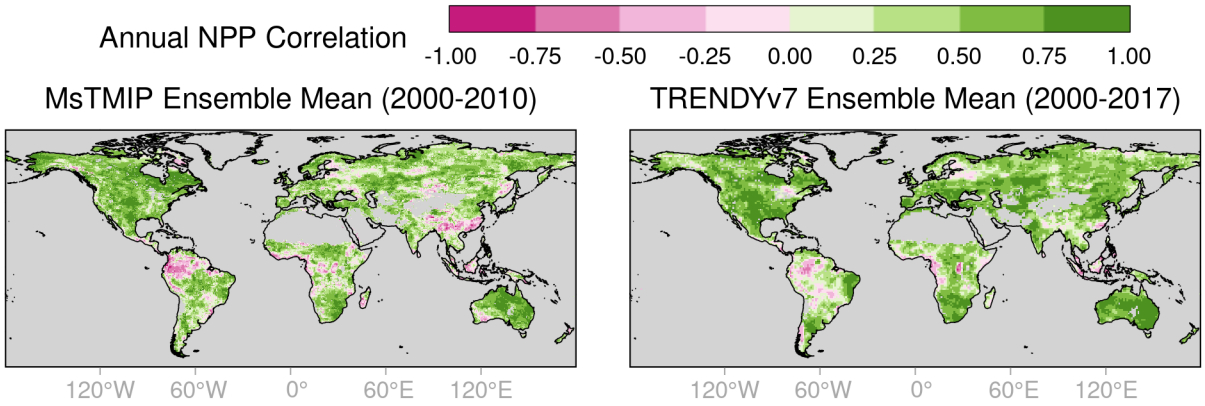

Figure 15: Plots of temporal correlations in annual NPP between the updated MOD17 product and two bottom-up modeling ensembles. The TRENDYv7 Ensemble Mean is shown on a 1-degree equirectangular grid, all others are shown on a 0.5-degree grid.

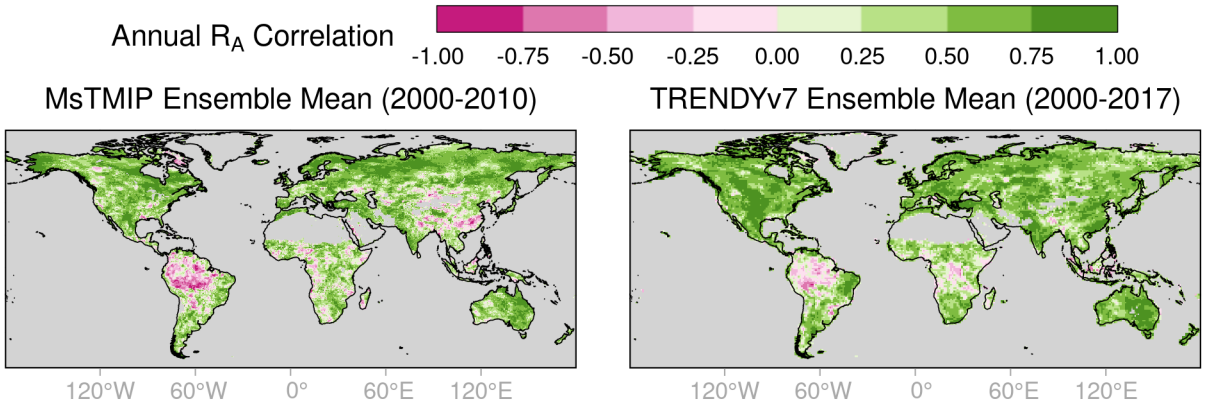

Figure 16: Plots of temporal correlations in annual autotrophic respiration (R_A) between the updated MOD17 product and two bottom-up modeling ensembles. The TRENDYv7 Ensemble Mean is shown on a 1-degree equirectangular grid, all others are shown on a 0.5-degree grid.

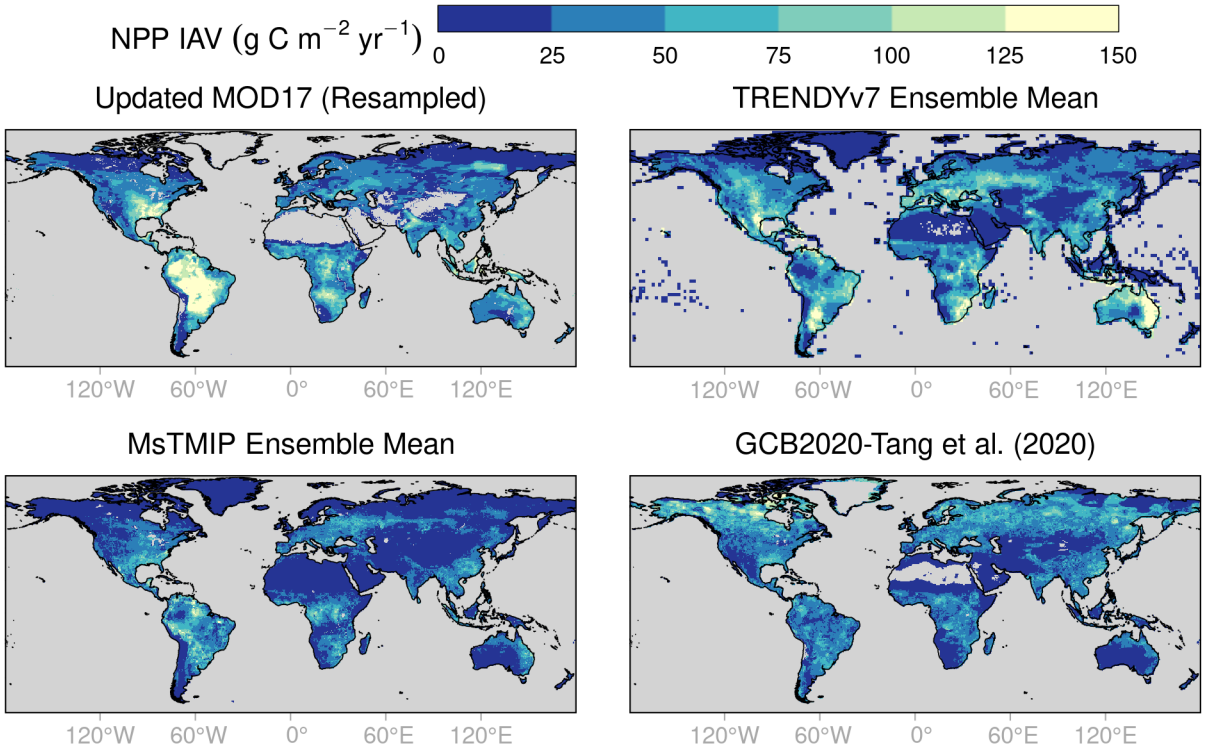

Figure 17: Interannual variability (standard deviation across the years 2000-2010) in annual NPP. The TRENDYv7 Ensemble Mean is shown on a 1-degree equirectangular grid, all others are shown on a 0.5-degree grid. The Updated MOD17 map is based on a bilinear resampling from the original 5-km, MODIS Sinusoidal projection.

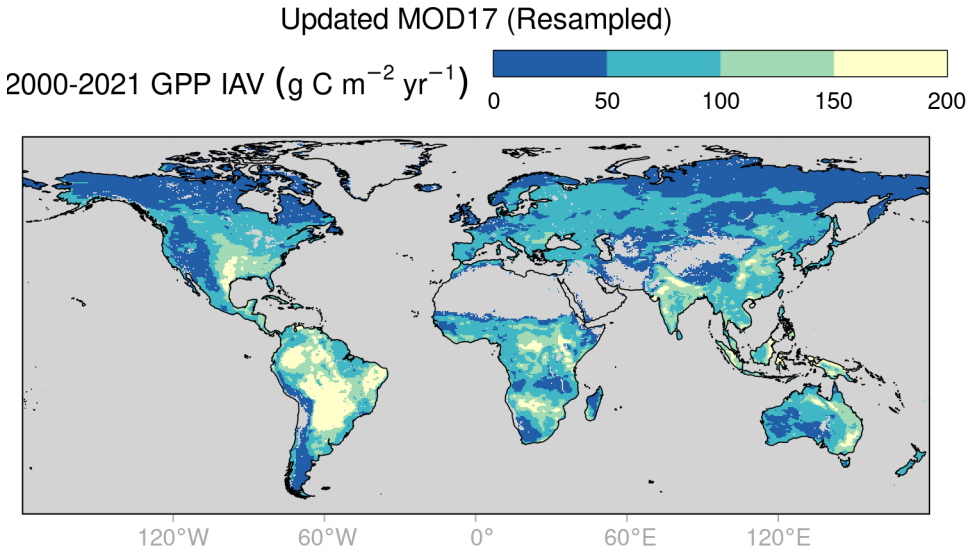

Figure 18: Interannual variability (standard deviation across the years 2000-2021) in annual GPP, based on the updated MOD17 BPLUT and resampling onto a 0.5-degree grid.

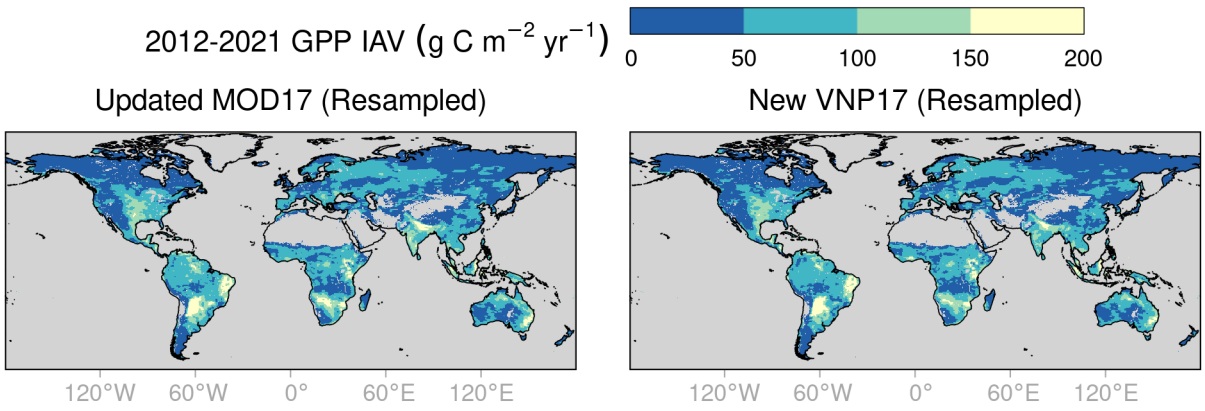

Figure 19: Interannual variability (standard deviation across the years 2012-2021) in annual GPP, based on resampling onto a 0.5-degree grid.

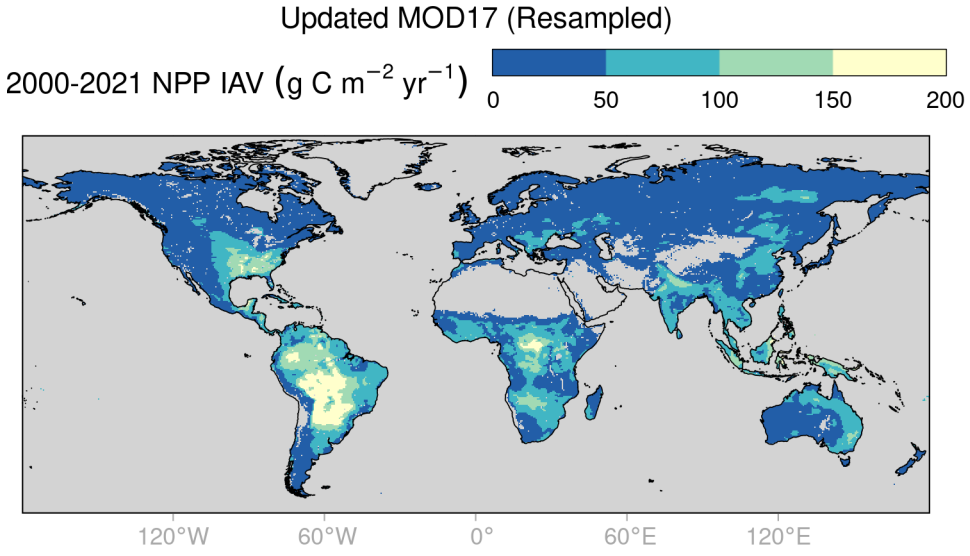

Figure 20: Interannual variability (standard deviation across the years 2000-2021) in annual NPP, based on the updated MOD17 BPLUT and resampling onto a 0.5-degree grid.

Table 17: Average root-mean squared error (RMSE) in annual GPP or NPP (g C m^{-2} $year^{-1}$) for each product, compared to independent datasets. The MOD17 and VNP17 (5-km resolution) data were projected onto a 0.5-degree or 1-degree equirectangular grid with bilinear resampling, prior to computing RMSE. Standard deviation across the years is also given.

NPP Dataset	Flux	MOD17 Update	New VNP17
TRENDYv7 Ensemble	Annual GPP	310 ±11	307 ±9
MsTMIP Ensemble	Annual GPP	383 ±8	n.a.
Global Carbon Budget-Tang et al.	Annual NPP	260 ±5	260 ±8
TRENDYv7 Ensemble	Annual NPP	192 ±12	179 ±4
MsTMIP Ensemble	Annual NPP	230 ±8	n.a.

Table 18: Pearson's correlation coefficients and RMSE, within each PFT group, between annual net primary production (NPP) estimated by MOD17/VNP17 and annual NPP based on the Global Carbon Budget (2020). 2010-2016 annual NPP is calculated from the Global Carbon Budget's estimate of net ecosystem exchange (NEE) based on atmospheric inversion and combined with an up-scaled, global, 1-degree map of heterotrophic respiration from Tang et al. (2020). Coefficients for the New VNP17 BPLUT are based on only the years 2012-2016.

PFT	RMSE (C61)	RMSE (MOD17 Update)	RMSE (VNP17 Update)	r (C61)	r (MOD17 Update)	r (VNP17 Update)
ENF	201	397	391	0.306	0.162	0.170
EBF	622	395	421	-0.513	-0.385	-0.464
DNF	138	148	62	-0.509	-0.407	-0.274
DBF	285	229	252	-0.178	-0.049	-0.153
MF	179	148	141	-0.133	-0.083	-0.122
CSH	171	265	270	-0.444	-0.421	-0.577
OSH	146	190	180	0.322	0.430	0.523
WSV	409	158	166	0.432	0.233	0.332
SAV	566	268	281	0.198	-0.047	-0.076
GRS	223	266	272	0.393	0.110	0.066
CRO	397	364	365	0.109	0.214	0.251

Table 19: Pearson's correlation coefficients and RMSE, within each PFT group, between annual net primary production (NPP) estimated by MOD17/VNP17 and mean annual NPP from the TRENDYv7 ensemble (2000-2017). Coefficients for the New VNP17 BPLUT are based on only the years 2012-2017.

PFT	RMSE (C61)	RMSE (MOD17 Update)	RMSE (VNP17 Update)	r (C61)	r (MOD17 Update)	r (VNP17 Update)
ENF	333	543	255	-0.169	-0.458	0.134
EBF	707	597	708	-0.631	-0.446	-0.474
DNF	348	354	81	0.651	0.766	-0.286
DBF	245	192	165	-0.028	0.260	0.383
MF	250	289	202	0.043	-0.219	-0.302
CSH	236	114	76	0.264	0.254	0.281
OSH	105	150	114	0.465	0.443	0.494
WSV	234	221	151	0.548	0.244	0.608
SAV	382	296	332	0.493	0.046	0.541
GRS	191	256	300	0.668	0.445	0.317
CRO	235	206	215	-0.005	0.043	-0.079

Table 20: Pearson's correlation coefficients and RMSE, within each PFT group, between annual net primary production (NPP) estimated by MOD17 and mean annual NPP from the MsTMIP ensemble (2000-2010).

PFT	RMSE (C61)	RMSE (MOD17 Update)	r (C61)	r (MOD17 Update)
ENF	265	455	-0.050	-0.349
EBF	823	651	-0.843	-0.563
DNF	199	206	0.412	0.596
DBF	212	163	0.286	0.547
MF	302	325	-0.258	-0.316
CSH	170	163	0.770	0.726
OSH	229	257	0.261	0.287
WSV	288	178	0.636	0.347
SAV	437	360	0.446	-0.116
GRS	203	235	0.685	0.514
CRO	279	245	0.141	0.263

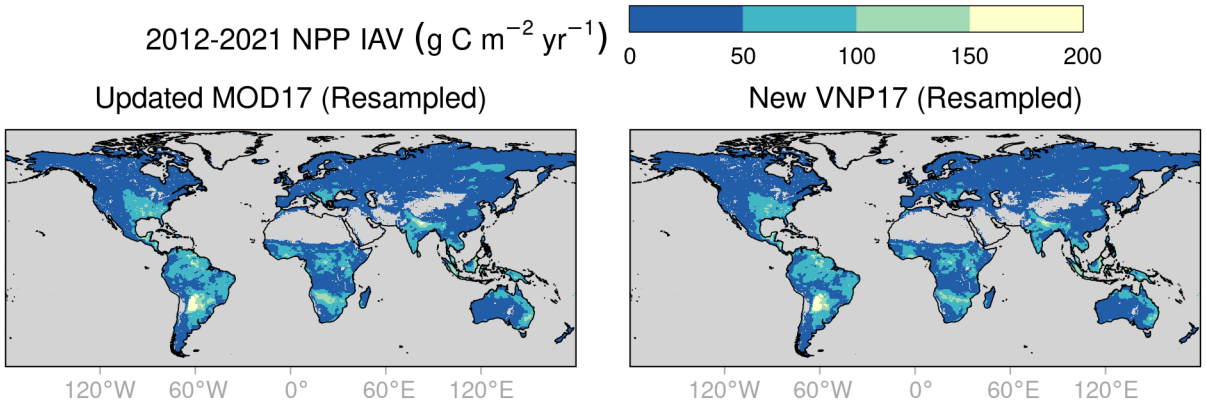

Figure 21: Interannual variability (standard deviation across the years 2012-2021) in annual NPP, based on resampling onto a 0.5-degree grid.

Table 21: Annual GPP and NPP fluxes (Pg C year^{-1}) for different products in different time periods.

Period	Product	GPP	NPP
2000-2010	Collection 6.1	117.4 ±2.2	58.2 ±1.7
2000-2010	FLUXCOM RS+METEO (ERA5)	115.7 ±0.4	n.a.
2000-2010	GCB2020-Tang et al.	n.a.	49.8 ±0.4
2000-2010	MOD17 Update	125.4 ±2.0	56.1 ±1.5
2000-2010	MsTMIP Ensemble Mean	109.9 ±1.7	51.6 ±0.9
2000-2010	TRENDYv7 Ensemble Mean	124.9 ±1.6	60.5 ±1.0
2000-2018	Collection 6.1	119.2 ±2.9	59.3 ±1.9
2000-2018	FLUXCOM RS+METEO (ERA5)	115.5 ±0.4	n.a.
2000-2018	GCB2020-Tang et al.	n.a.	49.6 ±0.6
2000-2018	MOD17 Update	127.2 ±2.8	57.1 ±1.8
2000-2018	MsTMIP Ensemble Mean	109.9 ±1.7	51.6 ±0.9
2000-2018	TRENDYv7 Ensemble Mean	126.3 ±2.4	61.2 ±1.3
2012-2018	Collection 6.1	121.6 ±1.6	60.7 ±1.1
2012-2018	FLUXCOM RS+METEO (ERA5)	115.2 ±0.2	n.a.
2012-2018	GCB2020-Tang et al.	n.a.	49.6 ±0.8
2012-2018	MOD17 Update	129.7 ±1.7	58.5 ±1.1
2012-2018	New VNP17	129.6 ±1.7	58.4 ±1.1
2012-2018	TRENDYv7 Ensemble Mean	128.6 ±1.4	62.3 ±0.9
2012-2021	Collection 6.1	121.9 ±1.4	60.7 ±0.9
2012-2021	FLUXCOM RS+METEO (ERA5)	115.2 ±0.2	n.a.
2012-2021	GCB2020-Tang et al.	n.a.	49.6 ±0.8
2012-2021	MOD17 Update	130.1 ±1.6	58.6 ±0.9
2012-2021	New VNP17	129.8 ±1.5	58.4 ±0.9
2012-2021	TRENDYv7 Ensemble Mean	128.6 ±1.4	62.3 ±0.9

Table 22: Error budget for the MOD17 daily GPP model. All units are g C m^{-2} day^{-1}. σ(fPAR) is the error in daily GPP due to error in MODIS MOD15A2HGF fPAR; $\sigma(\varepsilon_{max})$ is the error in daily GPP due to uncertainty in the maximum light-use efficiency parameter, ε_{max}. The "Overall" row corresponds to the pooled, stratified result, where every PFT is approximately equally represented.

PFT	Test RMSE	σ(fPAR)	$\sigma(\varepsilon_{max})$
ENF	2.23	1.84	0.08
EBF	2.44	2.88	0.12
DNF	2.47	2.57	0.07
DBF	2.02	1.57	0.05
MF	1.84	1.53	0.05
CSH	0.66	1.17	0.02
OSH	0.84	1.05	0.02
WSV	1.49	1.13	0.05
SAV	2.32	1.86	0.07
GRS	1.45	2.05	0.04
CRO	4.04	2.18	0.04
Overall	2.48	1.81	0.05

Table 23: Error budget for the VNP17 daily GPP model. All units are g C m^{-2} day^{-1}. σ(fPAR) is the error in daily GPP due to error in MODIS VNP15A2HGF fPAR; $\sigma(\varepsilon_{max})$ is the error in daily GPP due to uncertainty in the maximum light-use efficiency parameter, ε_{max}. The "Overall" row corresponds to the pooled, stratified result, where every PFT is approximately equally represented.

PFT	Test RMSE	σ(fPAR)	$\sigma(\varepsilon_{max})$
ENF	2.79	1.77	0.08
EBF	2.84	2.78	0.11
DNF	n.a.	2.55	0.07
DBF	1.53	1.55	0.05
MF	2.06	1.49	0.05
CSH	0.48	1.15	0.02
OSH	0.62	1.06	0.02
WSV	1.48	1.31	0.05
SAV	2.58	1.84	0.07
GRS	1.29	2.01	0.04
CRO	3.33	2.16	0.04
Overall	2.17	1.73	0.05

Table 24: Error budget for the MOD17 annual NPP model, where the error is expressed as the coefficient of variation in the RMSE due to uncertainty in a given parameter, relative to Test RMSE (units: g C m^{-2} $year^{-1}$). This budget assumes that the allometric parameters, `froot_leaf_ratio` and `livewood_leaf_ratio` are fixed at their true values.

PFT	SLA (LAI [kg C]$^{-1}$)	`Q10_froot`	`Q10_livewood`	`froot_mr_base`	`leaf_mr_base`	`livewood_mr_base`
ENF	60%	44%	1%	59%	9%	33%
EBF	65%	82%	<1%	23%	10%	2%
DNF	11%	5%	<1%	20%	8%	9%
DBF	31%	1%	<1%	7%	5%	1%
MF	28%	11%	<1%	6%	10%	<1%
CSH	n.a.	n.a.	n.a.	n.a.	n.a.	n.a.
OSH	2%	<1%	<1%	<1%	<1%	<1%
WSV	43%	7%	<1%	3%	32%	10%
SAV	23%	1%	<1%	3%	3%	7%
GRS	21%	2%	<1%	29%	3%	<1%
CRO	25%	27%	<1%	2%	1%	<1%
Overall	29%	16%	<1%	14%	7%	3%

Table 25: Error budget for the VNP17 annual NPP model, where the error is expressed as the coefficient of variation in the RMSE due to uncertainty in a given parameter, relative to Test RMSE (units: g C m^{-2} $year^{-1}$). This budget assumes that the allometric parameters, `froot_leaf_ratio` and `livewood_leaf_ratio` are fixed at their true values.

PFT	SLA (LAI [kg C]$^{-1}$)	`Q10_froot`	`Q10_livewood`	`froot_mr_base`	`leaf_mr_base`	`livewood_mr_base`
ENF	73%	53%	1%	70%	11%	37%
EBF	54%	72%	<1%	18%	8%	2%
DNF	10%	4%	<1%	17%	7%	8%
DBF	29%	1%	<1%	6%	4%	<1%
MF	28%	7%	<1%	5%	8%	<1%
CSH	n.a.	n.a.	n.a.	n.a.	n.a.	n.a.
OSH	1%	<1%	<1%	<1%	<1%	<1%
WSV	43%	6%	<1%	3%	31%	9%
SAV	23%	1%	<1%	3%	3%	7%
GRS	21%	2%	<1%	27%	3%	<1%
CRO	24%	26%	<1%	2%	1%	<1%
Overall	28%	16%	<1%	13%	7%	3%

manuscript submitted to *JGR: Biogeosciences*

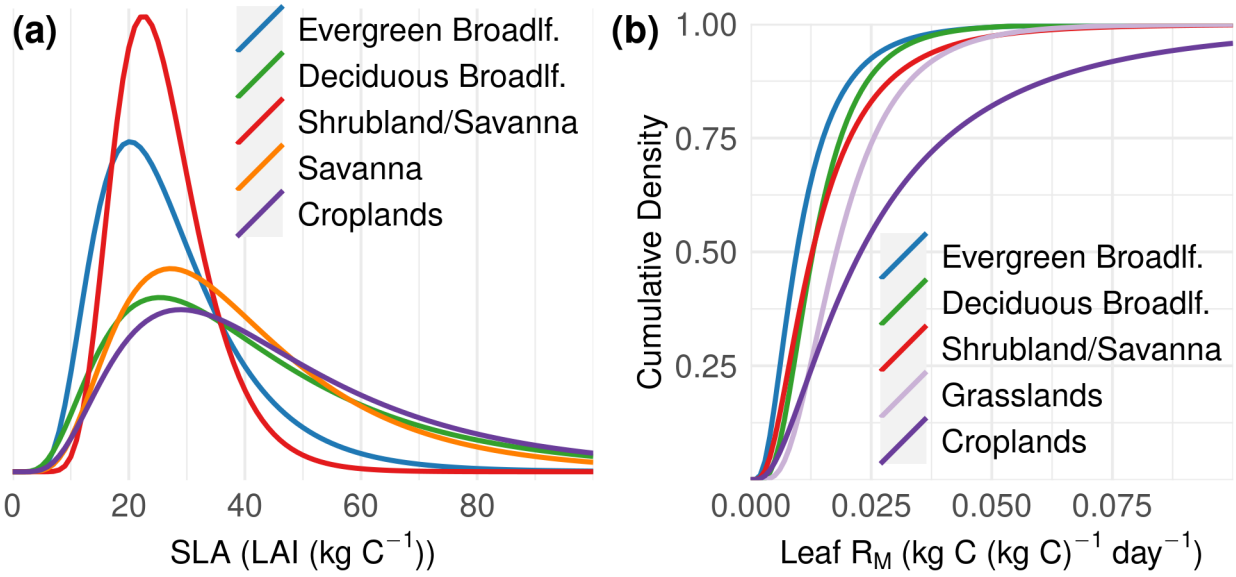

Figure 22: Uncertainty in TRY prior values, for select PFTs, as indicated by the prior probability density function for specific leaf area (a) and the prior cumulative density function for leaf R_M (b).